2017

Flow and transport from a stream to a well in an unconfined aquifer

Cynthia Louise Maroney
Iowa State University

Flow and transport from a stream to a well in an unconfined aquifer

by

Cynthia Louise Maroney

A dissertation submitted to the graduate faculty

in partial fulfillment of the requirements for the degree of

DOCTOR OF PHILOSOPHY

Major: Civil Engineering (Environmental Engineering)

Program of Study Committee:
Chris Rehmann, Major Professor
James Rossmanith
Kristie Franz
William Simpkins
Say Kee Ong
Shankar Subramaniam

The student author and the program of study committee are solely responsible for the content of this dissertation. The Graduate College will ensure this dissertation is globally accessible and will not permit alterations after degree is conferred.

Iowa State University

Ames, Iowa

2017

DEDICATION

This dissertation is dedicated to my children, James and Sarah, and my mother, Norma.

TABLE OF CONTENTS

LIST OF FIGURES

LIST OF TABLES

NOMENCLATURE

Roman symbols

A	$\pi e^{i\xi y'}\left(\omega^2+\alpha^2\right)\left(\omega\cos\left(\omega x'_D\right)-\alpha\sin\left(\omega x'_D\right)\Big/\sqrt{\omega^2+\alpha^2}\right)$
A_m	cell area in MODFLOW
a_L	longitudinal dispersivity
a_T	transverse dispersivity
b'	thickness of streambed
C	concentration of contaminant
C_b	$K_x A_m/d$, MODFLOW conductance
C_0	constant concentration in the river
C_w	concentration of solute at a well
Da	Damköhler number, λRT_0
D_L	longitudinal diffusion coefficient
D_T	transverse diffusion coefficient
d	distance from MODFLOW model boundary to constant head source
F	term resulting from inversion of Fourier transform
F_i	fraction of total flow carried by i^{th} streamline
F_r	F-term with change of variables for a point sink
$\breve{F}$	F-term for a partially penetrating vertical well
$\hat{f}$	hat denotes function in Fourier space
$\overline{f}$	bar denotes function in $\mathcal{R}$-space

$\tilde{f}$	tilde denotes function in both Fourier and $\mathcal{R}$-space
H	saturated thickness of aquifer
$H(z)$	Heaviside step function
h	hydraulic head
h_a	hydraulic head, MODFLOW
h_b	hydraulic head at a general head boundary, MODFLOW
$\tilde{h}$	head in both Fourier and $\mathcal{R}$-space
$\tilde{h}_s$	steady state head in both Fourier and $\mathcal{R}$-space
$\tilde{h}_0$	time varying term for head in both Fourier and $\mathcal{R}$-space
$\tilde{h}_n$	nth time varying term for head in both Fourier and $\mathcal{R}$-space
$\breve{h}$	hydraulic head for a partially penetrating vertical well
h_D	$\pi^2 K_x H h / Q$, dimensionless head
i	counter
K	hydraulic conductivity of aquifer
K_x	hydraulic conductivity of the aquifer in the x-direction
K_y	hydraulic conductivity of the aquifer in the y-direction
K_z	hydraulic conductivity of the aquifer in the z-direction
K'	hydraulic conductivity of streambed
L_x	distance from the stream to the center of a caisson or well
L_z	vertical position of laterals or half way point of vertical well screen
ℓ	length of vertical section of well screen

ℓ_i	length of the i^{th} lateral of a radial collector well
ℓ_T	total length of the laterals of a radial collector well
N	number of lateral well screens
N_s	number of streamlines
n	counter
Pe	Péclet number
p	$\omega/\sqrt{\kappa_z} = r\cos\phi$
Q	well discharge
Q_b	flow through general head boundary, MODFLOW
q	$\xi\sqrt{\kappa_y/\kappa_z} = r\sin\phi$
q_s	flow through the streambed
R	term resulting from inversion of the $\mathscr{R}$-transform for a radial collector well
R_c	retardation coefficient
R'	R-term resulting from inversion of the $\mathscr{R}$-transform for a point sink
R_r	R-term with change of variables
$\breve{R}$	R-term for a partially penetrating vertical well
r	$\sqrt{p^2+q^2}$
r_1	distance of observation point from well (Neuman,1974)
S	storage coefficient
S_s	specific storage
S_y	specific yield
s	drawdown

s_D	dimensionless drawdown
SDR	stream depletion rate
SDR′	dimensionless stream depletion rate for a point sink
$\widetilde{\mathrm{SDR}'}$	Fourier and $\mathcal{R}$-transform of stream depletion rate for a point sink
$\overline{\mathrm{SDR}'}$	stream depletion rate for a point sink in $\mathcal{R}$-space
SDR_H	stream depletion rate (Hantush, 1965) for a radial collector well
SDR'_H	stream depletion rate (Hantush, 1965)
SDR_T	stream depletion rate (Theis, 1941) for a radial collector well
SDR'_T	stream depletion rate (Theis, 1941)
SDR'_s	steady stream depletion rate for a point sink
$\overline{\mathrm{SDR}'_s}$	steady stream depletion rate in R-space for a point sink
T	aquifer transmissivity
T_i	travel time of water in *i*th streamtube
T_0	dimensionless time $\eta_e H L_x^2 / Q$
T_s	time to reach steady state
t	duration of pumping
t_D	$K_x t / \left(S_s H^2 \right)$, dimensionless time
x	horizontal coordinate (perpendicular to the stream)
x_D	x/H, dimensionless x-coordinate
x'	x-coordinate of point-sink

x'_D	x'/H , dimensionless *x*-location of point-sink
x_{0D}	*x*-coordinate of center of caisson normalized by *H*
y	horizontal coordinate (along the stream)
y_D	y/H , dimensionless *y*-coordinate
y'	*y*-coordinate of point-sink
y'_D	y'/H , dimensionless *y*-coordinate of point-sink
z	vertical coordinate (positive upward)
z_D	z/H , dimensionless *z*-coordinate
z'	*z*-coordinate of point-sink
z'_D	z'/H , dimensionless *z*-coordinate of point-sink
z_{0D}	z-coordinate of laterals normalized by *H*

Greek symbols

α	$-K'H/(K_x b')$
β_0	solution to $\tanh\beta_0 = \gamma\left(\beta_0^2\kappa_z - \kappa_y\xi^2 - \omega^2\right)/(\kappa_z\beta_0)$
β_n	solution to $\tan\beta_n = -\gamma\left(\beta_n^2\kappa_z + \kappa_y\xi^2 + \omega^2\right)/\beta_n\kappa_z$
γ	S_y/S non-dimensional parameter
$\delta(\,)$	dirac delta function
ε	$Q/(K_x H^2)$, flow parameter
ζ_0	root of $\tanh\zeta_0 = \gamma\left(\zeta_0^2\kappa_z - \omega^2\right)/(\kappa_z\zeta_0)$

$\breve{\zeta}_0$	root of $\tanh\zeta_0 = -\gamma\left(\zeta_0^2 - r^2\right)\big/\zeta_0$
ζ_n	roots of $\tan\zeta_n = -\gamma\left(\zeta_n^2\kappa_z + \omega^2\right)\big/\zeta_n\kappa_z$
$\breve{\zeta}_n$	roots of $\tan\zeta_n = -\gamma\left(\zeta_n^2 + r^2\right)\big/\zeta_n$
η_e	effective porosity
θ_i	orientation of i^{th} lateral of a radial collector well
κ_y	K_y/K_x horizontal anisotropy
κ_z	K_z/K_x vertical to horizontal anisotropy
Λ	ℓ/H ratio of length scale for vertical
Λ_i	ℓ_i/H ratio of length scale for the i^{th} lateral of a radial collector well
Λ_T	total length of the laterals ℓ_T normalized by H
λ	rate of decay
λ_s	$\sqrt{\left(\omega^2 + \kappa_y\xi^2\right)\big/\kappa_z}$
λ_0	$\beta_0^2\kappa_z - \kappa_y\xi^2 - \omega^2$
λ_n	$\beta_n^2\kappa_z + \kappa_y\xi^2 + \omega^2$
μ_0	$\zeta_0^2\kappa_z - \omega^2$
$\breve{\mu}_0$	$-\kappa_z\left(r^2 - \beta_0^2\right)$
μ_n	$\zeta_n^2\kappa_z - \omega^2$
$\breve{\mu}_n$	$\kappa_z\left(r^2 - \beta_n^2\right)$
ξ	y variable in Fourier space

ρ_x	L_x/H , horizontal ratio of length scale for well
ρ_z	L_z/H , vertical ratio of length scale for well
σ	variable for integration
τ	$Tt/\left(SL_x^2\right) = K_x t/S_s L_x^2$, dimensionless time parameter
Φ_s	steady state term in hydraulic head for a point sink
$\breve{\Phi}_s$	steady state term in hydraulic head for a partially penetrating vertical well
Φ_0	time dependent term in stream depletion rate for a radial collector well
Φ_0'	time dependent term in stream depletion rate for a point sink
$\breve{\Phi}_0$	time dependent term in hydraulic head for a partially penetrating vertical well
Φ_n	*n*th time dependent term in stream depletion rate for a radial collector well
Φ_n'	*n*th time dependent term in stream depletion rate for a point sink
$\breve{\Phi}_n$	*n*th time dependent term in head for a partially penetrating vertical well
ϕ	$\phi = \cos^{-1}\left(p/r\right) = \sin^{-1}\left(q/r\right)$
χ	$K'L_x/\left(K_x b'\right)$, streambed conductance coefficient
ω	*x* variable in $\boldsymbol{\mathcal{R}}$ space

Other notation

GHB	general head boundary, MODFLOW

HTY	Huang, Tsou, Yeh (2012)
MODFLOW	the United States Geological Survey's three-dimensional finite-difference groundwater model
PCG2	preconditioned conjugate gradient 2 solver package
$\mathcal{R}$-	transform that is a combination of Fourier sine and cosine transforms

ACKNOWLEDGMENTS

I would like to acknowledge and thank the Department of Civil, Construction, and Environmental Engineering for the financial support and teaching experiences that allowed me to complete the research for this degree and gain valuable experience.

My greatest thanks go to my advisor, Dr. Chris Rehmann who always had a tip, trick, or other piece of wisdom to keep my research and writing progressing. I learned a tremendous amount of academic knowledge along with how to keep going in spite of dead ends, lack of knowledge, and other obstacles. My path toward this degree has been a personal journey of growth in which Dr. Rehmann has served as a role model, mentor, and friend. Special thanks go to Dr. James Rossmanith and his infinite level of patience with my journey through the math department. I would also like to thank Dr. Bill Simpkins who also served on my master's committee at the end of the last century and provided practical suggestions for the improvement of my research. Finally, I want to acknowledge my other committee members Dr. Kristie Franz, Dr. Say Kee Ong, and Dr. Shankar Subramaniam for their support.

My mother's pride and belief in me has kept me going when things have felt too overwhelming. She has always been there for me through all my tears and joys. My children, James and Sarah, provided a unique kind of support by accepting that their mother went to school every day like they do. To my children, my pursuit of this degree was an ordinary activity for their not so normal mother. They kept my feet on the ground by reminding me that there are always meals to prepare, laundry to be washed, school activities to attend, and family adventures to be taken.

Special thanks go to my academic family Dr. Jen Jefferson, Lauren Schwab, Ian Willard, Rusen Sinir, Zhimin Li, and Yuqi Song. I also want to recognize the other people that I have worked in study groups with and other friends from campus including David Dziubanski, Dr. David Green, and Dr. Mike Lawrinenko. Additional thanks go to Dr. Beth Hartman, Dr. Kaoru Ikuma, Dr. Bob Horton, and Dr. Toby Ewing who have also served as mentors for me.

Many other people made this journey possible by assisting and supporting me as I made major changes to my life including Michael Abele, Vicky Arndt, Leilani McDonald, Denise Bachelder, Loretta Eue, Amy Gerhls, Anita White, all the other members of WATCH, Brenda Cloyd, Doug Truex, and Dr. Daria Schmidt.

ABSTRACT

Flow, stream depletion rate (SDR), and transport are evaluated with three analytical models for wells installed in a semi-infinite, homogeneous, anisotropic, unconfined aquifer near a fully penetrating stream with a streambed with reduced conductivity. The first model, presented in Maroney and Rehmann (2017), involves re-evaluating the calculations of Huang et al. (2012) for the SDR of a radial collector well. The present solution for SDR has a single integral that requires numerical evaluation, while the previous model has five. Analytical results show that at steady state the flow through the streambed equals the pumping rate of the well. That is, the steady SDR is one, and it does not depend on streambed or aquifer properties or the well design. Before the SDR reaches steady state, streambed conductance, aquifer anisotropy, and the position of the well relative to the stream affect SDR much more than the orientation, length, and depth of the lateral well screens.

The second model builds on the method developed for SDR for a radial collector well. It provides flow and SDR for a partially penetrating vertical well installed in a semi-infinite, homogeneous, unconfined aquifer adjacent to a stream with a reduced conductivity streambed. Like the model for SDR of a radial collector well, the SDR for this case has only one improper integral that must be evaluated numerically. Steady drawdown is symmetric across the horizontal plane at the center of the aquifer for a well centered in the aquifer. The supply of water from the stream decreases hydraulic gradients at the top and bottom of the aquifer. The model for a partially penetrating well provides quantitative guidance for practical applications. For example, for removing contaminants, a well with small degree of penetration should be placed near the level of the contamination, and for dewatering—which

aims for maximum drawdown and minimum SDR, the well should be placed as high in the aquifer as possible.

Streamlines from a river to a nearby well are used to compute the concentration of a contaminant in a well. Concentration at the stream is constant and transport to the well is through advection, retardation, and decay. Both the well and steam fully penetrate the aquifer, which has horizontal anisotropy. The stream has a streambed with reduced conductivity. As shown by dimensional analysis and supporting arguments, the concentration at the well depends on four dimensionless parameters: dimensionless time, a streambed conductance coefficient χ, the ratio κ_y of the horizontal hydraulic conductivities, and the Damköhler number, which accounts for advection, retardation, and decay by combining the properties of the aquifer, well, and contaminant. For fixed χ and κ_y, the timing and magnitude of the steady state concentration at the well depend only on the Damköhler number. The special case of no streambed ($\chi \to \infty$) yields conservative estimates of the time of first arrival, steady state concentration, and (except for low Damköhler number) the time to steady state.

CHAPTER 1: INTRODUCTION

1.1 Significance and Problem Definition

Alluvial aquifers are the primary source of water for supply, agriculture, and industry, and in many areas of the United States supplying enough water of acceptable quality is a challenge. Over-pumping of wells in an alluvial aquifer can reduce flow in the river and water levels in the aquifer. Such reductions along the Republican River have led to an interstate dispute between Kansas, Nebraska, and Colorado (Hendee, 2014). The interconnection between surface water and groundwater must be recognized for good management of water resource systems such as the Republican River and its associated aquifer.

Agricultural runoff is a source of nutrients and pesticides in rivers which require removal prior to delivery to the drinking water system. The interconnection between a river and its aquifer provides a path for contaminants to flow to wells and enter the drinking water system. When the level of nitrates in the Des Moines and Raccoon Rivers is high, nitrates that appear in the water produced by the riverbank filtration system increase the cost of water treatment substantially (KCCI, 2015).

Riverbank filtration (RBF) systems exploit the hydraulic connection between surface water and groundwater systems to produce water of good quality. Wells pumping in surficial aquifers near streams induce flow from the stream into the groundwater system. The surface water is filtered naturally as it flows through the subsurface materials. Straining, chemical reactions, sorption, dispersion, diffusion, and decay act to remove bacteria, nutrients, pesticides, and other contaminants. Quantifying the quantity and quality of flow from the

river to the well helps water managers, producers, and users plan treatment processes and manage the regional water system. Stream depletion rate (SDR), or the fraction of the well's flow that comes from the stream, quantifies the relationship between extraction of groundwater and flow through the streambed that results from pumping of a well. Water users and regulators also use the SDR to predict the quality of the pumped water and to determine how pumping influences the water budget (Ray et al., 2002). Although the SDR can be used to estimate contaminant concentrations in pumped water, the estimates do not account for removal in the aquifer. An approach to predict the quality of water in the well in terms of properties of the stream, aquifer, and well is needed.

1.2 Objectives

The objectives of this research are to increase the understanding of the flow and transport from rivers to wells by developing several analytical models that can be used to evaluate the flow of water to a well in an unconfined aquifer, estimate the contribution of streamflow to the well, and predict the concentration of the solute at the well. The non-dimensional parameters describing aquifer properties, streambed properties, well design and transport are evaluated to determine the effect they have on flow to the well or the development of stream depletion.

1) The objective of Chapter 2 is to investigate the SDR for riverbank filtration systems, particularly a radial collector well, in unconfined aquifers by re-evaluating the work of Huang et al. (2012), evaluating the effects of vertical flow in an aquifer on the SDR, and quantifying the effects of dimensionless parameters on the development of SDR.

2) The objective of Chapter 3 is to evaluate how flow to a partially penetrating vertical well in an unconfined aquifer is affected by a nearby stream and vertical flow in the aquifer and how SDR is affected by the amount of penetration and depth of the well screen.
3) The objective of Chapter 4 is to examine transport from a stream to a nearby well in an aquifer and predict the concentration of a contaminant accounting for advection, retardation, and decay and the effects of a reduced conductivity streambed.

1.3 Dissertation Organization

The following chapters discuss the flow of water and transport of contaminants to wells in unconfined aquifers that are bounded on one side by a river. The river is modeled as a feature that fully penetrates the aquifer. The SDR for a radial collector well is evaluated in Chapter 2 and has been published in the *Journal of Hydrology* (Maroney and Rehmann, 2017). A model for flow of water and SDR for a well that partially penetrates an unconfined aquifer builds on the research in Chapter 2 and is evaluated in Chapter 3. Chapter 4 presents a method to use velocity vectors generated from the flow model developed in Chapter 3 to estimate the steady state timing and concentration of a contaminant that travels from a stream to a nearby vertical well. The conclusions, significant findings, and suggestions for further research follow in Chapter 5.

References

Hendee, D., 2014. “Kansas' accusation that Nebraska violated Republican River pact lands at U.S. Supreme Court”, *Omaha World-Herald*, Oct. 13, 2014. http://www.omaha.com/news/nebraska/kansas-accusation-that-nebraska-violated-republican-river-pact-lands-at/article_14381236-2ad7-55b6-8417-c904ecdcf77e.html.

Huang, C.S., Tsou, P.R., Yeh, H.D., 2012. An analytical solution for a radial collector well near a stream with a low-permeability streambed. J. Hydrol., 446: 48-58. http://dx.doi.org/10.1016/j.jhydrol.2012.04.028

KCCI, 2015. “$1.5 million bill from Water Works record nitrate removal.” http://www.kcci.com/news/drinking-water-nitrate-removal-costs-15-million/34376516.

Maroney, C.L., Rehmann, C.R., 2017. Stream depletion rate for a radial collector well in an unconfined aquifer near a fully penetrating river. J. Hydrol., 547: 732-741. http://dx.doi.org/10.1016/j.jhydrol.2017.02.010

Ray, C., Schubert, J., Linsky, R.B., Melin, G., 2002. Riverbank filtration: Improving source-water quality. In: Ray, C., Melin, G., Linsky, R.B. (Eds.), Riverbank Filtration: Improving Source-Water Quality. Water Science and Technology Library, pp. 1-15.

CHAPTER 2: STREAM DEPLETION RATE FOR A RADIAL COLLECTOR WELL IN AN UNCONFINED AQUIFER NEAR A FULLY PENETRATING RIVER

A paper accepted by the *Journal of Hydrology*

Cynthia Maroney and Chris Rehmann

Abstract

The stream depletion rate (SDR) is computed for a radial collector well installed in a semi-infinite, anisotropic, homogeneous, unconfined aquifer near a fully penetrating stream with a streambed with reduced conductivity. For small pumping rates dimensional analysis and other arguments allow the SDR to be expressed as a function of eight parameters that describe the effect of properties of the aquifer and streambed as well as the configuration and placement of the well. The calculations employ some results from Huang et al. (2012, *J. Hydrol.*), who expressed the SDR as a quintuple integral, but by computing four of the integrals analytically, the present solution requires less computational effort. Analytical calculation shows that the SDR in steady state does not depend on the streambed properties (or any other parameters): Given enough time, the flow through the streambed will equal the pumping rate of the well. Values of SDR are supported by comparing to previous solutions for special cases corresponding to appropriate limiting values of the parameters. Effects of the eight dimensionless parameters are studied systematically: The properties of the streambed, anisotropy of the aquifer, and the position of the well affect the SDR more strongly than the orientation, length, and depth of the laterals.

2.1 Introduction

Wells located in high yielding aquifers next to a water body exploit the natural filtration by the soil and blending with groundwater to produce large volumes of water of acceptable quality. The quantity and quality of water produced by riverbank filtration systems varies because of the dynamic nature of the connection between the surface water and groundwater. To estimate the quality of the effluent and evaluate the effect of pumping on local and regional water budgets, producers and regulators use the stream depletion rate (SDR)

$$\text{SDR} = \frac{q_s}{Q} \tag{2.1}$$

or the ratio of the flow q_s from the stream and the pumping rate Q of the well. We evaluate the effect of several parameters on the SDR for a radial collector well in an unconfined aquifer so that radial collector wells can be designed and operated more effectively.

Dimensional analysis helps to identify the parameters that control the SDR for a radial collector well in a homogeneous, anisotropic, unconfined aquifer (Fig. 2.1). If the aquifer is infinitely long in the y-direction, the flow from the stream depends on the rate Q and duration t of pumping; the streambed hydraulic conductivity K' and thickness b'; aquifer properties including the saturated thickness H, horizontal hydraulic conductivity K_x (or transmissivity $T = K_xH$), vertical hydraulic conductivity K_z, specific yield S_y, and specific storage S_s (or storage coefficient $S = S_sH$); distance L_x from the stream to the caisson; and the length ℓ_i, vertical position L_z, and orientation θ_i of the laterals. The relationship can be simplified by realizing that the streambed parameters can be combined in a conductance coefficient (Hantush, 1965) and the specific yield, specific storage, and saturated thickness

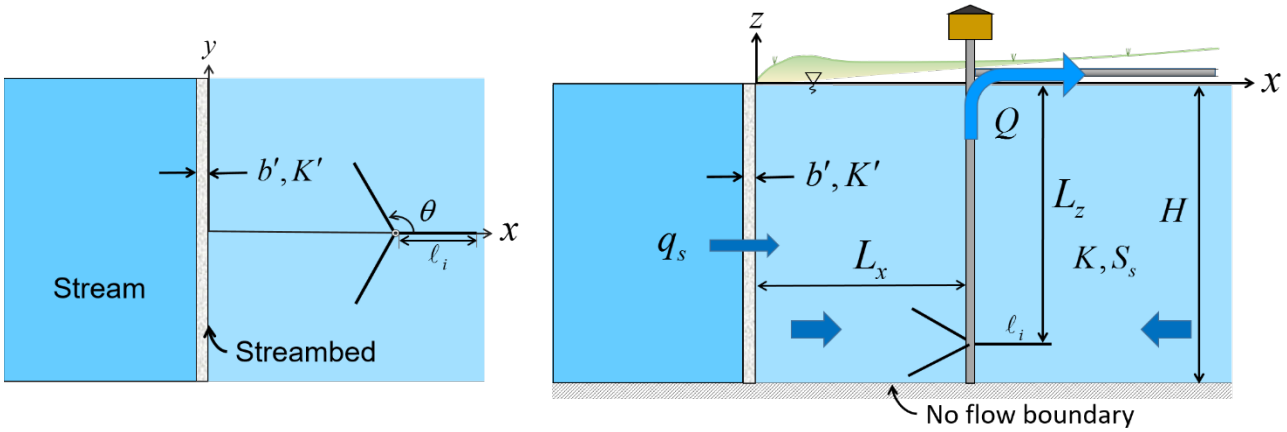

Fig. 2.1. Conceptual model for a radial collector well installed in an anisotropic, unconfined aquifer adjacent to a fully penetrating stream: (a) plan view, (b) profile view.

can be combined as the ratio S_y/S. Then, dimensional analysis yields

$$\mathrm{SDR} = f\left(\frac{Tt}{SL_x^2}, \frac{K'L_x}{K_x b'}, \theta_i, \frac{\ell_i}{H}, \frac{K_z}{K_x}, \frac{Q}{K_x H^2}, \frac{S_y}{S}, \frac{L_x}{H}, \frac{L_z}{H}\right) = f\left(\tau, \chi, \theta_i, \Lambda_i, \kappa_z, \varepsilon, \gamma, \rho_x, \rho_z\right) \qquad (2.2)$$

The second equality in (2.2) defines several dimensionless parameters to be considered (Table 2.1).

Previous work on this problem, which is summarized in Table 2.2, offers insight into the effects of the parameters in the dimensional analysis on SDR. For a fully penetrating vertical well in an aquifer near a fully penetrating stream, Theis (1941) and Glover and Balmer (1954) neglected vertical flow and found the SDR to be

$$\mathrm{SDR}'_T = \mathrm{erfc}\left(\frac{1}{2\tau^{1/2}}\right) \qquad (2.3)$$

Initially the SDR is small because the flow to the well is from the aquifer. As time passes, or τ increases, the cone of depression expands to include the streambed, and SDR increases. At large times, SDR approaches one, and the flow to the well is supplied entirely by the stream. The change in SDR depends on the diffusion time scale $L_x^2/(T/S)$ (Jenkins, 1968); changes

Table 2.1. Dimensionless parameters affecting the stream depletion rate.

Parameter	Description
$\tau = \frac{Tt}{SL_x^2}$	Time normalized by hydraulic diffusion time
$\chi = \frac{K'L_x}{K_x b'}$	Streambed conductance coefficient
$\kappa_z = \frac{K_z}{K_x}$	Anisotropy parameter: ratio of vertical and horizontal conductivities
$\Lambda_i = \frac{\ell_i}{H}$	Dimensionless length of i^{th} lateral
θ_i	Angle between the i^{th} lateral and positive x-axis
$\varepsilon = \frac{Q}{K_x H^2}$	Well strength
$\gamma = \frac{S_y}{S}$	Ratio of specific yield and storage coefficient
$\rho_x = \frac{L_x}{H}$	Dimensionless distance between stream and caisson
$\rho_z = \frac{L_z}{H}$	Dimensionless depth of laterals (defined as positive)

in SDR take longer for greater distances between the well and the stream, less conductive aquifers, or aquifers in which more water is released per unit change in head.

Several models have allowed for a streambed with reduced permeability. For a case with negligible vertical flow, the SDR depends on the conductance coefficient $\chi = K'L_x / K_x b'$, which characterizes the flow processes associated with the streambed (Hantush, 1965):

$$\mathrm{SDR}'_H = \mathrm{erfc}\left(\frac{1}{2\tau^{1/2}}\right) - \exp\left(-\frac{1}{4\tau}\right)\mathrm{erfcx}\left(\frac{1}{2\tau^{1/2}} + \chi\tau^{1/2}\right) \qquad (2.4)$$

Table 2.2. Survey of solutions for SDR with constant stream stage. Wells are vertical unless otherwise noted. BC = boundary condition.

References	Stream treatment	Streambed	Dupuit assumption?	Other features
Theis (1941) Glover and Balmer (1954)	Constant head BC	None	Yes	
Hantush (1965)	Third-type BC	Reduced permeability	Yes	
Hunt (1999)	Surface source: zero-width	Reduced permeability	Yes	Surface recharge
Zlotnik et al. (1999)	Surface source: finite-width	Reduced permeability	Yes	Finite width aquifer
Butler et al. (2001)	Surface source: finite-width	Reduced permeability	Yes	
Hunt (2003)	Surface source: zero-width	Aquitard	Yes, in aquifer	1D vertical flow in top layer
Zlotnik (2004)	Constant head BC	None	Yes, in aquifer	Leakage from below, two streams
Sun and Zhan (2007)	Constant head BC	Reduced permeability	Yes	Two streams
Yeh et al. (2008)	Constant head BC	None	Yes	Finite width aquifer, two streams
Zlotnik & Tartakovsky (2008)	Surface source: zero-width	Reduced permeability	Yes	Finite width aquifer, leakage from below
Hunt (2008)	Surface source: finite-width	Aquitard	Yes, in aquifer	Finite width aquifer, free surface aquitard
Hunt (2009)	Surface source: zero-width	Reduced permeability	Yes	Two layer aquifer, leakage from above
Tsou et al. (2010)	Constant head BC		Yes	Slanted or horizontal well
Ward and Lough (2011)	Surface source: zero-width	Reduced permeability	Yes	Two-layer aquifer
Sedghi et al. (2012)	Constant head BC	None	No	Two streams
Huang et al. (2012)	Third-type BC	Reduced permeability	No	Radial collector well
Huang et al. (2014)	Third-type BC	Reduced permeability	No	Two streams or stream and impermeable unit
Huang et al. (2016a)	Third-type BC	Reduced permeability	No	Two streams, lateral no-flow BC, radial collector well

where erfcx( ) is the scaled complementary error function, defined as $\mathrm{erfcx}(z) = \exp(z^2)\mathrm{erfc}(z)$. Small χ, which corresponds for example to a thick streambed with low conductivity, leads to smaller SDR. However, for any $\chi > 0$, the SDR approaches one given enough time; that is, even for streambeds with small conductivity, all of the flow to well will eventually come from the stream. This observation differs from results for a radial collector well in an unconfined, anisotropic aquifer with vertical flow, which show that the steady-state SDR decreases as K'/K_x decreases (Huang et al., 2012, hereafter HTY). However, steady SDR of less than one must be incorrect because a water balance applied to a semi-infinite aquifer shows that in steady state all of the well's flow must come from the stream.

The temporal evolution of the SDR becomes more complicated when gravity drainage supplies the well. Analytical solutions for both a semi-infinite aquifer (HTY) and an aquifer bounded by two streams and two no-flow boundaries (Huang et al., 2016a) predict an intermediate stage in which delayed yield from the aquifer (Neuman, 1972) maintains constant SDR. The unsteady behavior of SDR can be important in practice when times to steady state are large. For example, the Theis solution in Eq. (2.3) shows that SDR = 0.99 when $\tau = 3910$, and the Hantush solution in Eq. (2.4) shows that when streambed conductance is included, the time to steady state increases. The result from Eq. (2.3) applied to wells near the Cedar River in Iowa (Turco and Buchmiller, 2004) indicates that the time to steady state ranges from 1 d for wells close to the river in highly conductive soil to 3100 d for wells farther away in less conductive soil. Pumping tests to determine aquifer properties typically last less than 3 d (Chin, 2006, p. 744), and the post-construction tests of two radial

collector wells near the Des Moines River lasted 3 and 4 d (Moore et al., 2012), while a test of a radial collector well in the Tailan River Basin included 16 d of pumping (Appiah-Adjei et al., 2012). Therefore, understanding the unsteady behavior of SDR can help in interpreting data collected during short-term pumping tests, especially if water quality data are included.

Previous work allows the effect of several of the other parameters in Eq. (2.2) on SDR to be determined in cases with vertical flow. The value of the SDR in the intermediate stage depends on anisotropy, or the ratio of vertical and horizontal hydraulic conductivities, i.e., $\kappa_z = K_z/K_x$: As κ_z decreases, gravity drainage decreases, and more flow comes from the stream (Huang et al., 2016a). Lateral configuration affects SDR less than anisotropy. Lateral configurations that reduce the distance between the well and the stream—either by increasing the length of laterals pointed toward the stream or by orienting more laterals toward the stream—produce a slightly higher surface water percentage (i.e., SDR) before steady state is reached (Moore et al., 2012).

The last four parameters in Eq. (2.2) have not been studied in detail for flow to radial collector wells. As shown in section 2.2.1, the parameter Q/K_xH^2 determines whether the drawdown is large enough for nonlinear effects to be important. The parameter $\gamma = S_y/S$ determines the duration of the intermediate stage with constant drawdown (and presumably SDR); as γ increases, the duration of the intermediate stage also increases for a well pumping in an infinite unconfined aquifer (Neuman, 1975). The two ratios of length scales characterize the location of the well. Locating the well closer to the stream, or reducing $\rho_x = L_x/H$, increases the fraction of the well's flow that comes from the stream (Moore et al., 2012). Under certain conditions locating a radial collector well deeper in the aquifer can increase SDR (Huang et al., 2016a).

In this paper the HTY solution is re-evaluated to investigate the causes of differences between SDR in aquifers with and without vertical flow and to quantify the effects of the parameters from the dimensional analysis more fully. In section 2.2 we modify the Theis (1941) and Hantush (1965) solutions for use with a radial collector well and present a more efficient calculation of SDR from the HTY solution. We present the SDR as a function of various parameters in section 2.3, discuss the results in section 2.4, and list conclusions in section 2.5.

2.2 Methods

In this section we present the model of a radial collector well near a stream in an unconfined aquifer, the solution for the hydraulic head, the solution for stream depletion rate, and Theis and Hantush models for SDR adapted for radial collector wells. The first two subsections are similar to the development in HTY except for linearizing the water table boundary condition differently and computing roots of transcendental Eqs.s in a simpler and more robust way.

2.2.1. Model for an unconfined aquifer

The model of a radial collector well in a homogeneous, anisotropic unconfined aquifer follows that of HTY. The stage of the fully-penetrating stream is constant, and the well discharge Q is uniformly distributed along N lateral well screens. The origin of the coordinate system is at the top of the streambed and in line with the well. Then if a point sink of strength Q is located at (x', y', z'), the hydraulic head h is governed by

$$K_x \frac{\partial^2 h}{\partial x^2} + K_y \frac{\partial^2 h}{\partial y^2} + K_z \frac{\partial^2 h}{\partial z^2} = S_s \frac{\partial h}{\partial t} + Q\delta\left(x - x'\right)\delta\left(y - y'\right)\delta\left(z - z'\right) \qquad (2.5)$$

where K_y is the hydraulic conductivity in the y-direction and $\delta(\ )$ is the Dirac delta function. Before pumping begins at $t = 0$ and far from the well, there is no drawdown—that is, $h = 0$ at $t = 0$, as $x \to \infty$, and as $|y| \to \infty$. Because the unit underlying the aquifer is assumed to be impermeable, the vertical flow there is zero:

$$\frac{\partial h}{\partial z} = 0 \quad \text{at} \quad z = -H \tag{2.6}$$

At the interface between the streambed and aquifer, the flow in the aquifer equals the flow across the streambed:

$$K_x \frac{\partial h}{\partial x} - \frac{K'}{b'} h = 0 \quad \text{at} \quad x = 0 \tag{2.7}$$

As the conductivity of the streambed increases or the thickness of the streambed decreases, the stream approaches a constant-head boundary, as in the Theis (1941) solution for SDR.

In general the boundary condition for the water table depends nonlinearly on the head gradients (Yeh et al., 2010):

$$S_y \frac{\partial h}{\partial t} = K_x \left(\frac{\partial h}{\partial x} \right)^2 + K_y \left(\frac{\partial h}{\partial y} \right)^2 + K_z \left(\frac{\partial h}{\partial z} \right)^2 - K_z \frac{\partial h}{\partial z} \quad \text{at} \quad z = h \tag{2.8}$$

HTY assumed that small drawdown would make the nonlinear terms negligible and allow the boundary condition to be applied on $z = 0$, and Huang et al. (2016a) quantified the necessary criteria as $|h|/H < 0.1$ and $|\partial h/\partial x| + |\partial h/\partial y| < 0.01$. Another approach is to express the key assumptions in terms of input variables by estimating ratios of terms in Eq. (2.8). Neglecting the third term on the right side relative to the fourth on the right side requires

$$\frac{K_z (\partial h / \partial z)^2}{K_z \left(\partial h / \partial z \right)} = \frac{\partial h}{\partial z} \sim \frac{1}{H} \left(\frac{Q}{\pi^2 K_x H} \right) = \frac{\varepsilon}{\pi^2} << 1 \tag{2.9}$$

in which the scaling for the head [i.e., $h \sim Q/(\pi^2 K_x H)$] from HTY has been used. If the first and second terms on the right side are comparable to each other, then neglecting them requires

$$\frac{K_x(\partial h/\partial x)^2}{K_z\left(\partial h/\partial z\right)} \sim \frac{Q}{\pi^2 K_z L_x^2} = \frac{\varepsilon}{\pi^2 \kappa_z \rho_x^2} << 1 \qquad (2.10)$$

Expanding the last term in Eq. (2.8) in a Taylor series around $z = 0$ shows that if condition (2.9) is satisfied, the boundary condition can be applied at $z = 0$. If these conditions hold, then Eq. (2.8) can be approximated with

$$S_y \frac{\partial h}{\partial t} = -K_z \frac{\partial h}{\partial z} \quad \text{at} \quad z = 0 \qquad (2.11)$$

as in HTY. If $S_y = 0$, the boundary condition becomes a no-flux condition, and the aquifer becomes confined. The accuracy of the approximations leading to Eq. (2.11) varies: For the base-case example of HTY and a pumping test near the Russian River (Jasperse, 2009), the largest neglected terms are about 1% and 3% of the retained terms, respectively, while for a pumping test near the Ohio River (Schafer, 2006) and the Case D design of a radial collector well near the Des Moines River (Moore et al., 2012), the errors are 10% and 26%, respectively. However, conditions (2.9) and (2.10) are conservative for a radial collector well because distributing the total flow Q over the laterals will cause smaller maximum drawdown than for a point sink.

Computing the SDR requires calculating the flow from the stream. Darcy's law applied at the interface of the stream and the aquifer can be integrated over the area of that interface. Using the boundary condition in Eq. (2.7) yields

$$q_s = -\int_{-H}^{0}\int_{-\infty}^{\infty} K_x \left.\frac{\partial h}{\partial x}\right|_{x=0} dydz = -\int_{-H}^{0}\int_{-\infty}^{\infty} \frac{K'}{b'} h\big|_{x=0}\, dydz \qquad (2.12)$$

The problem of computing the flow q_s can be simplified by integrating the governing Eq. (2.5) over spatial coordinates. For example, integrating over y and using the boundary conditions for $|y| \to \infty$ removes one dimension from the problem. In a confined aquifer, another dimension can be removed by integrating over z. In an unconfined aquifer, however, the boundary condition (2.11) leads to the need for the head at the water table. Therefore, instead of integrating the governing Eq., we compute the flow from the stream and the SDR by using the solution of HTY for the head.

To use the solution of HTY for the head to compute stream depletion rate, we adopt the HTY notation regarding dimensionless variables:

$$\left(x_D, y_D, z_D\right) = \left(\frac{x}{H}, \frac{y}{H}, \frac{z}{H}\right), \quad \left(x'_D, y'_D, z'_D\right) = \left(\frac{x'}{H}, \frac{y'}{H}, \frac{z'}{H}\right), \quad t_D = \frac{K_x t}{S_s H^2}, \quad h_D = \frac{\pi^2 K_x H}{Q} h \quad (2.13)$$

The governing Eq. (2.5) becomes

$$\frac{\partial^2 h_D}{\partial x_D^2} + \kappa_y \frac{\partial^2 h_D}{\partial y_D^2} + \kappa_z \frac{\partial^2 h_D}{\partial z_D^2} = \frac{\partial h_D}{\partial t_D} + \pi^2 \delta\left(x_D - x'_D\right)\delta\left(y - y'_D\right)\delta\left(z - z'_D\right) \quad (2.14)$$

where $\kappa_y = K_y/K_x$, with $h_D = 0$ at $t_D = 0$, as $x_D \to \infty$, and as $|y_D| \to \infty$. The bottom boundary condition (2.6) becomes $\partial h_D / \partial z_D = 0$ at $z_D = -1$, and the top boundary condition (2.11) becomes

$$\gamma \frac{\partial h_D}{\partial t_D} = -\kappa_z \frac{\partial h_D}{\partial z_D} \quad \text{at} \quad z_D = 0 \quad (2.15)$$

The boundary condition at the streambed becomes

$$\frac{\partial h_D}{\partial x_D} + \alpha h_D = 0 \quad \text{at} \quad x_D = 0 \quad (2.16)$$

where $\alpha = -K'H / K_x b' = -\chi / \rho_x$, as defined by HTY. The flow from the stream can be expressed in dimensionless terms as the stream depletion rate:

$$\mathrm{SDR}' = \frac{\alpha}{\pi^2}\int_{-1}^{0}\int_{-\infty}^{\infty} h_D\big|_{x_D=0}\, dy_D dz_D \tag{2.17}$$

as shown by HTY.

2.2.2. Solution for stream depletion rate

HTY solved for the head by applying a Laplace transform in time, a Fourier transform in *y*, and an $\mathcal{R}$-transform in *x*. The Fourier transform pair is

$$\hat{f}(\xi) = \frac{1}{\sqrt{2\pi}}\int_{-\infty}^{\infty} f(y_D) e^{i\xi y_D} dy_D \quad \text{and} \quad f(y_D) = \frac{1}{\sqrt{2\pi}}\int_{-\infty}^{\infty} \hat{f}(\xi) e^{-i\xi y_D} d\xi \tag{2.18}$$

The $\mathcal{R}$-transform of a function $f(x)$ is

$$\overline{f}(\omega) = \sqrt{\frac{2}{\pi}}\int_0^{\infty} f(x_D)\frac{\omega\cos(\omega x_D) - \alpha\sin(\omega x_D)}{\left(\omega^2+\alpha^2\right)^{1/2}} dx_D \tag{2.19}$$

and the inverse $\mathcal{R}$-transform is

$$f(x_D) = \sqrt{\frac{2}{\pi}}\int_0^{\infty} \overline{f}(\omega)\frac{\omega\cos(\omega x_D) - \alpha\sin(\omega x_D)}{\left(\omega^2+\alpha^2\right)^{1/2}} d\omega \tag{2.20}$$

After inverting the Laplace transform, HTY found the Fourier- and $\mathcal{R}$-transform of the head (denoted by a tilde) to be

$$\tilde{h} = \tilde{h}_s + \tilde{h}_0 + \sum_{n=1}^{\infty}\tilde{h}_n \tag{2.21}$$

The first term on the right side of Eq. (2.21) is the transformed steady-state head distribution:

$$\tilde{h}_s = \begin{cases} -\dfrac{A\cosh\left[\lambda_s(1+z'_D)\right]\cosh\left(\lambda_s z_D\right)}{\kappa_z\lambda_s\sinh\lambda_s} & \text{for} \quad z'_D \le z_D \le 0 \\ -\dfrac{A\cosh\left[\lambda_s(1+z_D)\right]\cosh\left(\lambda_s z'_D\right)}{\kappa_z\lambda_s\sinh\lambda_s} & \text{for} \quad -1 \le z_D \le z'_D \end{cases} \tag{2.22}$$

where $\lambda_s = \sqrt{\left(\omega^2 + \kappa_y\xi^2\right)/\kappa_z}$ and

$$A = \pi e^{i\xi y'_D}\,\frac{\omega\cos\left(\omega x'_D\right) - \alpha\sin\left(\omega x'_D\right)}{\sqrt{\omega^2+\alpha^2}} \tag{2.23}$$

The last two terms on the right side of Eq. (2.21) represent the transformed time-varying portion of the head. The first of those is defined as

$$\tilde{h}_0 = \frac{2A\cosh\left[\beta_0(1+z'_D)\right]\left[-\beta_0\kappa_z\cosh\left(\beta_0 z_D\right) + \gamma\lambda_0\sinh\left(\beta_0 z_D\right)\right]}{\lambda_0\left[\left(1+2\gamma\right)\beta_0\kappa_z\cosh\beta_0 + \left(\kappa_z+\gamma\lambda_0\right)\sinh\beta_0\right]}e^{\lambda_0\rho_x^2\tau} \tag{2.24}$$

for $z'_D \le z_D \le 0$ and

$$\tilde{h}_0 = \frac{2A\cosh\left[\beta_0(1+z_D)\right]\left[-\beta_0\kappa_z\cosh\left(\beta_0 z'_D\right) + \gamma\lambda_0\sinh\left(\beta_0 z'_D\right)\right]}{\lambda_0\left[\left(1+2\gamma\right)\beta_0\kappa_z\cosh\beta_0 + \left(\kappa_z+\gamma\lambda_0\right)\sinh\beta_0\right]}e^{\lambda_0\rho_x^2\tau} \tag{2.25}$$

for $-1 \le z_D \le z'_D$, where $\lambda_0 = \beta_0^2\kappa_z - \kappa_y\xi^2 - \omega^2$ and β_0 is the solution to

$$\tanh\beta_0 = -\frac{\gamma}{\kappa_z\beta_0}\left(\beta_0^2\kappa_z - \kappa_y\xi^2 - \omega^2\right) \tag{2.26}$$

Eq. (2.26) is equivalent to Eq. (29) of HTY, but solving it is simpler because the hyperbolic tangent is bounded. The summand of the final term in Eq. (2.21) is given by

$$\tilde{h}_n = \frac{2A\cos\left[\beta_n(1+z'_D)\right]\left[\beta_n\kappa_z\cos\left(\beta_n z_D\right) + \gamma\lambda_n\sin\left(\beta_n z_D\right)\right]}{\lambda_n\left[\left(1+2\gamma\right)\beta_n\kappa_z\cos\beta_n + \left(\kappa_z-\gamma\lambda_n\right)\sin\beta_n\right]}e^{-\lambda_n\rho_x^2\tau} \tag{2.27}$$

for $z'_D \le z_D \le 0$ and

$$\tilde{h}_n = \frac{2A\cos\left[\beta_n(1+z_D)\right]\left[\beta_n\kappa_z\cos\left(\beta_n z'_D\right)+\gamma\lambda_n\sin\left(\beta_n z'_D\right)\right]}{\lambda_n\left[\left(1+2\gamma\right)\beta_n\kappa_z\cos\beta_n+\left(\kappa_z-\gamma\lambda_n\right)\sin\beta_n\right]}e^{-\lambda_n\rho_x^2\tau} \tag{2.28}$$

for $-1 \le z_D \le z'_D$, where $\lambda_n = \beta_n^2\kappa_z + \kappa_y\xi^2 + \omega^2$ and β_n is the solution to

$$\tan\beta_n = -\frac{\gamma\left(\beta_n^2\kappa_z+\kappa_y\xi^2+\omega^2\right)}{\beta_n\kappa_z} \tag{2.29}$$

as presented in HTY.[1] To avoid spurious roots—especially for smaller values of γ, we obtained β_n by solving

$$\beta_n\sin\beta_n = -\gamma\cos\beta_n\left(\beta_n^2+\frac{\kappa_y}{\kappa_z}\xi^2+\frac{\omega^2}{\kappa_z}\right) \tag{2.30}$$

HTY computed the head for a point sink by inverting the Fourier- and $\mathcal{R}$-transforms in Eqs. (2.22), (2.24), (2.25), (2.27), and (2.28).

2.2.3. Solution for the stream depletion rate

To compute SDR, HTY integrated over the laterals to obtain the head distribution caused by pumping from a radial collector well, and then they computed the flow from the stream (and thus SDR) using Eq. (2.12). These calculations involve five numerical integrations. Because our focus is the stream depletion rate, we compute as many of the integrals as possible analytically. The Fourier transform and $\mathcal{R}$-transform of the SDR in Eq. (2.17) is

$$\widetilde{\mathrm{SDR}'} = \frac{\alpha}{\pi^2}\int_{-1}^{0}\int_{-\infty}^{\infty} h_D\big|_{x_D=0}\,dy_D\,dz_D \tag{2.31}$$

The integration over y_D can be accomplished by using Eq. (2.18) with $\xi = 0$ because

[1]Typographical sign errors in the denominators of equations (2.27) and (2.28) were verified with H.D. Yeh (pers. comm., 2014) and corrected here.

$$\int_{-\infty}^{\infty} f\left(y_D\right) dy_D = \sqrt{2\pi}\,\hat{f}\left(0\right) \tag{2.32}$$

Using Eq. (2.32), Eq. (2.31) becomes

$$\overline{\mathrm{SDR}'} = \frac{\alpha\sqrt{2\pi}}{\pi^2}\int_{-1}^{0} \bar{h}_D dz_D \tag{2.33}$$

For the steady SDR, integrating the transformed steady head distribution in Eq. (2.22) over z_D and using identities for hyperbolic functions yields

$$\overline{\mathrm{SDR}'}_s = -\left.\frac{\alpha\sqrt{2\pi}A}{\pi^2\kappa_z\lambda_s^2}\right|_{\xi=0} \tag{2.34}$$

and because $\lambda_s^2 = \omega/\sqrt{\kappa_z}$ when $\xi = 0$,

$$\overline{\mathrm{SDR}'}_s = -\sqrt{\frac{2}{\pi}}\alpha\frac{\omega\cos\left(\omega x_D'\right) - \alpha\sin\left(\omega x_D'\right)}{\omega^2\sqrt{\omega^2+\alpha^2}} \tag{2.35}$$

Inverting the $\mathcal{R}$-transform with Eq. (2.20), using trigonometric identities, and evaluating the result at $x_D = 0$ gives

$$\begin{aligned}\mathrm{SDR}_s' &= -\frac{2\alpha}{\pi}\int_0^{\infty}\left(\frac{\omega\cos\left(\omega x_D'\right) - \alpha\sin\left(\omega x_D'\right)}{\omega^2\sqrt{\omega^2+\alpha^2}}\right)\left(\left.\frac{\omega\cos\left(\omega x_D\right) - \alpha\sin\left(\omega x_D\right)}{\sqrt{\omega^2+\alpha^2}}\right)\right|_{x_D=0} d\omega \\ &= -\frac{2\alpha}{\pi}\int_0^{\infty}\frac{1}{\omega^2+\alpha^2}\left(\cos\left(\omega x_D'\right) - \frac{\alpha}{\omega}\sin\left(\omega x_D'\right)\right) d\omega \\ &= 1\end{aligned} \tag{2.36}$$

where the final integral was evaluated using methods in sections 10.13-10.15 of Hildebrand (1976). Therefore, the stream depletion rate in steady state is 1. That is, all of the water pumped by the well—whether it is a point sink or a radial collector well—eventually comes from the stream.

For the unsteady terms in the SDR, all but the integral over ω, which results from the inverse $\mathcal{R}$-transform, can be computed analytically using steps similar to those for the steady term. The integral over y_D is again computed using the property in Eq. (2.32). The transformed unsteady head distributions in Eqs. (2.24) and (2.25) and Eqs. (2.27) and (2.28) are integrated over z_D, and identities for hyperbolic and trigonometric functions are used to yield the unsteady SDR for a point sink:

$$\mathrm{SDR}' = 1 + \frac{2\alpha}{\pi}\int_0^\infty \left(\Phi_0' + \sum_{n=1}^{\infty} \Phi_n' \right) R' d\omega \tag{2.37}$$

where

$$\Phi_0' = \frac{2\gamma \cosh\left[\zeta_0\left(1+z_D'\right)\right] e^{\mu_0 \rho_x^2 \tau}}{\zeta_0\left[\left(2\gamma+1\right)\zeta_0\kappa_z \cosh\left(\zeta_0\right) + \left(\gamma\mu_0 + \kappa_z\right)\sinh\left(\zeta_0\right)\right]} \tag{2.38}$$

$$\Phi_n' = -\frac{2\gamma \cos\left[\zeta_n\left(1+z_D'\right)\right] e^{-\mu_n \rho_x^2 \tau}}{\zeta_n\left[\left(2\gamma+1\right)\zeta_n\kappa_z \cos\left(\zeta_n\right) + \left(\kappa_z - \gamma\mu_n\right)\sin\left(\zeta_n\right)\right]} \tag{2.39}$$

$$R' = \frac{\omega\left[\omega\cos\left(\omega x_D'\right) - \alpha\sin\left(\omega x_D'\right)\right]}{\omega^2 + \alpha^2} \tag{2.40}$$

and $\mu_0 = \zeta_0^2\kappa_z - \omega^2$, $\mu_n = \zeta_n^2\kappa_z + \omega^2$, and ζ_0 and ζ_n are the roots of Eqs. (2.26) and (2.30), respectively, with $\xi = 0$. If the total flow to the well is distributed evenly over the laterals, then the SDR for the radial collector well can be computed by integrating over the laterals. Because the laterals are horizontal, $x_D' = x_{0D} + \sigma\cos\left(\theta_i\right)$ and $z_D' = z_{0D}$, where x_{0D} and z_{0D} are the x- and z-coordinates of the center of the laterals, normalized by H. Then

$$\mathrm{SDR} = \frac{1}{\Lambda_T}\sum_{i=1}^{N}\int_0^{\Lambda_i} \mathrm{SDR}' d\sigma \tag{2.41}$$

where Λ_T is the total length ℓ_T of the laterals, normalized by H. The result of the integration is

$$\mathrm{SDR} = 1 + \frac{2\alpha}{\pi \Lambda_T} \sum_{i=1}^{N} \int_0^{\infty} \left(\Phi_0 + \sum_{n=1}^{\infty} \Phi_n \right) R \, d\omega \tag{2.42}$$

where

$$R = \frac{-1}{\left(\omega^2 + \alpha^2\right)\cos\left(\theta_i\right)} \Big[\alpha \left\{ \cos\left(\omega x_{0D}\right) - \cos\left[\omega \left(\Lambda_i \cos\left(\theta_i\right) + x_{0D} \right) \right] \right\} + \omega \left\{ \sin\left(\omega x_{0D}\right) - \sin\left[\omega \left(\Lambda_i \cos\left(\theta_i\right) + x_{0D} \right) \right] \right\} \Big] \tag{2.43}$$

and Φ_0 and Φ_n are the same as Φ_0' and Φ_n' in Eqs. (2.38) and (2.39) except with z_{0D} replacing z_D'. The integral in Eq. (2.42) was evaluated numerically with Matlab's quadgk function, which uses adaptive Gauss-Kronrod quadrature with a maximum of 650 intervals. Matlab functions for computing the stream depletion rate with Eq. (2.42) are included in the supplementary material.

2.2.4. Cases without vertical flow

To investigate the importance of vertical flow, the SDR for the full model is compared to SDR from the Theis (1941) and Hantush (1965) solutions modified for use with radial collector wells. In terms of the model described in section 2.1, both solutions correspond to the case of $\gamma = 0$, and the Theis (1941) solution would also have $\chi \to \infty$. Integrating Eq. (2.3) over the laterals as in Eq. (2.41) gives

$$\mathrm{SDR}_T = \frac{L_x}{\ell_T} \sum_{i=1}^{N} \left\{ \frac{\ell_i}{L_x} \operatorname{erfc}\left(\frac{1 + (\ell_i / L_x)\cos\theta_i}{2\tau^{1/2}} \right) - \frac{2\tau^{1/2}}{\sqrt{\pi}\cos\theta_i} \left(e^{-\left[1 + (\ell_i / L_x)\cos\theta_i\right]^2 / 4\tau} - e^{-1/4\tau} \right) - \frac{1}{\cos\theta_i} \left[\operatorname{erf}\left(\frac{1 + (\ell_i / L_x)\cos\theta_i}{2\tau^{1/2}} \right) - \operatorname{erf}\left(\frac{1}{2\tau^{1/2}} \right) \right] \right\} \tag{2.44}$$

and integrating Eq. (2.4) over the laterals gives

$$\mathrm{SDR}_H = \mathrm{SDR}_T - \frac{L_x}{\ell_T}\sum_{i=1}^{N}\frac{1}{\chi\cos\theta_i}\left\{\mathrm{erf}\left(\frac{1+(\ell_i/L_x)\cos\theta_i}{2\tau^{1/2}}\right)-\mathrm{erf}\left(\frac{1}{2\tau^{1/2}}\right)+ e^{-\left[1+(\ell_i/L_x)\cos\theta_i\right]^2/4\tau}\mathrm{erfcx}\left(\frac{1+2\chi\tau+(\ell_i/L_x)\cos\theta_i}{2\tau^{1/2}}\right)-e^{-1/4\tau}\mathrm{erfcx}\left(\frac{1+2\chi\tau}{2\tau^{1/2}}\right)\right\} \quad (2.45)$$

Eqs. (2.44) and (2.45)—which we refer to as the Theis and Hantush models, respectively—provide special cases to be used in interpreting the full solution for SDR for a radial collector well.

2.2.5. Parameter values and ranges

Unless otherwise noted, the simulations for the following sections use the default values for the dimensionless parameters shown in Table 2.3. The radial collector well has three laterals equal in length and spacing (Fig. 2.1). The default values of χ, κ_z, and γ are taken from Table 1 of Huang et al. (2012), and typical ranges are estimated from previous work. The streambed conductance coefficient $\chi = K'L_x/K_xb'$ can vary over many orders of magnitude because of wide variation in hydraulic conductivities of the streambed (Calver, 2001) and typical aquifer material (Chin, 2006, Table 6.2); values of $\chi > 10^{-4}$ are considered in the analysis. The ratio κ_z of vertical and horizontal conductivities for glacial outwash and fluvial

Table 2.3. Values for the dimensionless parameters. The example from Moore et al. (2012) is Case C at Site 1.

Parameter	Default value	Moore et al. (2012)	Range considered
(θ_1, θ_2, θ_3)	(0, 2π/3, 4π/3)	(π/2, 3π/4, π, 5π/4, 3π/2)	See Fig. 1
Λ_i	1	4.67	0.5-2
χ	2	0.12	$> 10^{-4}$
κ_z	0.1	0.2	10^{-4}-10^{0}
γ	300	167	10^{0}-10^{3}
ρ_x	2	2.03	0.5-4
ρ_z	0.8	0.75	0.35-0.8

deposits can range from 0.01 to 0.5. (Freeze and Cherry, 1979; Todd and Mays, 1980); we consider values between 10^{-4} and 1. Neuman (1972) determined a range of γ of 3 to 1400 using results from the field study of Prickett (1965); these values are consistent with ranges estimated from data in Tables 6.2 and 6.5 in Chin (2006) and estimates of typical saturated thicknesses.

2.3. Results

2.3.1. Effect of hydrogeologic parameters

The streambed conductance coefficient χ affects the SDR much more strongly than the orientation of the laterals (Fig. 2.2). In particular, larger χ, which results from more conductive or thinner streambeds, leads to larger SDR. For infinite χ the full solution approaches the Theis solution in Eq. (2.44). As in the Hantush solution given by Eq. (2.45), the increase in SDR from zero occurs later for cases with smaller streambed conductance coefficient. Also, with smaller χ the SDR for the full model departs from the Hantush solution at a smaller value of SDR. That is, when the resistance from the streambed is larger, gravity drainage supplies more of the flow to the well. For a fixed value of κ_z, the value of SDR in the intermediate stage can decrease so much as χ decreases that the curve appears to have no intermediate stage. However, comparing the full solution and Hantush solution for $\chi = 10^{-4}$ (say) shows that little water from the stream flows to the well during the elastic release stage. The SDR eventually reaches one for all non-zero values of χ, as in the Hantush model.

The ratio of the vertical and horizontal conductivities controls the value of the SDR in the intermediate stage (Fig. 2.3), while the ratio of specific yield and storage coefficient

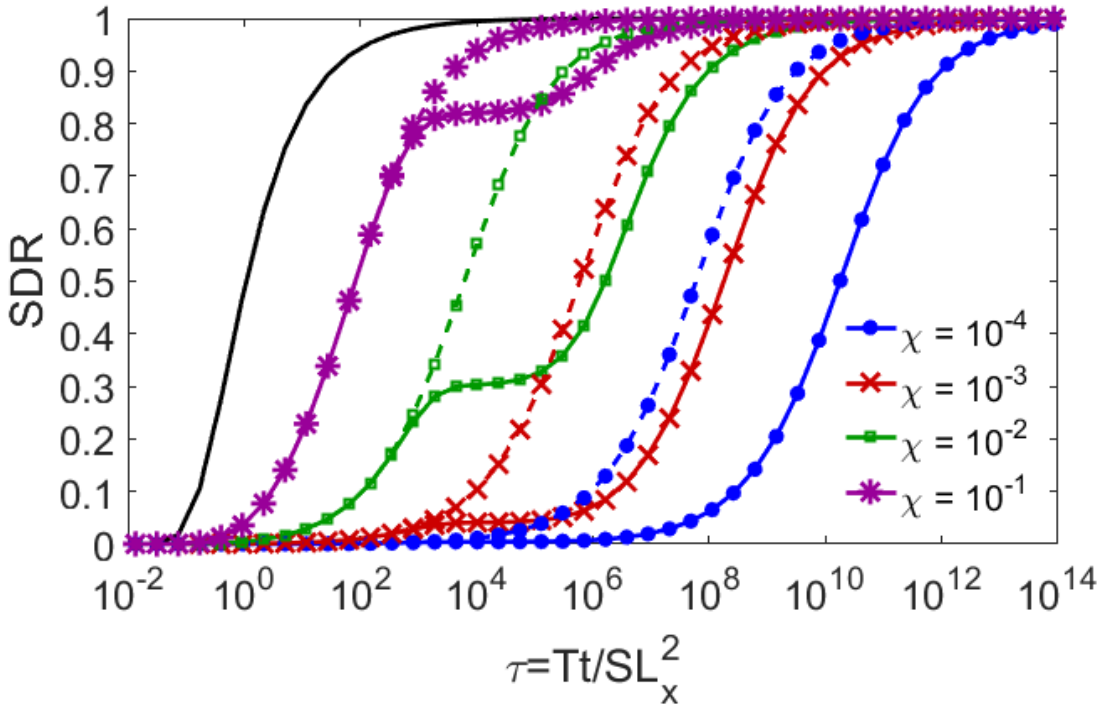

Fig. 2.2. Effect of streambed conductance coefficient on stream depletion rate: solid lines with symbols, current SDR model; dashed lines, Hantush (1965); plain solid line, Theis (1941). The anisotropy parameter is $\kappa_z = 7\times10^{-5}$.

controls the duration (Fig. 2.4). For a fixed value of $\kappa_z = K_z/K_x$, the value of the SDR in the intermediate stage increases with χ (Fig. 2.2), while for a fixed value of χ, it decreases as κ_z increases (Fig. 2.3). When gravity drainage occurs, a larger vertical conductivity increases vertical flow and reduces the fraction of the well's flow that comes from the stream. For the curves in Fig. 2.3 the intermediate stage is apparent, though for $\kappa_z = 1$ SDR ≈ 0 in the intermediate stage and for $\kappa_z = 10^{-4}$ the intermediate stage is close to steady state. Huang et al. (2016a) noted that larger vertical conductivity (with other parameters fixed) leads the SDR to behave as in a confined aquifer and that vertical flow can be neglected. For large κ_z the SDR can be computed with the simpler Hantush model, but the storage

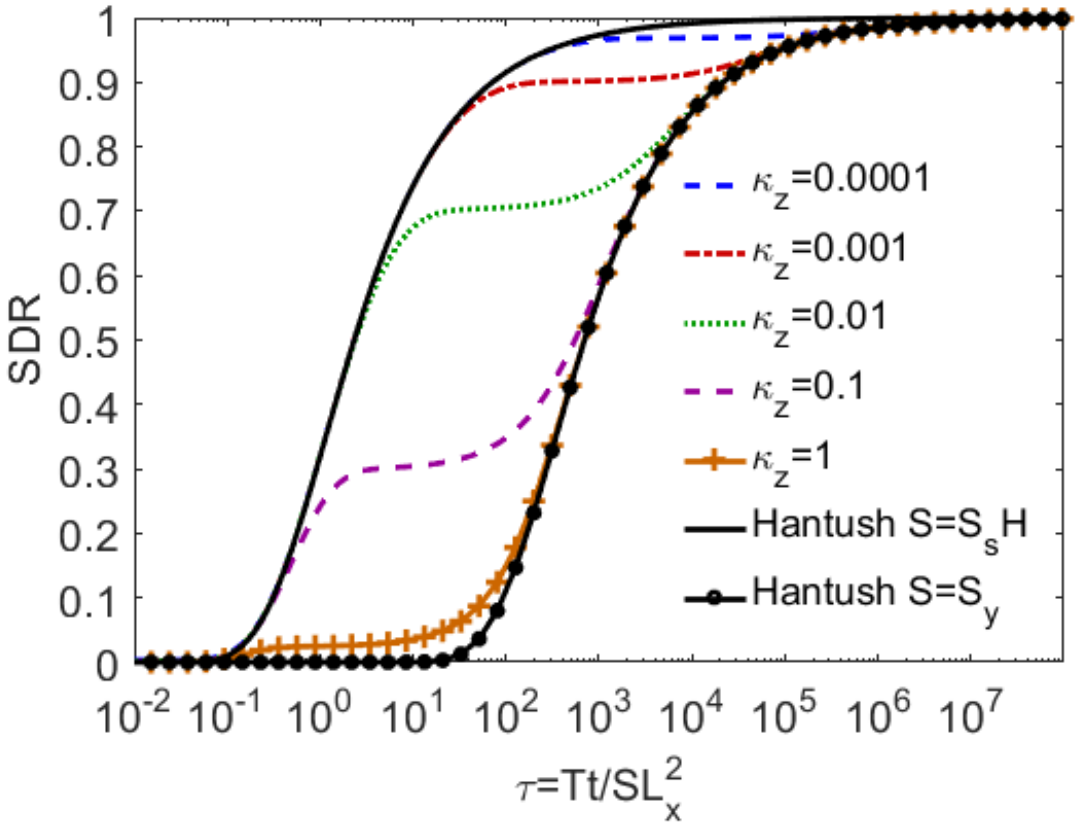

Fig.. 2.3. Effect of anisotropy (i.e., $\kappa_z = K_z/K_x$) on stream depletion rate.

coefficient S must be taken as the specific yield instead of S_sH. The vertical flow is still important when κ_z is large; gravity drainage causes stream depletion to occur later in time.

The duration of the intermediate stage increases as γ, the ratio of the specific yield and storage coefficient, increases (Fig. 2.4). For γ less than $O(10^2)$, the plateau in the SDR curve is not reached, while at $\gamma = 10^3$, it extends over two orders of magnitude in τ. As noted in section 2.1, similar behavior is observed for drawdown caused by a well pumping in an unconfined aquifer with no stream (Neuman, 1975). When the specific yield is much greater than the storage coefficient, the delay between gravity drainage and elastic release increases.

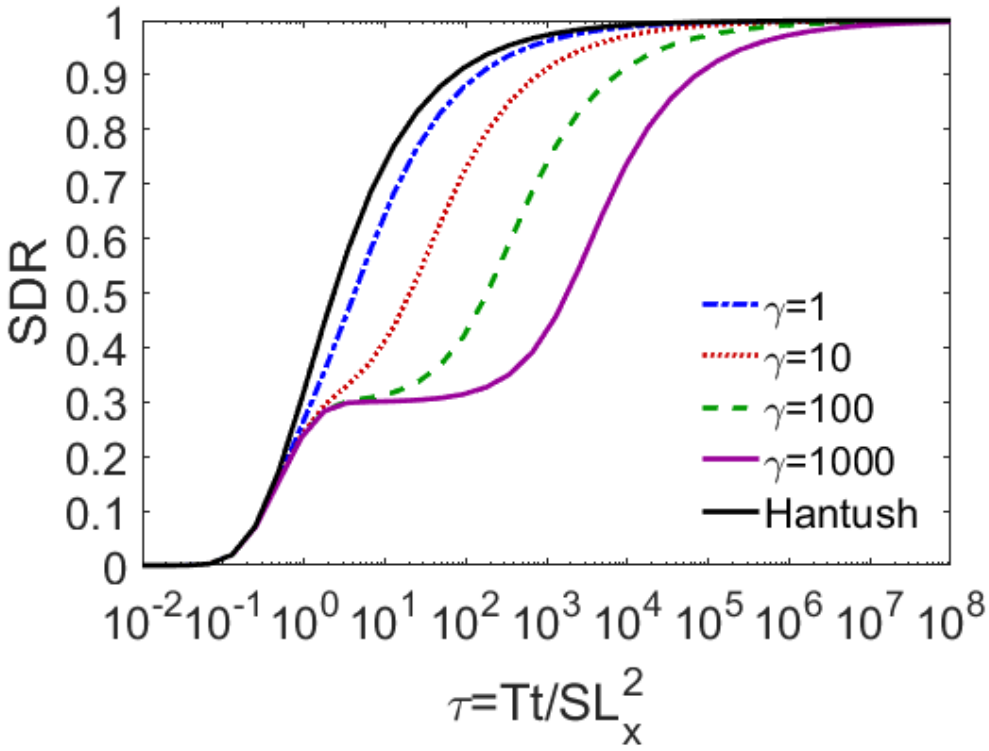

Fig. 2.4. Effect of the ratio $\gamma = S_y/(S_sH)$ on stream depletion rate.

Also, when the specific yield (and γ) approaches zero, the aquifer behaves as if it were confined, as noted in section 2.2.3.

2.3.2. Effect of well design parameters

The results regarding the effect of lateral configuration are similar to those of Moore et al. (2012) (Fig. 2.5). The SDR is larger for configurations in which more laterals point toward the stream, and beyond a certain time, the effect of the configuration is small. In the intermediate stage, SDR for case (b) (streamward laterals) exceeds the SDR for case (a) (symmetric laterals) by about 0.05 and SDR for case (c) (landward laterals) by about 0.1. Numerical modeling by Moore et al. (2012) of radial collector wells near the Des Moines

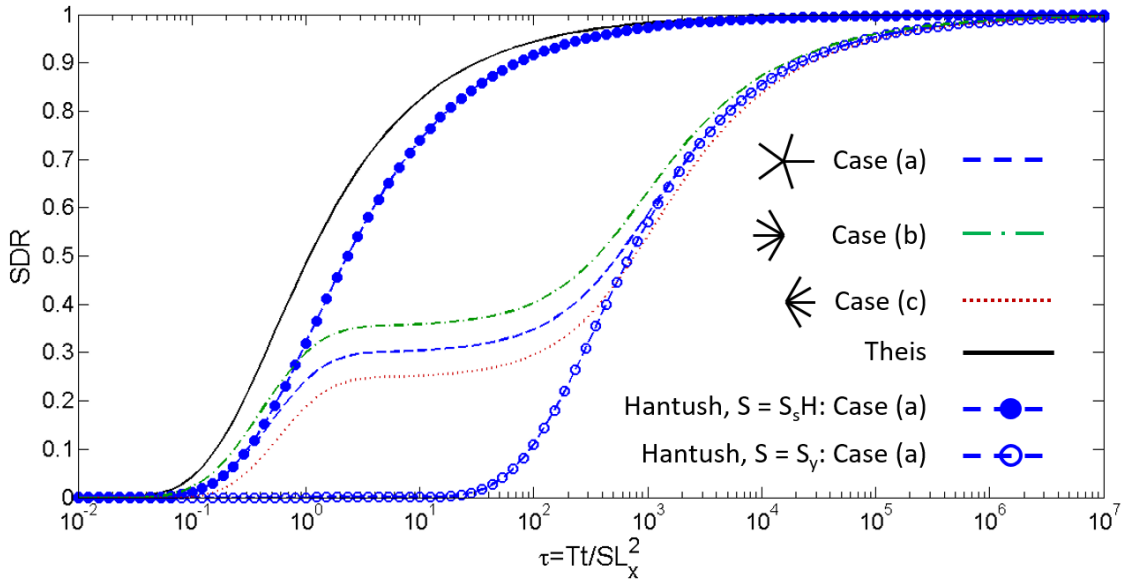

Fig. 2.5. Effect of lateral configuration on stream depletion rate.

River yielded qualitatively similar results: SDR values in their cases that direct laterals streamward exceed SDR from a case with symmetrical laterals, as for the curves in Fig. 2.5.

Longer laterals, measured by an increase in the normalized lateral length $\Lambda = \ell/H$, produce only a slight increase in SDR (Fig. 2.6). The effect of Λ is largest during the early stages of the SDR's evolution. Still, even when the laterals are four times longer, the SDR in Fig. 2.6 increases by at most 0.05. One might expect a larger increase in SDR when Λ is larger because some of the laterals are closer to the stream; however, the effect is offset somewhat by distributing the flow to the well over a greater total lateral length. As the laterals become shorter and as time and the horizontal scale of the cone of depression increase, the SDR of the radial collector well approaches the SDR of a point sink, computed

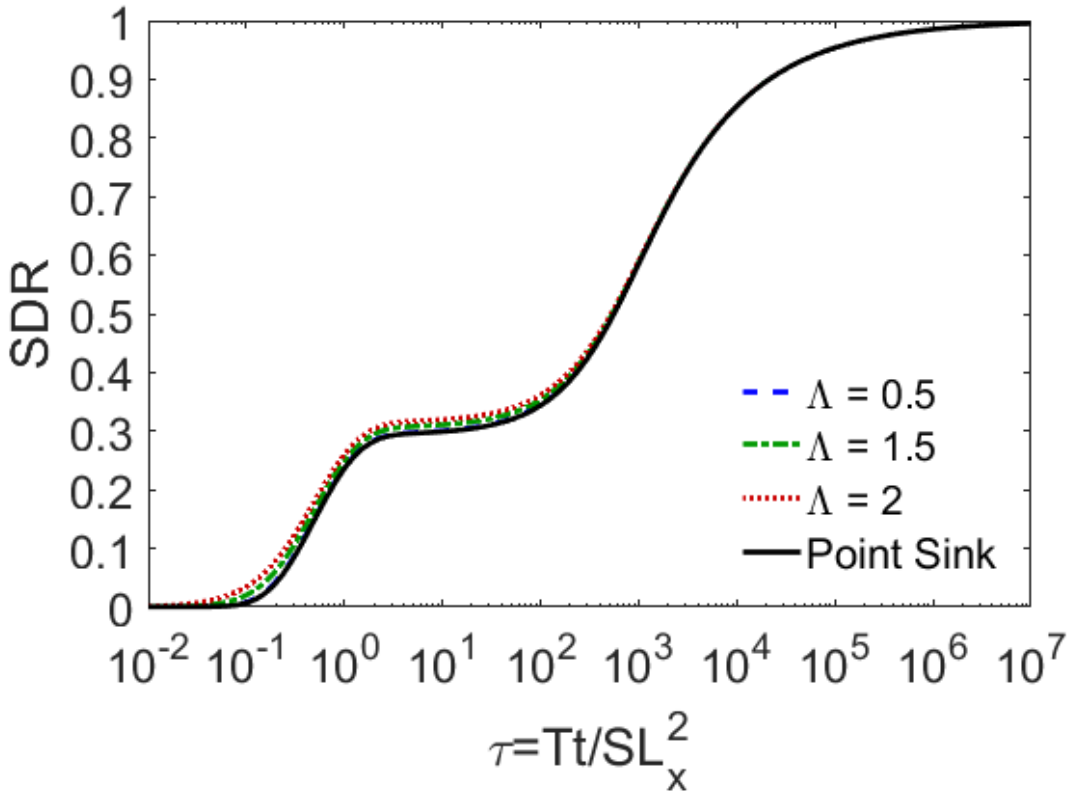

Fig. 2.6. Effect of normalized lateral length $\Lambda = \ell_i/H$ on stream depletion rate. Lateral configuration (a) in Fig. 2.5 is used.

with Eq. (2.37). In fact for $\Lambda = 0.5$, the SDR is indistinguishable from that of a point sink over the entire evolution.

The stream depletion rate is larger when the caisson is closer to the stream, as measured by the aspect ratio $\rho_x = L_x/H$ (Fig. 2.7). The HTY scaling in Eq. (2.13) and their solution show that the horizontal scale of the cone of depression is the aquifer thickness H rather than the distance L_x between the caisson and the stream. Therefore, the aspect ratio ρ_x measures relative distance from the stream because an increase in L_x or decrease in H means the cone of depression takes longer to reach the stream. As a result, for smaller ρ_x the total flow from the stream is larger, and the initial increase in SDR, the intermediate stage, and steady state are reached earlier—that is, at smaller values of t_D.

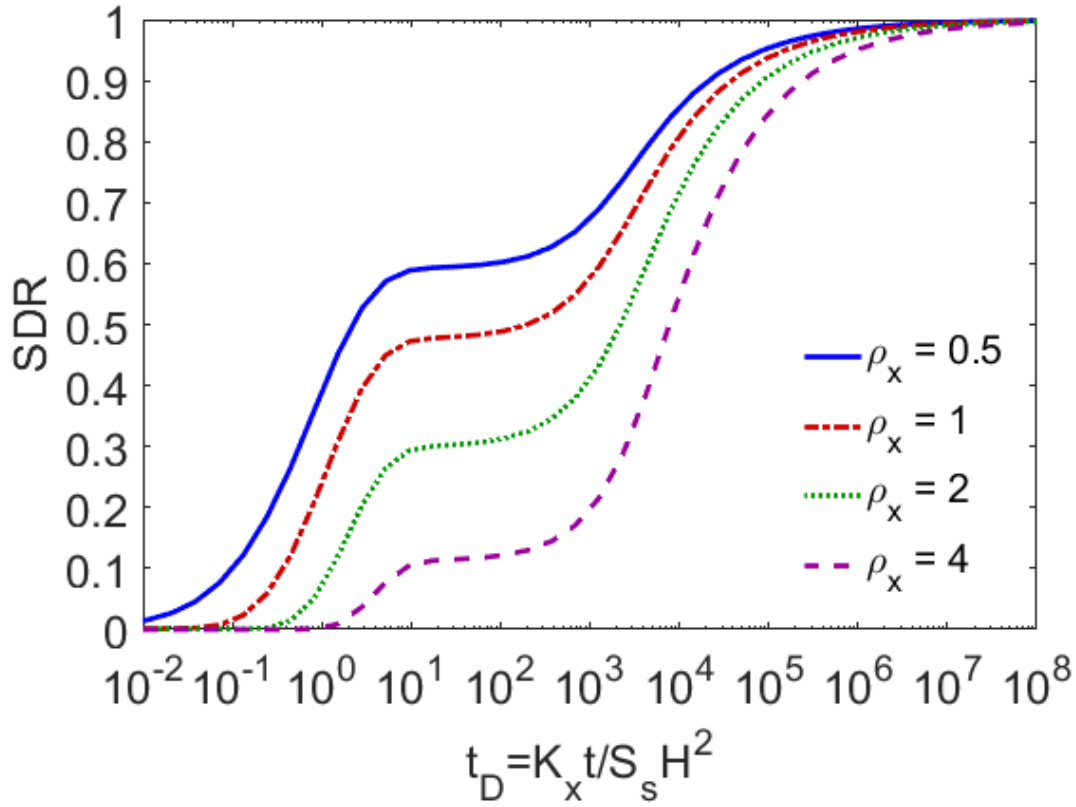

Fig. 2.7. Effect of the aspect ratio $\rho_x = L_x/H$ on stream depletion rate. The SDR is plotted against t_D rather than τ because the interpretation is simpler, as discussed in section 2.4.1.

Stream depletion rate is also larger when the laterals are deeper in the aquifer (Fig. 2.8). The SDR does not depend strongly on $\rho_z = L_z/H$ before or after the intermediate stage, but during the intermediate stage the SDR for $\rho_z = 0.8$ is about 0.1 higher than the SDR for $\rho_z = 0.35$ when $\kappa_z = 0.1$. The increase in flow from the stream results from the larger potential gradient of hydraulic head when the laterals are deeper in the aquifer. When κ_z decreases, the SDR in the intermediate stage increases, as in Fig. 2.3, and the effect of the vertical position of the laterals becomes larger. The decreased vertical flow not only increases the fraction of the well's flow that come from the stream but also magnifies the differences caused by the vertical position. The dependence on lateral depth and vertical hydraulic

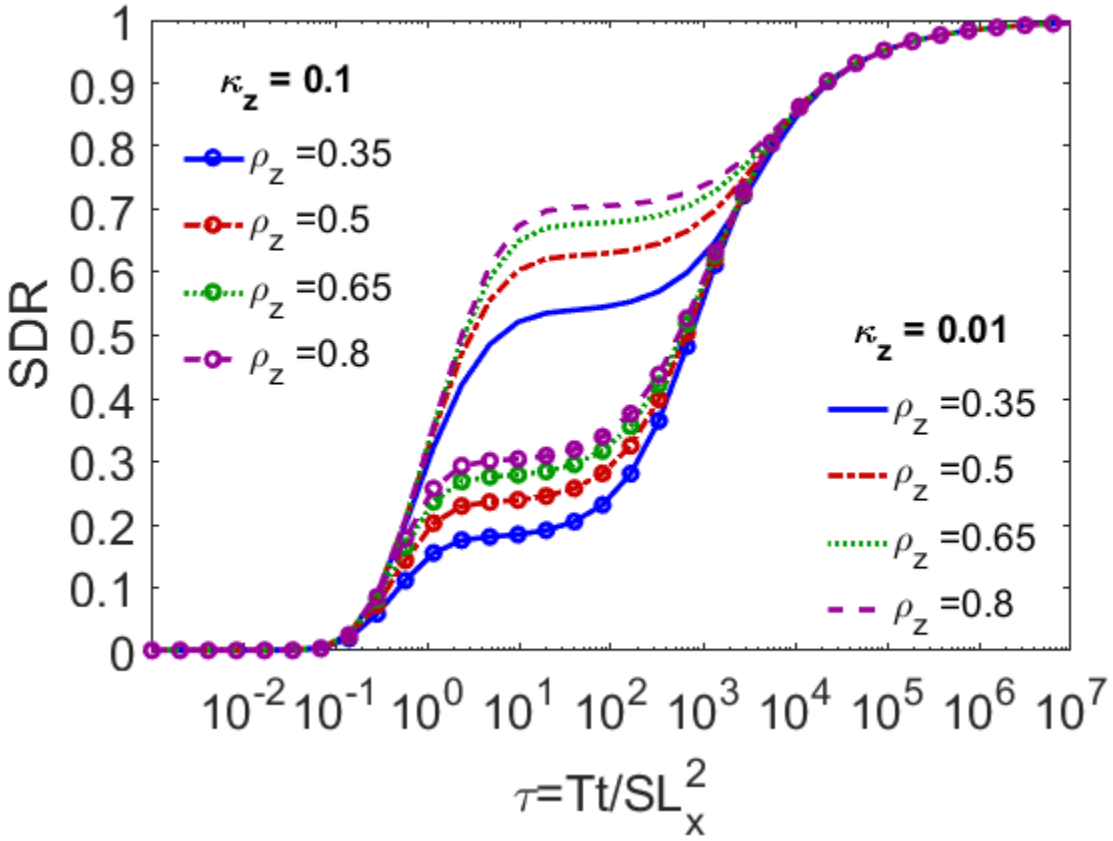

Fig. 2.8. Effect of the ratio $\rho_z = L_z/H$ on stream depletion rate. The curves are plotted for two values of the anisotropy parameter: $\kappa_z = 0.01$ and $\kappa_z = 0.1$.

conductivity for a semi-infinite aquifer is consistent with the calculations of Huang et al. (2016a) for an aquifer bounded by two streams and two no-flow boundaries. The implications of these results and others involving the position and configuration of the well are discussed in section 2.4.3.

2.4 Discussion

2.4.1. Choice of dimensionless parameters

Even in this idealized model of a radial collector well near a river, understanding what affects and controls the stream depletion rate is complicated because the flow from the stream depends on thirteen parameters and variables. The dimensional analysis leading to Eq.

(2.2) simplifies the problem by showing that for small pumping rates (i.e., $\varepsilon = Q/K_xH^2 << 1$ as assumed for this problem) the SDR can be expressed as a function of eight dimensionless parameters, and the analysis in section 2.3 evaluates the effect of each parameter on the SDR systematically. This large number of parameters and the ability to recast them by combining dimensionless groups in different ways leads to some formulations being more informative than others.

The main factor that influences the choice of dimensionless parameters is the length scale of changes in the horizontal direction. For an aquifer bounded by two streams and two impermeable boundaries, the length scale is the distance between the caisson and the stream (Huang et al., 2014, 2016a). However, as noted in the discussion of Fig. 2.7, for a semi-infinite aquifer the aquifer thickness H controls the scale of changes in the horizontal direction (Huang et al., 2012). The ratio of terms in Eq. (2.7) is related to $\alpha = -K'H/K_xb'$, and the parameter α appears naturally in the HTY solution. In contrast, in the Hantush model for a confined aquifer, changes in the horizontal direction occur on the length scale L_x, and the parameter $\chi = K'L_x/K_xb'$ appears in the solution. Therefore, the comparison with the Hantush model in Fig. 2.2 focuses on χ. HTY discussed the conductance of the streambed in terms of the ratio K'/K_x. Although for a fixed value of $\rho_x = L_x/H$ any of the three parameters can be used to describe the effects of the streambed, by including the thickness of the streambed, the parameters α and χ emphasize its importance in determining the streambed's conductance.

The difference in horizontal length scales between the semi-infinite and bounded aquifers affects the parameter measuring differences between vertical and horizontal hydraulic conductivities. For the semi-infinite aquifer in the present analysis and in HTY, the

key parameter measuring the effects of anisotropy is $\kappa_z = K_z/K_x$, while for the bounded aquifers of Huang et al. (2014, 2016a), the parameter involves the square of the ratio of horizontal and vertical length scales, such as $K_z L_x^2 / K_x H^2$ in our notation. Huang et al. (2016a) argued that the horizontal length scale in this parameter should be the smallest distance between the stream and the end of a lateral. In any case, the parameter for measuring the effect of the vertical-horizontal anisotropy arises naturally by comparing the magnitudes of the first and third terms in Eq. (2.5).

A similar choice of scales is involved with the dimensionless time. In the scaling and solution of HTY the time variable $t_D = Tt/SH^2$ arises. However, because the aquifer thickness does not appear explicitly in the solutions for confined aquifers, the comparisons to the Theis and Hantush models in section 2.3 require the time variable $\tau = Tt / SL_x^2$, and for consistency τ is used in the discussion of the effects of most of the other parameters. The exception is the aspect ratio $\rho_x = L_x/H$ (Fig. 2.7), for which plotting SDR against t_D simplifies the interpretation. Although for the cases of Theis (1941) and Hantush (1965) the time scale $L_x^2 / (T / S)$ emerges from the one-dimensional diffusion equation governing the flow—where T/S is the hydraulic diffusivity (Freeze and Cherry, 1979, p. 61), in the current case with multi-dimensional flow, the time scale $H^2/(T/S)$ is more appropriate.

2.4.2. Merits of the present approach

The expression for stream depletion rate presented here has some advantages over previously reported results. The solution in Eq. (2.42) satisfies analytical limits and matches the Theis and Hantush models for simpler cases, as shown in Figs. 2.2, 2.3, and 2.5. The present solution is much simpler to compute than that of HTY because, as noted in section 2.2, Eq.

(2.42) requires one numerical integration, while the original version of HTY requires five: two for inverting transforms, two for integrating over the area between the streambed and aquifer, and one for accounting for sinks over the length of the laterals. Furthermore, the two integrals in the inverse transforms and the integral over *y* are improper. Therefore, computing SDR with the HTY approach requires significant care and computational effort. These demands motivated Huang et al. (2016a) to consider a radial collector well in an aquifer bounded by two streams and two no-flow boundaries; in that case, the SDR can be expressed in terms of double infinite sums, which are simpler to compute accurately than multiple integrals. Huang et al. (2016a) note that the solution for the bounded case matches the solution of HTY for small time, but after the no-flow boundaries and second stream affect the flow, the two solutions diverge.

Like all models, the approach here is limited by its assumptions, including the fully penetrating, straight stream and homogeneous aquifer and streambed. We followed HTY in invoking the assumption that a partially-penetrating stream can be approximated by a fully-penetrating stream if $\rho_x > 1.5$ (Jacob, 1950). Spalding and Khaleel (1991) used a two-dimensional numerical model to compute the SDR for a vertical well near a partially-penetrating stream, and they compared to predictions from analytical solutions, including those of Theis (1941) and Hantush (1965). Although ignoring disconnection between the stream and water table led to only small errors, treating the stream as fully-penetrating caused larger errors (e.g., 20% after 58.5 d of pumping) even though the distance from the well to the stream was 2.5 times the aquifer thickness. The effect of partial penetration can be considered by extending the model of Hunt (1999) for a zero-width stream or the model of Butler et al. (2001) for a finite-width stream.

The conditions under which assuming homogeneity is acceptable can be assessed with the work of Lackey et al. (2015), who modeled pumping near a sinusoidally meandering stream with heterogeneous conductivity in the streambed—high K' in the pools (bends) and low K' in the riffles (straight sections) during high flow and the opposite during low flow. The heterogeneity of the streambed conductivity is less important in three conditions. If the distance L_x between the well and the stream is larger than the scale of the heterogeneity (e.g., the wavelength of the meandering), then differences in K' are averaged over the cone of depression in the stream depletion process. Also, Lackey et al. (2015) defined ranges over which the SDR was sensitive to K'; outside those ranges, the conductance can be taken as homogeneous. The calculations of Lackey et al. (2015) show that the importance of heterogeneity depends on the target value of SDR; as it decreases—for example, because of stricter limitations on stream depletion, differences between cases with homogeneous streambeds and cases with heterogeneous streambeds become smaller.

2.4.3. Implications for designing and operating radial collector wells

As noted in section 2.4.2, one of the benefits of a systematic analysis of the parameters affecting stream depletion rate is that it can help in the design and operation of a radial collector well. Parameters affecting SDR the most include properties of the streambed, anisotropy of the aquifer, and the position of the well, which are represented by χ (or α), κ_z, and ρ_x and shown in Figs. 2.2, 2.3, and 2.7, respectively. However, once a site is chosen, the properties of the aquifer and streambed are set. Of the parameters remaining for design—the horizontal position of the well and the lateral orientation, length, and depth, which are represented by ρ_x, θ_i, Λ_i, and ρ_z and examined in Figs. 2.7, 2.5, 2.6, and 2.8, respectively—

the horizontal position affects the SDR more strongly than the others during unsteady conditions.

Our analysis focuses on the effect of the parameters on stream depletion rate, but other considerations will also affect the choice of values. Orienting the laterals toward the stream increases the SDR (Fig. 2.5), but the orientation and the length of the laterals can be constrained by subsurface obstacles such as foundations of structures or boulders and other geologic features. Although Moore et al. (2012) stated that increasing the lateral length would reduce hydraulic interference between laterals, calculations with Eq. (2.42) show the SDR to increase only slightly with longer laterals at times before steady state (Fig. 2.6). Still, the reduced velocity into longer laterals will reduce clogging and required maintenance. The depth dependence of the equivalent 2D entry resistance computed by Haitjema et al. (2010) suggests placing the laterals at mid-depth (Moore et al., 2012). Because raising the laterals increased the head in the caisson by only a small amount, Moore et al. (2012) recommended choosing the lateral elevation to allow sufficient suction head and efficient construction. Our calculations for a homogeneous aquifer indicate that an increased lateral depth increases SDR during unsteady conditions (Fig. 2.8).

Given enough time, a steady state will be reached in which all of the water to the well comes from the stream. The time to steady state, which is proportional to SL_x^2 / T, decreases for smaller distances between the caisson and the stream and for more conductive soils, which have larger transmissivities and smaller storage coefficients. In practice the times to reach steady state can be quite large; in particular, by causing the intermediate stage with constant SDR, vertical flow increases the time to steady state, as illustrated in Fig. 2.2. For example, using the conditions at Site 1 in Moore et al. (2012) in the simpler SDR models

yields times for SDR to reach 95% and 99% of 0.03 d and 0.8 d for the Theis model and 11d and 293 d for the Hantush model. The full model gives times that are orders of magnitude larger: 1900 d for SDR = 0.95 and 49,000 d for SDR = 0.99. For cases in which steady state occurs after a long time, the intermediate stage becomes more important. As shown in Fig. 2.4, for large γ the intermediate stage can last long enough that it acts as a quasi-steady state. In such a case the value of the vertical hydraulic conductivity (or more precisely, the ratio κ_z) is important because it sets the value of the SDR in the intermediate stage (Fig. 3).

2.5 Conclusion

The stream depletion rate for a radial collector well pumping in a homogeneous anisotropic unconfined aquifer near a fully penetrating stream with a low-conductivity streambed was recomputed using the solution of Huang et al. (2012). Dimensional analysis and other arguments showed that for small pumping rates (i.e., $\varepsilon = Q/K_xH^2 << 1$ as assumed for this problem) the SDR can be expressed as a function of eight dimensionless parameters. The effects of these parameters were examined systematically using comparisons with two simpler cases derived from the solutions of Theis (1941) and Hantush (1965). Key conclusions are as follows:

1. While the HTY solution requires five numerical integrations to compute SDR, Eq. (2.42) requires only one. The present solution avoids much of the computational cost and challenges related to computing the integrals accurately.

2. Quantitative values of SDR computed with Eq. (2.42) match the Hantush model for appropriate limiting values of the parameters. In particular, in steady state the SDR is one—that is, the flow through the streambed is equal to the pumping rate of the well.

3. At a given time before steady state, SDR is smaller for smaller streambed conductance coefficient $\chi = K'L_x/K_x b'$. Either χ or $\alpha = -K'H/K_x b'$, defined by HTY, can be used to describe the conductance of the streambed. These two parameters are better than the ratio K'/K_x because they include the thickness b' of the streambed.

4. The value of SDR in the intermediate stage of the evolution decreases as $\kappa_z = K_z/K_x$ increases, and the duration of the intermediate stage increases as $\gamma = S_y/S_s H$ increases.

5. The properties of the streambed, anisotropy of the aquifer, and distance between the well and the stream affect the SDR more strongly than the lateral orientation, length, and depth of the laterals. However, for a selected site, properties of the aquifer and streambed are set, and the other parameters are left for design of the well. Increasing the length and depth of the laterals, reducing the distance between the caisson and the stream, or orienting more laterals toward the stream increases the SDR during unsteady conditions.

References

Appiah-Adjei, E.K., Shu, L.C., Adjei, K.A., Lu, C.P., Deng, M.J., 2012. Interpretation of pumping test with radial collector well using a reservoir model. J. Hydrol. Eng., 17(12): 1397-1407. http://dx.doi.org/10.1061/(asce)he.1943-5584.0000598

Butler, J.J., Zlotnik, V.A., Tsou, M.S., 2001. Drawdown and stream depletion produced by pumping in the vicinity of a partially penetrating stream. Ground Water, 39(5): 651-659. http://dx.doi.org/10.1111/j.1745-6584.2001.tb02354.x

Calver, A., 2001. Riverbed permeabilities: information from pooled data. Ground Water, 39(4): 546-553. http://dx.doi.org/10.1111/j.1745-6584.2001.tb02343.x

Chin, D.A., 2006. Water-Resources Engineering. Pearson Prentice Hall, Upper Saddle River, NJ, 962 pp.

Freeze, R.A., Cherry, J.A., 1979. Groundwater. Prentice-Hall, Englewood Cliffs, NJ, 604 pp.

Glover, R.E., Balmer, G.G., 1954. River depletion resulting from pumping a well near a river. EOS Trans. Am. Geophys. Union, 35(3): 468-470.

Haitjema, H., Kuzin, S., Kelson, V., Abrams, D., 2010. Modeling flow into horizontal wells in a Dupuit-Forchheimer model. Ground Water, 48(6): 878-883. http://dx.doi.org/10.1111/j.1745-6584.2010.00694.x

Hantush, M.S., 1965. Wells near streams with semipervious beds. J. Geophys. Res., 70(12): 2829-2838. http://dx.doi.org/10.1029/JZ070i012p02829

Hildebrand, F.B., 1976. Advanced Calculus for Applications. Prentice-Hall, Englewood Cliffs, NJ, 733 pp.

Huang, C.S., Tsou, P.R., Yeh, H.D., 2012. An analytical solution for a radial collector well near a stream with a low-permeability streambed. J. Hydrol., 446: 48-58. http://dx.doi.org/10.1016/j.jhydrol.2012.04.028

Huang, C.-S., Lin, W.-S., Yeh, H.-D., 2014. Stream filtration induced by pumping in a confined, unconfined or leaky aquifer bounded by two parallel streams or by a stream and an impervious stratum. J. Hydrol., 513: 28-44. http://dx.doi.org/10.1016/j.jhydrol.2014.03.039

Huang, C.S., Chen, J.J., Yeh, H.D., 2016a. Approximate analysis of three-dimensional groundwater flow toward a radial collector well in a finite-extent unconfined aquifer. Hydrology and Earth System Sciences, 20(1): 55-71. http://dx.doi.org/10.5194/hess-20-55-2016

Huang, C.S., Tsou, P.R., Yeh, H.D., 2016b. Corrigendum to "An analytical solution for a radial collector well near a stream with a low-permeability streambed" [J. Hydrol. 446-447 (2012) 48-58]. J. Hydrol., 542: 1002-1002. http://dx.doi.org/10.1016/j.jhydro1.2016.09.013

Hunt, B., 1999. Unsteady stream depletion from ground water pumping. Ground Water, 37(1): 98-102. http://dx.doi.org/10.1111/j.1745-6584.1999.tb00962.x

Hunt, B., 2003. Unsteady stream depletion when pumping from semiconfined aquifer. J. Hydrol. Eng., 8(1): 12-19. http://dx.doi.org/10.1061/(asce)1084-0699(2003)8:1(12)

Hunt, B., 2008. Stream depletion for streams and aquifers with finite widths. J. Hydrol. Eng., 13(2): 80-89. http://dx.doi.org/10.1061/(asce)1084-0699(2008)13:2(80)

Hunt, B., 2009. Stream depletion in a two-layer leaky aquifer system. J. Hydrol. Eng., 14(9): 895-903. http://dx.doi.org/10.1061/(asce)he.1943-5584.0000063

Jacob, C.E., 1950. Engineering Hydraulics. Wiley, New York, NY.

Jasperse, J., 2009. Planning, design and operations of Collector 6, Sonoma County Water Agency. In: Ray, C., Shamrukh, M. (Eds.), Riverbank Filtration for Water Security in Desert Countries. NATO Science for Peace and Security Series C-Environmental Security, pp. 169-202. http://dx.doi.org/10.1007/978-94-007-0026-0_11

Jenkins, C.T., 1968. Techniques for computing rate and volume of stream depletion by wells. Ground Water, 6(2): 37-46.

Lackey, G., Neupauer, R.M., Pitlick, J., 2015. Effects of streambed conductance on stream depletion. Water, 7(1): 271-287. http://dx.doi.org/10.3390/w7010271

Moore, R., Kelson, V., Wittman, J., Rash, V., 2012. A modeling framework for the design of collector wells. Ground Water, 50(3): 355-366. http://dx.doi.org/10.1111/j.1745-6584.2011.00850.x

Neuman, S.P., 1972. Theory of flow in unconfined aquifers considering delayed response of the water table. Water Resour. Res., 8(4): 1031-1045. http://dx.doi.org/10.1029/WR008i004p01031

Neuman, S.P., 1975. Analysis of pumping test data from aniostropic unconfined aquifers considering delayed gravity response. Water Resour. Res., 11(2): 329-342. http://dx.doi.org/10.1029/WR011i002p00329

Prickett, T., 1965. Type-curve solution to aquifer tests under water-table conditions. Ground Water, 3(3): 5-14.

Schafer, D.C., 2006. Use of aquifer testing and groundwater modeling to evaluate aquifer/river hydraulics at Louisville Water Company, Louisville, Kentucky, USA. In: Hubbs, S.A. (Ed.), Riverbank Filtration Hydrology. NATO Science Series IV Earth and Environmental Sciences. Springer, Dordrecht, pp. 179-198.

Sedghi, M.M., Samani, N., Sleep, B., 2012. Boundary depletion rate and drawdown in leaky wedge-shaped aquifers. Hydrol. Process., 26(20): 3101-3113. http://dx.doi.org/10.1002/hyp.8338

Spalding, C.P., Khaleel, R., 1991. An evaluation of analytical solutions to estimate drawdowns and stream depletions by wells. Water Resour. Res., 27(4): 597-609. http://dx.doi.org/10.1029/91wr00001

Sun, D.M., Zhan, H.B., 2007. Pumping induced depletion from two streams. Adv. Water Resour., 30(4): 1016-1026. http://dx.doi.org/10.1016/j.advwatres.2006.09.001

Theis, C.V., 1941. The effect of a well on the flow of a nearby stream. Transactions-American Geophysical Union, 22: 734-738.

Todd, D.K., Mays, L.W., 1980. Groundwater Hydrology. John Wiley & Sons, New York, 535 pp.

Tsou, P.R., Feng, Z.Y., Yeh, H.D., Huang, C.S., 2010. Stream depletion rate with horizontal or slanted wells in confined aquifers near a stream. Hydrology and Earth System Sciences, 14(8): 1477-1485. http://dx.doi.org/10.5194/hess-14-1477-2010

Turco, M.J., Buchmiller, R.C., 2004. Simulation of ground-water flow in the Cedar River alluvial aquifer flow system, Cedar Rapids, Iowa: U.S. Geological Survey Scientific Investigations Report 2004-5130, 39 pp.

Ward, N.D., Lough, H., 2011. Stream depletion from pumping a semiconfined aquifer in a two-layer leaky aquifer system. J. Hydrol. Eng., 16(11): 955-959. http://dx.doi.org/10.1061/(asce)he.1943-5584.0000382

Yeh, H.D., Chang, Y.C., Zlotnik, V.A., 2008. Stream depletion rate and volume from groundwater pumping in wedge-shape aquifers. J. Hydrol., 349(3-4): 501-511. http://dx.doi.org/10.1016/j.jhydrol.2007.11.025

Yeh, H.D., Huang, C.S., Chang, Y.C., Jeng, D.S., 2010. An analytical solution for tidal fluctuations in unconfined aquifers with a vertical beach. Water Resour. Res., 46. http://dx.doi.org/10.1029/2009wr008746

Zlotnik, V.A., 2004. A concept of maximum stream depletion rate for leaky aquifers in alluvial valleys. Water Resour. Res., 40(6). http://dx.doi.org/10.1029/2003wr002932

Zlotnik, V.A., Tartakovsky, D.M., 2008. Stream depletion by groundwater pumping in leaky aquifers. J. Hydrol. Eng., 13(2): 43-50. http://dx.doi.org/10.1061/(asce)1084-0699(2008)13:2(43)

Zlotnik, V.A., Huang, H., Butler, J.J., 1999. Evaluation of stream depletion considering finite stream width, shallow penetration, and properties of streambed sediments, in *Proc. of Water 99 Joint Congress*, July 6-8, 1999, Brisbane, Australia, pp. 221-226.

Supplemental material

```
SDR = compute_SDR(1E4,0.1,7E-5,[1,1,1],[0,2*pi/3,4*pi/3],300,2,-0.8)

function SDR = compute_SDR(tau,chi,kappaz,Lambda,theta,gam,rhox,rhoz)
%  COMPUTE_SDR   Compute the stream depletion rate for a radial collector
well
%
%  Cynthia Maroney and Chris Rehmann

%  Set constants

   Nt      = 20;                     %  Number of terms to sum for PhiN

%  Define variables from the main dimensionless variables in Table 1

   N       = length(Lambda);         %  Number of laterals
   alpha   = -chi/rhox;              %  Alternate form of streambed
conductance coefficient
   LambdaT = sum(Lambda);            %  Total length of laterals
normalized by aquifer thickness
   x0D     = rhox;                   %  Dimensionless distance from
stream to caisson
   z0D     = -rhoz;                  %  Dimensionless vertical position
of laterals
   tD      = rhox^2*tau;             %  Alternate form of dimensionless
time

%  Compute integrals in equation (42)

   intPhi0R = NaN*ones(N,1);
   intPhinR = NaN*ones(N,Nt);
   for i = 1:N
      intPhi0R =
quadgk(@(omega)Phi0R(omega,gam,kappaz,alpha,tD,x0D,z0D,Lambda(i),theta(i))
,0,Inf);
      for n = 1:Nt
         intPhinR(i,n) =
quadgk(@(omega)PhinR(omega,gam,kappaz,alpha,tD,x0D,z0D,Lambda(i),theta(i),
n),0,Inf);
      end
   end

%  Compute SDR

 SDR = 1 + (2*alpha/(pi*LambdaT))*sum(intPhi0R);
%     SDR = 1 + (2*alpha/(pi*LambdaT))*sum(sum(intPhinR,2));
%    SDR = 1 + (2*alpha/(pi*LambdaT))*sum(intPhi0R+sum(intPhinR,2));
%  Eq. 42 of paper

function intgd = Phi0R(omega,gam,kappaz,alpha,tD,x0D,z0D,Lam,theta)
%
%  PHI0R  Product of Phi0 and R
```

```
%
%     Cynthia Maroney and Chris Rehmann, 12-27-16

%  Compute zeta0

   zeta0 = NaN*ones(size(omega));
   zetap = (-
kappaz+sqrt(kappaz^2+4*gam^2*kappaz*omega.^2))/(2*gam*kappaz);         %
Initial guesses--see HTY
   for i = 1:length(omega);
       zeta0(i) = fzero('fzeta0',zetap(i)+1e-9,[],omega(i),kappaz,gam);
   end
   zeta0 = abs(zeta0);
%    [omega',zeta0']
%  Compute integrand

   mu0   = zeta0.^2*kappaz-omega.^2
%    [omega',mu0']
   Phi0  =
2*gam*cosh(zeta0*(1+z0D)).*exp(mu0*tD)./(zeta0.*((2*gam+1).*zeta0*kappaz.*
cosh(zeta0)+(gam*mu0+kappaz).*sinh(zeta0)));
%    [omega',Phi0']

   R     = -(alpha*(cos(omega*x0D)-
cos(omega*(Lam*cos(theta)+x0D)))+omega.*(sin(omega*x0D)-
sin(omega*(Lam*cos(theta)+x0D)))) ...
           ./(cos(theta)*(omega.^2+alpha^2));
   intgd = Phi0.*R;
%    zindx = find(om == 0);
%    if ~isempty(zindx)
%        intgd(zindx) = (1-alpha*x0D)/alpha^2;
%    end

   nandx = find(isnan(intgd));
   if ~isempty(nandx)
       intgd(nandx) = 0;
   end

function intgd = PhinR(omega,gam,kappaz,alpha,tD,x0D,z0D,Lam,theta,n)

%  PHINR  Product of Phin and R
%
%     Cynthia Maroney and Chris Rehmann, 12-27-16

%  Compute zetan

   zetan = NaN*ones(size(omega));
   zetap = ((2*n-1)*pi/2)*ones(size(omega));
%  Initial guesses--see HTY
   for i = 1:length(omega);
       zetan(i) = fzero('fzetan',zetap(i)+1e-9,[],omega(i),kappaz,gam);
   end
   zetan = abs(zetan);
```

```
%  Compute integrand

   mun   = zetan.^2*kappaz+omega.^2;
   Phin  = -2*gam*cos(zetan*(1+z0D)).*exp(-
mun*tD)./(zetan.*((2*gam+1).*zetan*kappaz.*cos(zetan)+(kappaz-
gam*mun).*sin(zetan)));
   R     = -(alpha*(cos(omega*x0D)-
cos(omega*(Lam*cos(theta)+x0D)))+omega.*(sin(omega*x0D)-
sin(omega*(Lam*cos(theta)+x0D)))) ...
           ./(cos(theta)*(omega.^2+alpha^2));
   intgd = Phin.*R;
%    zindx = find(om == 0);
%    if ~isempty(zindx)
%        intgd(zindx) = (1-alpha*x0D)/alpha^2;
%    end

   nandx = find(isnan(intgd));
   if ~isempty(nandx)
       intgd(nandx) = 0;
   end

function y = fzeta0(zeta0,omega,kappaz,gam)
%  FZETA0   Equation (26) with xi = 0
%  Use the tanh version because the exp and sinh/cosh versions become
large

y = zeta0*tanh(zeta0)+gam*(kappaz*zeta0.^2-omega^2)/kappaz;

function y = fzetan(zetan,omega,kappaz,gam)

y = zetan.*sin(zetan)+cos(zetan)*gam.*(zetan.^2+omega.^2/kappaz);
```

CHAPTER 3: FLOW TO A PARTIALLY PENETRATING VERTICAL WELL IN AN UNCONFINED AQUIFER NEAR A STREAM

A paper to be submitted to the *Journal of Hydrology*

Cynthia Maroney and Chris Rehmann

Abstract

The flow and stream depletion rate are computed for a vertical well that partially penetrates a semi-infinite, anisotropic, homogeneous, unconfined aquifer adjacent to a stream. The stream fully penetrates the aquifer and has a streambed with lower conductivity. The stream depletion rate (SDR) is developed using the method in Maroney and Rehmann (2017, *J. Hydrol*.) and can be expressed in terms of one improper integral. SDR increases as the degree of penetration decreases and as the depth of the well increases. The steady state drawdown is symmetric about the middle of a well located in the center of the aquifer. The intermediate stage drawdown for a partially penetrating well located in the middle of the aquifer is largest at the center of the well. The stream provides a source of water to reduce hydraulic gradients near the top and bottom of the aquifer. The theoretical model provides quantitative guidance for managing drawdown and SDR in practical applications, such as supplying water, dewatering, and remediating contaminated sites.

3.1 Introduction

Understanding the flow of groundwater and surface water to wells located near a stream in an unconfined alluvial aquifer is important for achieving designs for maximizing water production, dewatering, or remediating aquifers. The development of drawdown for a well located next to a stream in an unconfined aquifer is influenced by vertical and horizontal

flow within the aquifer and flow of surface water into the groundwater system that occurs as a result of pumping. Vertical wells may be screened only in small portions of the aquifer to prevent the water table from moving below the top of the well screen or to focus on collecting contaminants, and calculations are needed to determine how the length and location of the well screen affect the flow of water to the well. This chapter builds on previous work summarized in Table 3.1 for evaluating saturated flow to wells in confined, leaky and unconfined aquifers and Table 2 of Maroney and Rehmann (2017) for stream depletion rate (SDR), or the fraction of the well's flow that comes from the stream. Presented here is a model for flow to a vertical well adjacent to a stream and with a screen section that does not cover the saturated thickness of the unconfined aquifer. In particular, this chapter evaluates how flow to a vertical well in an unconfined aquifer is influenced by vertical flow in the aquifer, the length of the screen relative to the saturated thickness of the aquifer, and the presence of a stream with a reduced permeability streambed.

The concept of delayed response for flow to a well in an unconfined aquifer was extended by Neuman (1972, 1973) in the three-dimensional analytical model for a homogeneous, anisotropic, unconfined aquifer that models the water table as a free surface allowing for vertical flow. In this model aquifer the vertical wells are screened through the entire saturated thickness and have a constant discharge. Flow to a well initially comes from release of water from storage by aquifer compression and water expansion, and with time, gravity drainage contributes to and eventually dominates the flow producing the delayed response observed in time-drawdown curves. Vertical hydraulic conductivity K_z, storativity S_s and specific yield S_y control the level and duration of the intermediate stage of the evolution of drawdown and the development of SDR. With all other parameters fixed

Table 3.1. References for analytical solutions for saturated flow to wells.

Reference	Well Type	Aquifer Type	Stream	Other Features
Theis (1935)	Full vertical	Confined	None	
Hantush and Jacob (1955)	Full vertical	Leaky	None	Overlying aquitard
Boulton (1954)	Full vertical	Unconfined-no vertical flow	None	Overlying aquitard
Hantush and Papadopoulos (1962)	Radial collector well	Vertical flow	Constant head	
Hantush (1964)	Full vertical	Confined	None	
Hantush (1965)	Full vertical	Unconfined-vertical flow	Streambed	
Cooley and Case (1973)	Full vertical	Leaky	None	Unsaturated flow
Neuman (1972, 1973)	Full vertical	Unconfined-vertical flow	None	
Neuman (1974)	Full vertical, Partial	Unconfined-vertical flow	None	
Murdoch (1994)	Interceptor trench	Confined	None	
Hunt (1999)	Full vertical	Unconfined- no vertical flow	Surface source: zero width	
Kawecki (2000)	Horizontal	Confined Unconfined	None	Approximation of vertical flow
Zhan and Cao (2000)	Horizontal	Confined	None	
Butler et al. (2001)	Full vertical	Unconfined-no vertical flow	Surface source: finite width	Finite width aquifer
Zhan et al. (2001)	Horizontal	Confined	None	
Fox et al. (2002)	Full vertical	Unconfined-no vertical flow	Surface source: finite width	
Zhan and Zlotnik (2002)	Slanted; partial	Unconfined-vertical flow	None	

Table 3.1. continued

Reference	Well Type	Aquifer Type	Stream	Other Features
Hunt (2003)	Full vertical	Leaky	Surface source: zero width	Stream in aquitard
Kompani-Zare et al. (2005)	Horizontal	Confined	None	
Sun and Zhan (2006)	Horizontal	Leaky aquifer	Constant head	Reservoir
Hunt (2005)	Partially penetrating, nonvertical	Leaky top	None	
Hunt (2006)	Partially penetrating, nonvertical	Unconfined-vertical flow	None	
Butler et al. (2007)	Full vertical	Leaky	Surface source: constant flux	Underlying aquitard
Sun and Zhan (2007)	Full vertical	Unconfined-no vertical flow	Surface source: constant flux	Two streams
Yeh et al. (2008)	Full vertical	Confined	Constant head	Wedge, two streams
Hunt (2009)	Full vertical	Unconfined-no vertical flow	Surface source: zero width	Underlying aquitard
Sedghi, et al.(2009)	Full vertical, partially penetrating	Confined, unconfined	None	Wedge shaped
Tsou et al. (.2010)	Horizontal, slanted	Confined	Streambed	
Huang et al, (2012)	Radial collector well	Unconfined-vertical flow	Streambed	
Sedghi, et al. (2012)	Full vertical	Unconfined-vertical flow	None	Wedge shaped underlying aquitard
Huang et al. (2016a)	Radial collector well	Confined, unconfined-vertical flow	Streambed	Two streams

drawdown increases as the vertical to horizontal anisotropy $\kappa_z = K_z/K_x$ increases. The duration of the intermediate stage of drawdown increases as the ratio $\gamma = S_y/S$ increases and gravity drainage is delayed (Neuman, 1975). As specific yield nears zero, drawdown evolves as for a confined aquifer.

As the degree of penetration decreases, the drawdown takes longer to develop and the delayed response occurs when the drawdown is smaller. The effect of partial penetration for a well in an unconfined aquifer that is infinite in extent is less further away from the well and as the ratio of the vertical to horizontal hydraulic conductivity K_z/K_x increases (Neuman, 1974). At distances exceeding $H(K_x/K_z)^{1/2}$ where H is the saturated thickness and times greater than $10S_y r_1^2 / T$ —where S_y is the specific yield, r_1 is the distance from the well, and T is the transmissivity—the degree of penetration of a well is less important. The Hantush (1964) model for unsteady flow to a well in a compressible confined aquifer and Dagan's (1967) solution for a homogeneous, rigid water table aquifer serve as bounds for Neuman's (1974) model for a partially penetrating well. The Hantush (1964) solution is the early time bound, while Dagan's (1967) provides the late time bound.

Flow to a partially penetrating well in a homogeneous, anisotropic aquifer with leakage through an overlying unit matches the Hantush (1964) model for a confined aquifer but differs from the same Hantush model with a leaky boundary (Hunt, 2005). For a confined aquifer, partial penetration has minimal effect on drawdown about one aquifer thickness away from the well. Applying the Zhan and Zlotnik (2002) model for a well in an unconfined aquifer shows that drawdown increases when the degree of penetration of the screen decreases for a well at the bottom of the aquifer (Hunt, 2006). In a wedge shaped unconfined

aquifer decreasing the penetration of the well results in reduced stream depletion from a constant head stream boundary (Sedghi et al., 2009).

The presence of a streambed reduces drawdown and delays SDR (Hantush, 1965), Hantush's (1965) solution builds on a model for a fully penetrating vertical well installed in a semi-infinite aquifer near a constant head stream that neglects vertical flow (Theis, 1941; Glover and Balmer, 1954) by allowing for a reduced permeability streambed using the conductance coefficient $\chi = K'L_x / K_x b'$, where L_x is the distance between the river and well and K' and b' are the conductivity and thickness of the streambed. As χ increases, the development of SDR is delayed. Streambed properties, aquifer anisotropy, and the position of a radial collector well have a greater impact on SDR than the configuration of the collector well laterals for a collector well located near a fully penetrating stream in a homogeneous, anisotropic, unconfined aquifer with vertical flow (Maroney and Rehmann, 2017). Large streambed conductance χ caused by a high streambed conductivity or a thin streambed increases SDR, and as χ approaches infinity, the SDR approaches the value predicted by the Theis (1941) model. As χ decreases, SDR is reduced and delayed compared to the Hantush (1965) model, and gravity drainage contributes more flow to the well.

Drawdown can develop on both sides of a shallow stream modeled as a surface source in unconfined aquifers with no vertical flow (Hunt, 1999). Drawdown in Butler's (2001) solution for a well in a finite aquifer with a shallow stream approaches that of an infinite aquifer as modeled by Theis (1935) when the stream conductance parameter is small. When the conductance parameter is large, drawdown approaches the Theis (1941) model for a fully penetrating stream. Drawdown for a well near a wide stream is reduced compared to

that for a well near a stream of negligible width in an aquifer of semi-infinite extent (Fox et al., 2002)

Previous work has not evaluated the flow to a well that partially penetrates an unconfined aquifer and is installed near a stream that fully penetrates the aquifer. This chapter investigates how flow to vertical wells with screened intervals that are less than the saturated thickness of an unconfined aquifers is influenced by the presence of a stream, the vertical flow in the aquifer and how the SDR is affected by the degree of penetration of the well screen and 4) the depth of the well screen. A model for hydraulic head for vertical well located near a stream in an unconfined aquifer is given in section 3.2. A general solution for SDR as a function of dimensionless parameters is also presented in section 3.2. The results are presented in section 3.3 with a discussion of the results in section 3.4 and conclusions in section 3.5.

3.2 Methods

3.2.1. Model for an unconfined aquifer

The model presented in this chapter is similar to the model for a radial collector well (Maroney and Rehmann, 2017). The assumptions are that the well is located near a stream in a homogeneous, anisotropic, unconfined aquifer that is infinite in extent along the stream (y-direction) and away from the stream (x-direction) (Fig. 3.1). Flow into the well is uniform along the length of the well screen. The streambed hydraulic conductivity K' and thickness b' and the aquifer properties of saturated thickness H, horizontal hydraulic conductivity K_x, vertical hydraulic conductivity K_z, specific storage S_s, and specific yield S_y are site specific

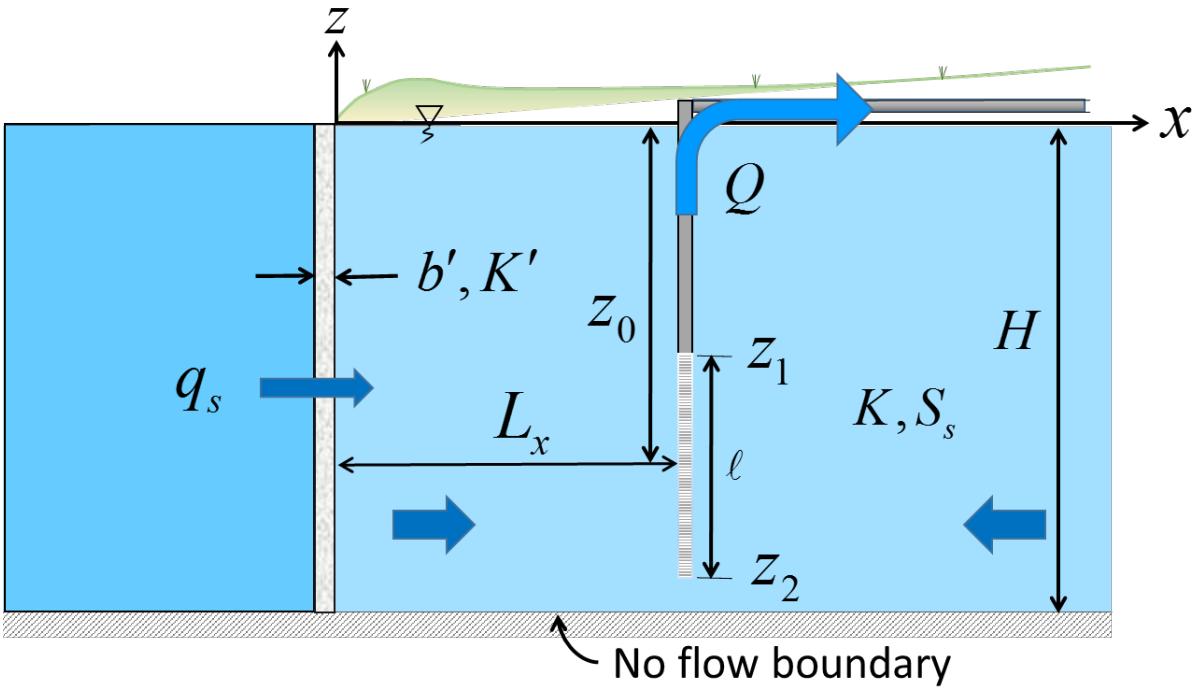

Fig. 3.1. Conceptual model for a partially penetrating well installed in an anisotropic, unconfined aquifer adjacent to a fully penetrating stream.

parameters that control the flow from the stream. The rate Q and duration t of pumping along with distance from the stream to the center point of the well L_x, the vertical position of the center of the well screen L_z, and length of the well screen ℓ are parameters that can be designed to suit the goals of the project.

The streambed parameters combine to create a streambed conductance coefficient described by Hantush (1965) and modified by HTY for an unconfined aquifer. The specific yield and storage coefficient ($S = S_sH$) form the ratio S_y/S and the ratio of vertical to horizontal hydraulic conductivity forms a parameter that reflects the anisotropy of the aquifer. The dimensional analysis becomes

$$\text{SDR} = f\left(\frac{Tt}{SH^2}, -\frac{K'H}{K_x b'}, \frac{\ell}{H}, \frac{K_z}{K_x}, \frac{Q}{K_x H^2}, \frac{S_y}{S}, \frac{L_x}{H}, \frac{L_z}{H}\right) = f\left(t_D, \alpha, \Lambda, \kappa_z, \varepsilon, \gamma, \rho_x, \rho_z\right) \qquad (3.1)$$

where the right-hand side identifies the dimensionless parameters for the model presented in this chapter. These dimensionless parameters are the same parameters used by HTY and Maroney and Rehmann (2017) except with the horizontal angle θ omitted and are discussed in Maroney and Rehmann (2017) for a radial collector well. In this chapter Λ represents the ratio of the length of well screen to initial saturated thickness and is referred to as the degree of penetration.

The stream fully penetrates the aquifer and the stream stage is constant. The origin of the coordinate system is located at the intersection of the streambed and pre-pumping water level with the *x*-direction in line with the well. For a point sink *Q* located at (*x′*, *y′*, *z'*), the governing equation for hydraulic head *h* becomes

$$K_x \frac{\partial^2 h}{\partial x^2} + K_y \frac{\partial^2 h}{\partial y^2} + K_z \frac{\partial^2 h}{\partial z^2} = S_s \frac{\partial h}{\partial t} + Q\delta\left(x - x'\right)\delta\left(y - y'\right)\delta\left(z - z'\right) \tag{3.2}$$

where $\delta(\ )$ is the Dirac delta function. There is no drawdown prior to the start of pumping. At any time far away from the well, pumping has no effect and $h = 0$ as $x \to \infty$, and as $|y| \to \infty$. Assuming the unit underlying the aquifer is impermeable, there is no vertical flux through the bottom of the aquifer:

$$\frac{\partial h}{\partial z} = 0 \quad \text{at} \quad z = -H \tag{3.3}$$

At the streambed boundary, flow through the streambed equals flow in the aquifer:

$$K_x \frac{\partial h}{\partial x} - \frac{K'}{b'} h = 0 \quad \text{at} \quad x = 0 \tag{3.4}$$

The water table is represented with a linearized free surface equation:

$$S_y \frac{\partial h}{\partial t} = -K_z \frac{\partial h}{\partial z} \quad \text{at} \quad z = 0 \tag{3.5}$$

Maroney and Rehmann (2017) showed that for a point sink Eq. (3.5) holds when $\varepsilon << \pi^2$ and $\varepsilon << \pi^2 \kappa_z \rho_x^2$. They showed that these conditions are satisfied for certain cases of radial collector wells. They argued that these conditions are conservative because the well's flow will be distributed over a lateral or well screen. The linearized condition for vertical wells will usually apply because pumping rates for vertical wells are typically much smaller than for radial collector wells.

3.2.2. *Solution for stream depletion rate*

The SDR for a point sink can be found by applying Darcy's law across the streambed and following the method for hydraulic head described by Huang et al. (2012) and for SDR defined by Maroney and Rehmann (2017). In this chapter x_{0D} is the distance from the stream to the well and z_{0D} is the vertical coordinate of the center of the well screen, normalized by H.

$$\mathrm{SDR}' = 1 + \frac{2\alpha}{\pi} \int_0^\infty \left(\Phi_0' + \sum_{n=1}^{\infty} \Phi_n' \right) R' d\omega \tag{3.6}$$

where

$$\Phi_0' = \frac{2\gamma \cosh\left[\zeta_0 \left(1 + z_{0D}\right)\right] e^{\mu_0 t_D}}{\zeta_0 \left[\left(2\gamma + 1\right)\zeta_0 \kappa_z \cosh\left(\zeta_0\right) + \left(\gamma \mu_0 + \kappa_z\right)\sinh\left(\zeta_0\right)\right]} \tag{3.7}$$

$$\Phi_n' = -\frac{2\gamma \cos\left[\zeta_n \left(1 + z_{0D}\right)\right] e^{-\mu_n t_D}}{\zeta_n \left[\left(2\gamma + 1\right)\zeta_n \kappa_z \cos\left(\zeta_n\right) + \left(\kappa_z - \gamma \mu_n\right)\sin\left(\zeta_n\right)\right]} \tag{3.8}$$

$$R' = \frac{\omega\left[\omega \cos\left(\omega x_{0D}\right) - \alpha \sin\left(\omega x_{0D}\right)\right]}{\omega^2 + \alpha^2} \tag{3.9}$$

where ω is the $\mathcal{R}$-transform variable, $\mu_0 = \zeta_0^2 \kappa_z - \omega^2$, $\mu_n = \zeta_n^2 \kappa_z - \omega^2$, and ζ_0 and ζ_n are the roots of

$$\tanh \zeta_0 = -\frac{\gamma}{\kappa_z \zeta_0}\left(\zeta_0^2 \kappa_z - \omega^2\right) \tag{3.10}$$

$$\tan \zeta_n = -\frac{\gamma\left(\zeta_n^2 \kappa_z + \omega^2\right)}{\zeta_n \kappa_z} \tag{3.11}$$

For flow that is uniform along the screen section of the well, the SDR for a partially penetrating vertical well can be found by integrating over the screened portion of the well. This gives

$$SDR = 1 + \frac{2\alpha}{\Lambda \pi}\int_0^\infty \left\{\Phi_0 + \sum_{n=1}^{\infty} \Phi_n\right\} R d\omega \tag{3.12}$$

where

$$\Phi_0 = \frac{4\gamma \cosh\left[\zeta_0\left(1 + z_{0D}\right)\right]\sinh\left(\frac{\Lambda}{2}\zeta_0\right)e^{\mu_0 t_D}}{\zeta_0{}^2\left[\left(2\gamma + 1\right)\zeta_0 \kappa_z \cosh\left(\zeta_0\right) + \left(\kappa_z + \gamma\mu_0\right)\sinh\left(\zeta_0\right)\right]} \tag{3.13}$$

$$\Phi_n = \frac{-2\gamma\left\{\sin\left[\zeta_n\left(1 + \rho_z + \frac{\Lambda}{2}\right)\right] - \sin\left[\zeta_n\left(1 + \rho_z - \frac{\Lambda}{2}\right)\right]\right\}e^{-\mu_n t_D}}{\zeta_n^2\left[\left(2\gamma + 1\right)\zeta_n \kappa_z \cos\left(\zeta_n\right) + \left(\kappa_z - \gamma\mu_n\right)\sin\left(\zeta_n\right)\right]} \tag{3.14}$$

$$R = \frac{\omega\left[\omega\cos\left(\omega x_{0D}\right) - \alpha\sin\left(\omega x_{0D}\right)\right]}{\left(\omega^2 + \alpha^2\right)} \tag{3.15}$$

The $\mathcal{R}$-inversion was performed numerically with Matlab's quadgk function using a maximum of 650 intervals.

3.2.3. Solution for hydraulic head for a partially penetrating well

A solution for the hydraulic head for a partially penetrating well near a stream is found by beginning with Eqs. (16) and (17) from Huang et al. (2012) solution for the hydraulic head for a point sink in an unconfined aquifer near a fully penetrating stream. The Huang et al. (2012) notation for dimensionless variables given in Eq. (2.13) is followed as described in Maroney and Rehmann (2017). Huang et al (2012) found a solution for head by using a Laplace transform in time, a Fourier transform in *y*, and an $\mathcal{R}$-transform in *x*. After solving the problem in the transformed space, the Laplace transform of the solution was inverted analytically and the integrals for the Fourier transform and $\mathcal{R}$-transform were inverted numerically. The integrand for this problem is doubly oscillating and difficult to integrate numerically.

An alternate approach is to apply a change of variables to the problem by setting $p = \omega/\sqrt{\kappa_z}$ and $q = \xi\sqrt{\kappa_y/\kappa_z}$ where ξ is the Fourier transform variable. Next change (p,q) to (r,ϕ) by setting $r = \sqrt{p^2 + r^2}$ where $p = r\cos\phi$ and $q = r\sin\phi$. The solution for a point sink becomes

$$\begin{aligned} h_{Da} &= \frac{2\kappa_z}{\sqrt{\kappa_y}}\int_0^{\pi/2}\int_0^{\infty}\left\{\Phi_s + \Phi_0 + \sum_{n=1}^{\infty}\Phi_n\right\}F_r R_r r dr d\phi \quad \text{for} \quad z_{0D} < z_D < 0 \\ h_{Db} &= \frac{2\kappa_z}{\sqrt{\kappa_y}}\int_0^{\pi/2}\int_0^{\infty}\left\{\Psi_s + \Psi_0 + \sum_{n=1}^{\infty}\Psi_n\right\}F_r R_r r dr d\phi \quad \text{for} \quad -1 < z_D < z_{0D} \end{aligned} \tag{3.16}$$

where

$$F_r = \cos\left[\sqrt{\frac{\kappa_z}{\kappa_y}}\left(y_D - y_{0D}\right) r\sin\left(\phi\right)\right] \tag{3.17}$$

$$R_r = \frac{1}{\left[\alpha^2 + \kappa_z r^2 \cos^2(\phi)\right]}\left\{\alpha^2 \sin\left[\sqrt{\kappa_z} x_D r\cos(\phi)\right]\sin\left[\sqrt{\kappa_z} x_{0D} r\cos(\phi)\right]\right.$$
$$-\alpha\sqrt{\kappa_z} r\cos(\phi)\sin\left[\sqrt{\kappa_z}\left(x_D + x_{0D}\right) r\cos(\phi)\right] \qquad (3.18)$$
$$\left.+\kappa_z r^2 \cos^2(\phi)\cos\left[\sqrt{\kappa_z} x_D r\cos(\phi)\right]\cos\left[\sqrt{\kappa_z} x_{0D} r\cos(\phi)\right]\right\}$$

Evaluating the problem for a vertical well that partially penetrates the aquifer requires integrating Equation (3.16) from the top of the well screen z_{D1} to the bottom of the well z_{D2}. Now

$$\breve{h} = \frac{2\kappa_z}{\Lambda\sqrt{\kappa_y}}\int_0^{\pi/2}\int_0^{\infty}\left\{\breve{\Phi}_s + \breve{\Phi}_0 + \sum_{n=1}^{\infty}\breve{\Phi}_n\right\}\breve{F}\breve{R}\,dr\,d\phi \qquad (3.19)$$

where

$$\breve{\Phi}_s = \begin{cases} -\dfrac{\cosh(z_D r)\left\{\sinh\left[(1+z_{D1})r\right] - \sinh\left[(1+z_{D2})r\right]\right\}}{\kappa_z r\sinh(r)} \\ for \quad z_{D1} \le z_D \le 0 \\ -\dfrac{\sinh(r) + \sinh(z_{D1} r)\cosh\left[(1+z_D)r\right] - \cosh(z_D r)\sinh\left[(1+z_{D2})r\right]}{\kappa_z r\sinh(r)} \\ for \quad z_{D2} \le z_D \le z_{D1} \\ -\dfrac{\left\{\sinh(z_{D1} r) - \sinh(z_{D2} r)\right\}\cosh\left[(1+z_D)r\right]}{\kappa_z r\sinh(r)} \\ for \quad -1 \le z_D \le z_{D2} \end{cases} \qquad (3.20)$$

$$\breve{\Phi}_0 = \begin{cases} \dfrac{2r\left\{\sinh\left[\left(1+z_{D1}\right)\breve{\zeta}_0\right]-\sinh\left[\left(1+z_{D2}\right)\breve{\zeta}_0\right]\right\}\left[\gamma\breve{\mu}_0\sinh\left(z_D\breve{\zeta}_0\right)-\breve{\zeta}_0\kappa_z\cosh\left(z_D\breve{\zeta}_0\right)\right]e^{\breve{\mu}_0 t_D}}{\breve{\mu}_0\beta_0\left[\left(1+2\gamma\right)\beta_0\kappa_z\cosh\left(\beta_0\right)+\left(\kappa_z+\gamma\breve{\mu}_0\right)\sinh\left(\beta_0\right)\right]} \\ \quad for \quad z_{D1}\le z_D\le 0 \\ \dfrac{-2re^{\breve{\mu}_0\tau}}{\breve{\mu}_0\beta_0\left[\left(1+2\gamma\right)\beta_0\kappa_z\cosh\left(\beta_0\right)+\left(\kappa_z+\gamma\breve{\mu}_0\right)\sinh\left(\beta_0\right)\right]}\left\{\gamma\breve{\mu}_0\cosh\left(\breve{\zeta}_0\right)+\breve{\zeta}_0\kappa_z\sinh\left(\breve{\zeta}_0\right)\right. \\ \qquad -\gamma\breve{\mu}_0\left\{\cosh\left[\left(1+z_D\right)\breve{\zeta}_0\right]\cosh\left(z_{D1}\breve{\zeta}_0\right)-\sinh\left[\left(1+z_{D2}\right)\breve{\zeta}_0\right]\sinh\left(z_D\breve{\zeta}_0\right)\right\} \\ \qquad \left.-\kappa_z\breve{\zeta}_0\left\{\cosh\left[\left(1+z_D\right)\breve{\zeta}_0\right]\sinh\left(z_{D1}\breve{\zeta}_0\right)-\sinh\left[\left(1+z_{D2}\right)\breve{\zeta}_0\right]\cosh\left(z_D\breve{\zeta}_0\right)\right\}\right\} \\ \quad for \quad z_{D2}\le z_D\le z_{D1} \\ \dfrac{2r\cosh\left[\left(1+z_D\right)\breve{\zeta}_0\right]\left\{\gamma\breve{\mu}_0\left[\cosh\left(z_{D1}\breve{\zeta}_0\right)-\cosh\left(z_{D2}\breve{\zeta}_0\right)\right]-\breve{\zeta}_0\kappa_z\left[\sinh\left(z_{D1}\breve{\zeta}_0\right)-\sinh\left(z_{D2}\breve{\zeta}_0\right)\right]\right\}e^{\breve{\mu}_0 t_D}}{\breve{\mu}_0\beta_0\left[\left(1+2\gamma\right)\beta_0\kappa_z\cosh\left(\beta_0\right)+\left(\kappa_z+\gamma\breve{\lambda}_0\right)\sinh\left(\beta_0\right)\right]} \\ \quad for \quad -1\le z_D\le z_{D2} \end{cases}$$

(3.21)

$$\breve{\Phi}_n = \begin{cases} \dfrac{2r\left\{\sin\left[\left(1+z_{D1}\right)\breve{\zeta}_n\right]-\sin\left[\left(1+z_{D2}\right)\breve{\zeta}_n\right]\right\}\left[\gamma\breve{\mu}_n\sin\left(z_D\breve{\zeta}_n\right)+\breve{\zeta}_n\kappa_z\cos\left(z_D\breve{\zeta}_n\right)\right]e^{-\breve{\mu}_n t_D}}{\breve{\mu}_n\breve{\zeta}_n\left[\left(1+2\gamma\right)\breve{\zeta}_n\kappa_z\cos\left(\breve{\zeta}_n\right)+\left(\kappa_z+\gamma\breve{\mu}_n\right)\sin\left(\breve{\zeta}_n\right)\right]} \\ \quad for \quad z_{D1}\le z_D\le 0 \\ \dfrac{2re^{-\breve{\mu}_n\tau}}{\breve{\mu}_n\breve{\zeta}_n\left[\left(1+2\gamma\right)\breve{\zeta}_n\kappa_z\cos\left(\breve{\zeta}_n\right)+\left(\kappa_z+\gamma\breve{\mu}_n\right)\sin\left(\breve{\zeta}_n\right)\right]}\left\{-\gamma\breve{\mu}_n\cos\left(\breve{\zeta}_n\right)-\breve{\zeta}_n\kappa_z\sin\left(\breve{\zeta}_n\right)\right. \\ \qquad +\gamma\breve{\mu}_n\left\{\sin\left(z_D\breve{\zeta}_n\right)\sin\left[\left(1+z_{D1}\right)\breve{\zeta}_n\right]+\cos\left(z_{D2}\breve{\zeta}_n\right)\cos\left[\left(1+z_D\right)\breve{\zeta}_n\right]\right\} \\ \qquad \left.+\kappa_z\breve{\zeta}_n\left\{\cos\left(z_D\breve{\zeta}_n\right)\sin\left[\left(1+z_{D1}\right)\breve{\zeta}_n\right]-\sin\left(z_{D2}\breve{\zeta}_n\right)\cos\left[\left(1+z_D\right)\breve{\zeta}_n\right]\right\}\right\} \\ \quad for \quad z_{D2}\le z_D\le z_{D1} \\ \dfrac{2r\cos\left[\left(1+z_D\right)\breve{\zeta}_n\right]\left\{-\gamma\breve{\mu}_n\left[\cos\left(z_{D1}\breve{\zeta}_n\right)-\cos\left(z_{D2}\breve{\zeta}_n\right)\right]+\breve{\zeta}_n\kappa_z\left[\sin\left(z_{D1}\breve{\zeta}_n\right)-\sin\left(z_{D2}\breve{\zeta}_n\right)\right]\right\}e^{-\breve{\mu}_n t_D}}{\breve{\mu}_n\breve{\zeta}_n\left[\left(1+2\gamma\right)\breve{\zeta}_n\kappa_z\cos\left(\breve{\zeta}_n\right)+\left(\kappa_z+\gamma\breve{\mu}_n\right)\sin\left(\breve{\zeta}_n\right)\right]} \\ \quad for \quad -1\le z_D\le z_{D2} \end{cases}$$

(3.22)

$$\breve{\mu}_0 = -\kappa_z \left(r^2 - \zeta_0^2 \right) \tag{3.23}$$

$$\breve{\mu}_n = \kappa_z \left(r^2 + \zeta_n^2 \right) \tag{3.24}$$

where $\breve{\zeta}_0$ and $\breve{\zeta}_n$ are the roots of

$$\tanh\left(\zeta_0\right) = -\frac{\gamma}{\zeta_0}\left(\zeta_0^2 - r^2\right) \tag{3.25}$$

$$\tan\left(\zeta_n\right) = -\frac{\gamma}{\zeta_n}\left(\zeta_n^2 + r^2\right) \tag{3.26}$$

The improper integral in Eq. (3.19) was computed numerically using Matlab's quadgk function that applies adaptive Gauss-Kronrod quadrature for a maximum of 2000 intervals. The finite limit integral was evaluated with the Matlab trapz function for a maximum of 200 intervals.

3.2.4. Parameter values and ranges

The default values for the calculations for the calculations for SDR and hydraulic head in Section 3.3 are given in Table 3.2. The default values used for κ_y, κ_z, γ, and α are the same as those listed in Table 1 of Huang et al. (2012) with typical ranges described in Maroney and Rehmann (2017). The vertical well is assumed to have a screen length that extends for 20% of the full depth of the saturated thickness of the aquifer and may be located at the base of the of the aquifer for water supply or collection of dense non-aqueous phase liquids (DNAPLs), in the center of the saturated thickness to dewater a site, or at the top of the zone of saturation to collect contaminants at near the water table.

Table 3.2. Default values for the dimensionless parameters used for simulations for SDR and hydraulic head.

Parameter	Default value	Range considered
Λ	0.2	0.2 to 1
α	−1	−0.1 to −1
κ_z	0.1	10^{-3}, 10^{-1}
κ_y	1	1
γ	300	300
x_{0D}	2	2
y_{0D}	0	0
z_{0D}	0.5	−1 to 0

3.2.5. Finite difference model

A finite-difference model was developed for the conceptual model described in section 3.1.3 and Fig. 3.1 using the United States Geological Survey (USGS) groundwater flow model MODFLOW 2000 (Harbaugh et al., 2000). The dimensional data used in this model is similar to the East Well Field located in the alluvial aquifer of the Cedar River near Cedar Rapids, Iowa (Turco and Buchmiller, 2004). There is a direct connection between the river and the aquifer deposits which are composed of fine- to coarse-grained sands and gravels up to 100 feet thick. Siltation has occurred upstream of a low head dam resulting in a reduced permeability streambed. The typical well is screened for 20 feet and rests at the bottom of the aquifer. The saturated thickness is approximately 65 feet.

The model has 350 rows, 250 columns, and 13 layers with the horizontal cell sizes ranging from 2 feet near the river to 1000 feet at the boundary of the model. The top layer is 10 feet thick and the other layers are each 5 feet thick. The parameters used for this model are uniform unless specified (Table 3.3). A free surface represents the water table. No flow passes through the bottom of the model. The well is operated with a constant pumping rate

Table 3.3. Parameters used in the MODFLOW model and dimensionless parameters used in the analytical model.

Parameter	Value	Dimensionless parameter	Value
Model top elevation, ft	70	Λ	0.31
Model bottom elevation, ft	0	α	−0.38
Well pumping rate, ft^3/d	−150,000	κ_z	0.1
Horizontal hydraulic conductivity, ft/d	170	γ	130
Vertical hydraulic conductivity, ft/d	17	x_{0D}	1.92
Specific storage, ft^{-1}	0.00005	z_{0D}	−0.85
Specific yield	0.42		
Steady state groundwater level, ft	65		
Stream stage, ft	65		
Riverbed hydraulic conductivity, ft/d	1		
Riverbed thickness, ft	1		

and is modeled with MODFLOW's well package. The well is located 125 feet away from the river with the pumping flow split between layers 10 through 13. The horizontal hydraulic conductivity is uniform and the same in all layers. The vertical to horizontal anisotropy ratio is set at 0.1 (Turco and Buchmiller, 2004).

General head boundaries are used to allow for the aquifer's presence beyond the model area as the analytical model is semi-infinite in extent. MODFLOW's general head boundary (GHB) package calculates the flow Q_b through the boundary by $Q_b = C_b(h_b - h_a)$, where $C_b = K_x A_m/d$ is the conductance, h_b is the head at the boundary outside of the model (distance to constant head), h_a is the head in the model, K_x is the horizontal hydraulic conductivity of the material between the boundary and the model, A_m is the area of the cell, and d is the distance to the boundary (Anderson and Woessner, 2002). The hydraulic conductivity of the aquifer is used to determine the conductance between the boundary of the model and the remote constant head boundary. The distance to the boundary head is set at 1,000,000 feet to represent the head infinitely far away. The stream is also modeled as a head

dependent boundary to represent the fully penetrating stream condition of the analytical model presented in this chapter. The GHB package is used and the constant head boundary is set at 1 foot outside the model limits. The streambed hydraulic conductivity is used to determine the conductance between the river and the boundary cell.

The model is solved using the preconditioned conjugate gradient 2 (PCG2) solver package. A head change requirement of 0.0001 feet was chosen for closure, which occurred after 219 iterations. The final mass balance discrepancy for the entire model was 0.01%. Flow out of the model is entirely through the well, and flow into the model is through the lateral boundaries with more than 99% entering through the boundary cells representing the river and less than 0.01% entering through the GHB cells representing the continuation of the aquifer.

3.3. Results

3.3.1. Stream depletion rate

Vertical wells with screens that penetrate a larger portion of the saturated thickness of the aquifer and have the lowest end located at the base of the aquifer demonstrate a reduction in the SDR during the intermediate stage (Fig. 3.2). During the intermediate stage, the SDR for a well screened through the entire saturated thickness ($\Lambda = 1$) is about 0.15 lower than the SDR for a well screened in the lower tenth of the aquifer ($\Lambda = 0.1$) when $\kappa_z = 0.001$. The present model (Eq. 3.8) matches the Hantush (1965) model for SDR for the special cases shown in Fig. 3.2 for a well located at the bottom of the aquifer with the Hantush solution providing the analytical limits. The curves follow the Hantush model with $S = S_s H$ for small time $\tau = K_x t / S_s L_x^2$ and follow the Hantush case with $S = S_y$ for large time. As κ_z increases

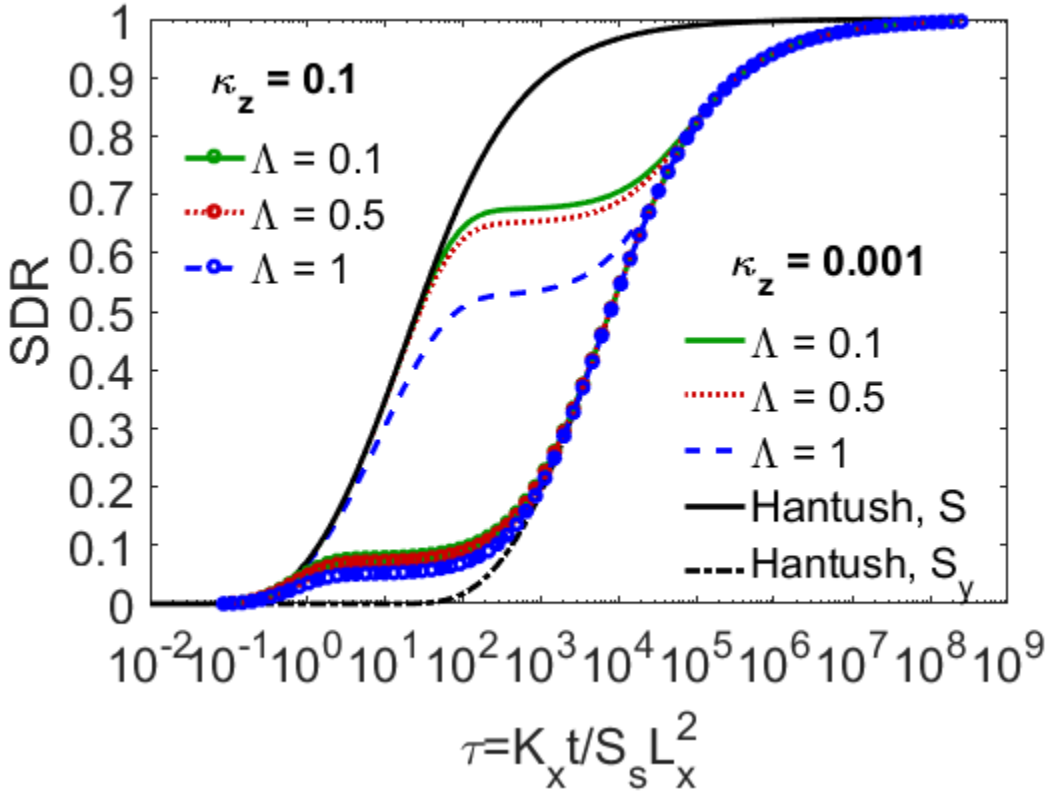

Fig. 3.2. Effect of degree of penetration of the well screen for a vertical well located at the bottom of an unconfined aquifer.

the degree of penetration for a well located as the base of the aquifer has less impact on the development of SDR; however, the SDR is reduced during the intermediate stage and approaches the Hantush (1965) model with $S = S_y$ (Fig. 3.2). SDR increases as κ_z decreases, as in the case of a radial collector well (Maroney and Rehmann, 2017), with the SDR increasing more for a well with a smaller Λ compared to a well with large Λ. For a well screened at the bottom of the aquifer and small Λ the potential gradient of the hydraulic head is larger compared to a well with a larger Λ.

Wells screened near the top of the saturated zone have smaller SDR during the intermediate stage (Fig. 3.3). For a well screened in the top tenth of the saturated zone and κ_z = 0.001 the SDR during the intermediate stage is about 0.52 less than that of a well screened

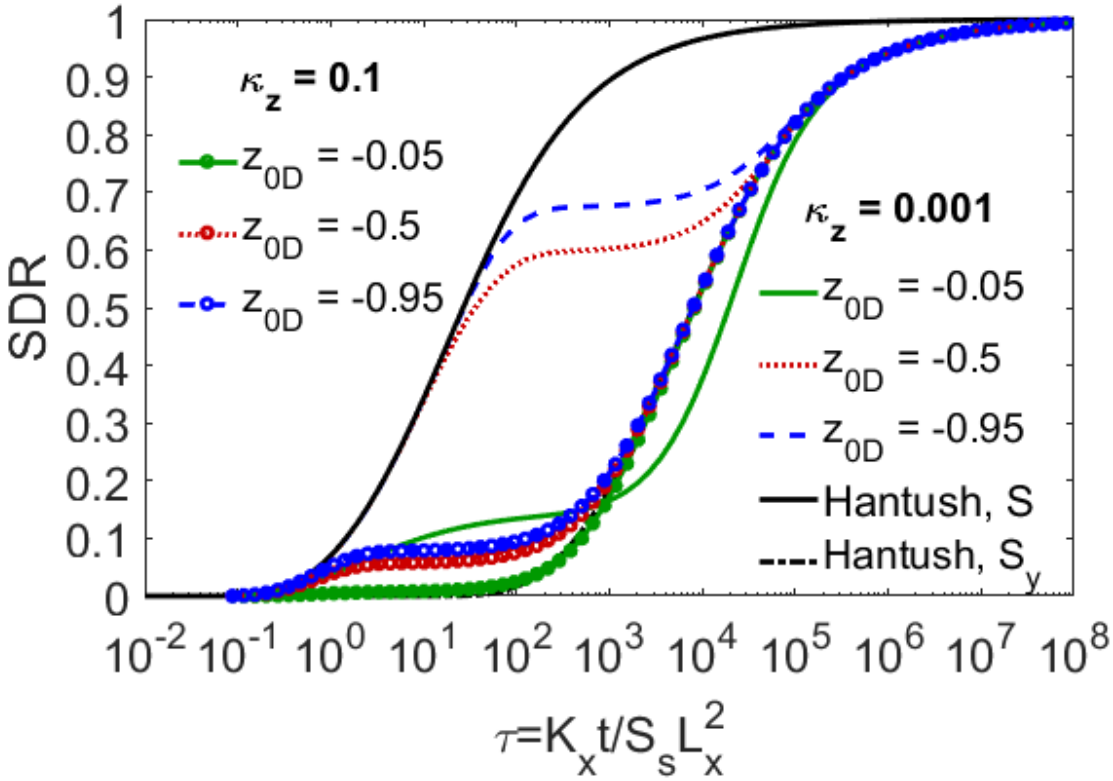

Fig. 3.3. Effect of the well screen location for a vertical well with Λ = 0.1.

in the lowest tenth of the saturated thickness. When Λ is small the deeper well has an increased hydraulic gradient compared to a shallow well with the same Λ. When the degree of penetration of the well is small—particularly when the well is located at the top of the aquifer the intermediate and late stages of SDR develop more slowly, and the curves no longer follow the Hantush model with $S = S_y$ at late time (Fig. 3.3).

3.3.2. Comparison of numerical and analytical solutions

The numerical model and the analytical model in Eq. (3.19) produce comparable hydraulic heads in the vicinity of the well, and the numerical model slightly under-predicts hydraulic head at larger values of *x* (Fig. 3.4). Relative error ranges from less than 1% to 15% within 125 feet of the well to 61% at 1000 feet from the well. The finite—difference

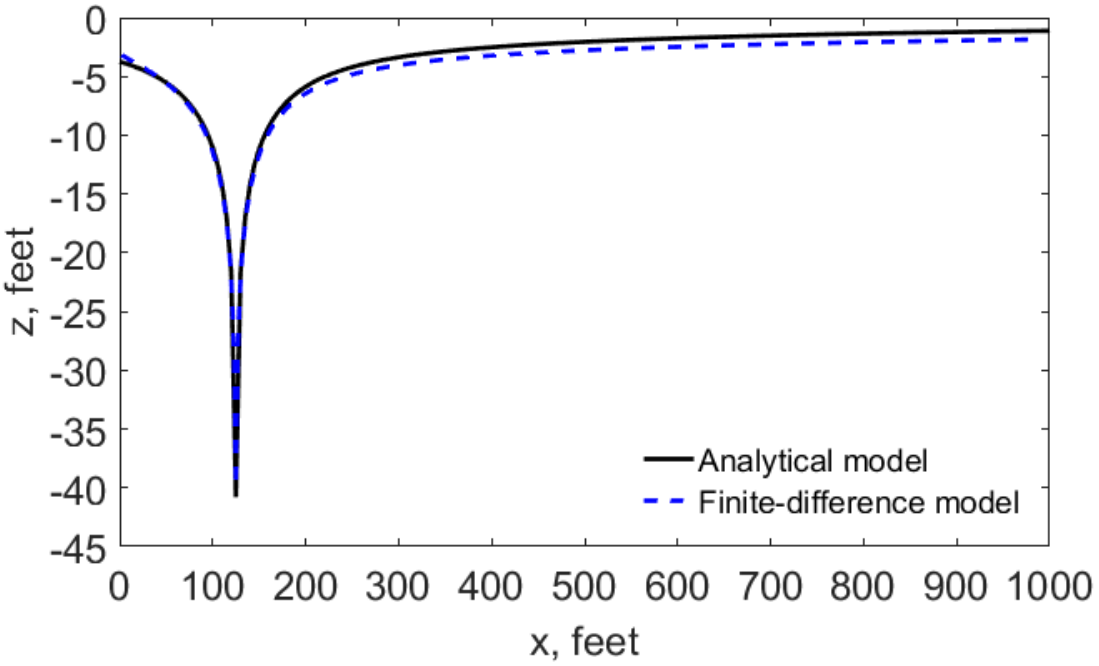

Fig. 3.4. Comparison of hydraulic head at 52.5 feet below the initial water table (level 11 of the finite-difference model.

model draws less than 1% of the water through the GHB that represents the infinite extent of the aquifer with more than 99% passing through the river boundary. Increasing the resolution of the analytical model did not change the solution, while the results from the finite-difference model continued to change as the resolution increased.

3.3.3. Drawdown

For a fully penetrating well, the drawdown develops in three stages as observed by Neuman (1972) (Fig. 3.5). Initially water is released because of the compressibility of the water and aquifer material. In the intermediate stage gravity drainage delays the spreading of the cone of depression. Eventually gravity drainage dominates the flow, and drawdown approaches a steady state value. The curves follow the Hantush (1965) model with $S = S_s H$ during the early time and with $S = S_y$ for large time. Compared to the intermediate stage of

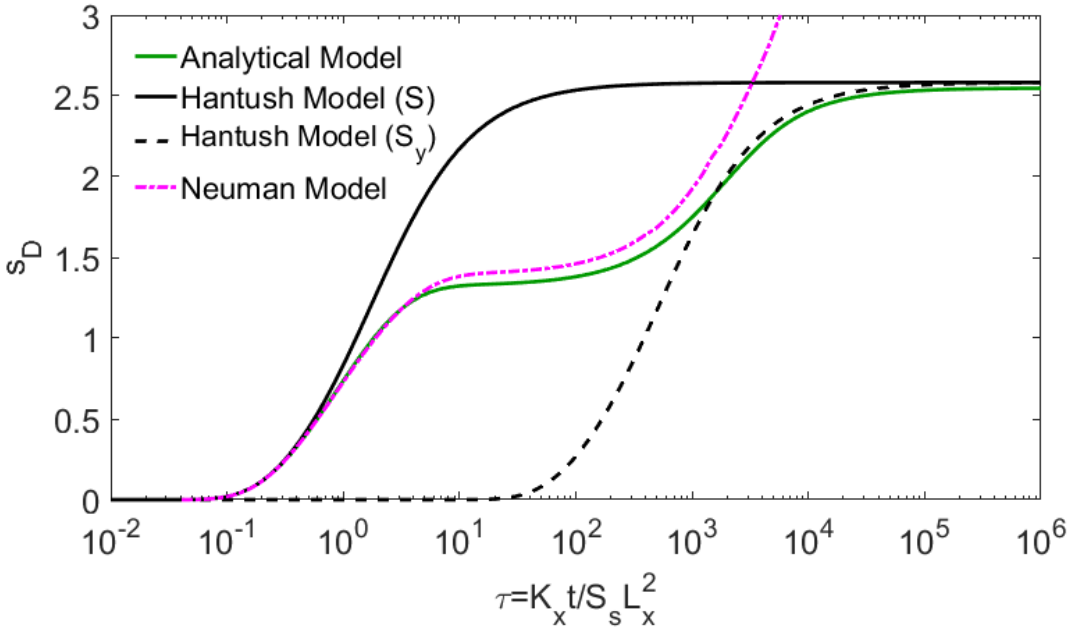

Fig. 3.5. Comparison of development of drawdown for a vertical well that fully penetrates an unconfined aquifer observed at $x_D = 1$, $y_D = 0$, and $z_D = -0.5$.

the Neuman (1974), the intermediate stage in the present model for a fully penetrating well has less drawdown.

For a partially penetrating well, the drawdown depends on position of the screen, the degree of penetration, and the vertical position of the observation (Fig. 3.6). Steady state drawdown for a well centered in the aquifer $z_{0D} = -0.5$ is symmetric about the observation point of $z_D = -0.5$ with drawdown decreasing as the observation point moves away from the center of the aquifer with drawdowns for $z_D = -0.3$ and -0.7 similar and $z_D = -0.1$ and -0.9 similar. At the center of the aquifer the drawdown is smaller for larger Λ as the well has more area for flow to enter. At the top and bottom of the aquifer, the opposite occurs with smaller drawdown occurring for smaller Λ. For all levels of observation and all degrees of

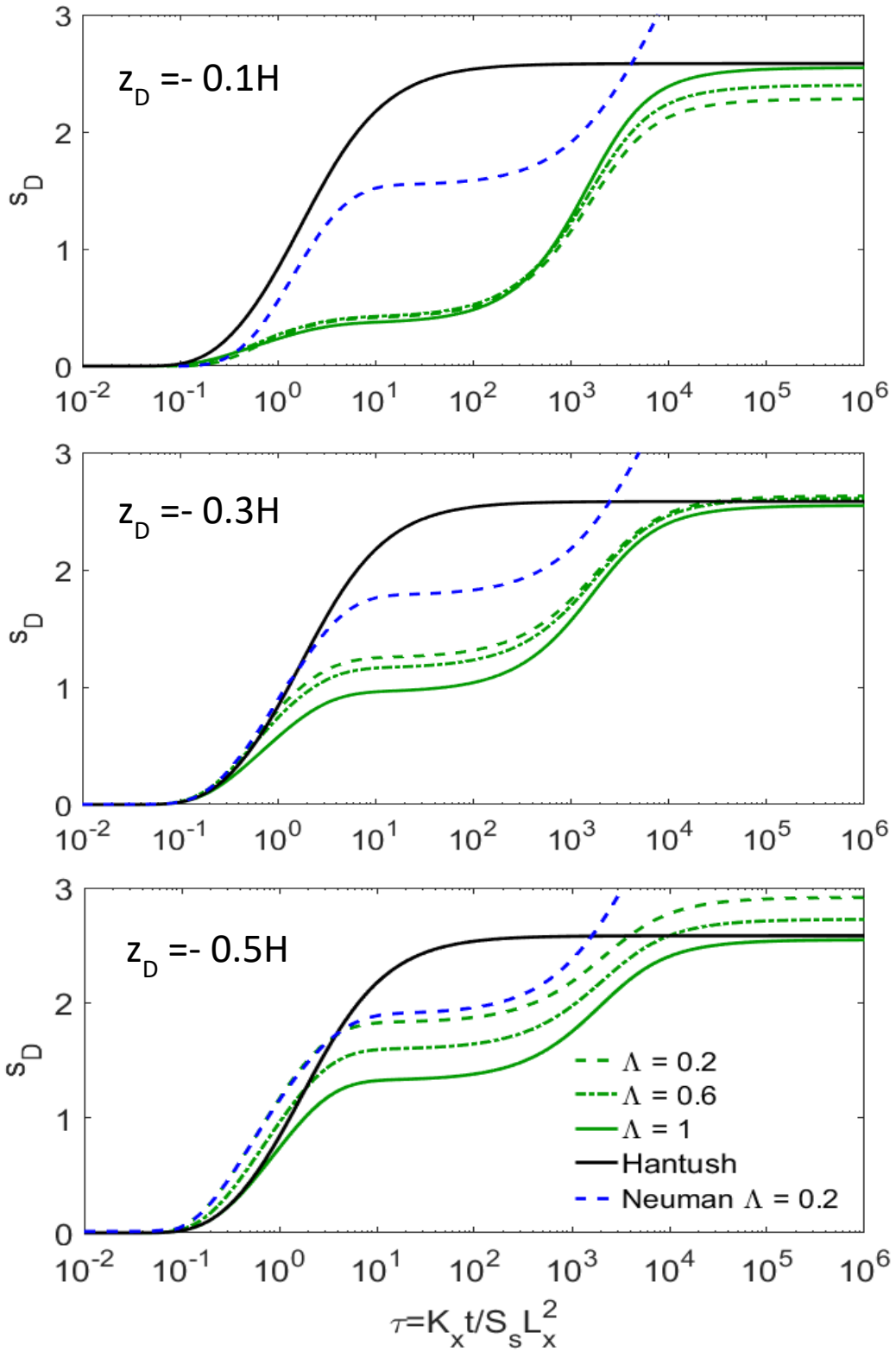

Fig. 3.6. Development of drawdown for wells with $z_{0D} = -0.5$ predicted at $x_D = 1$ and $y_D = 0$ for various reference levels z_D.

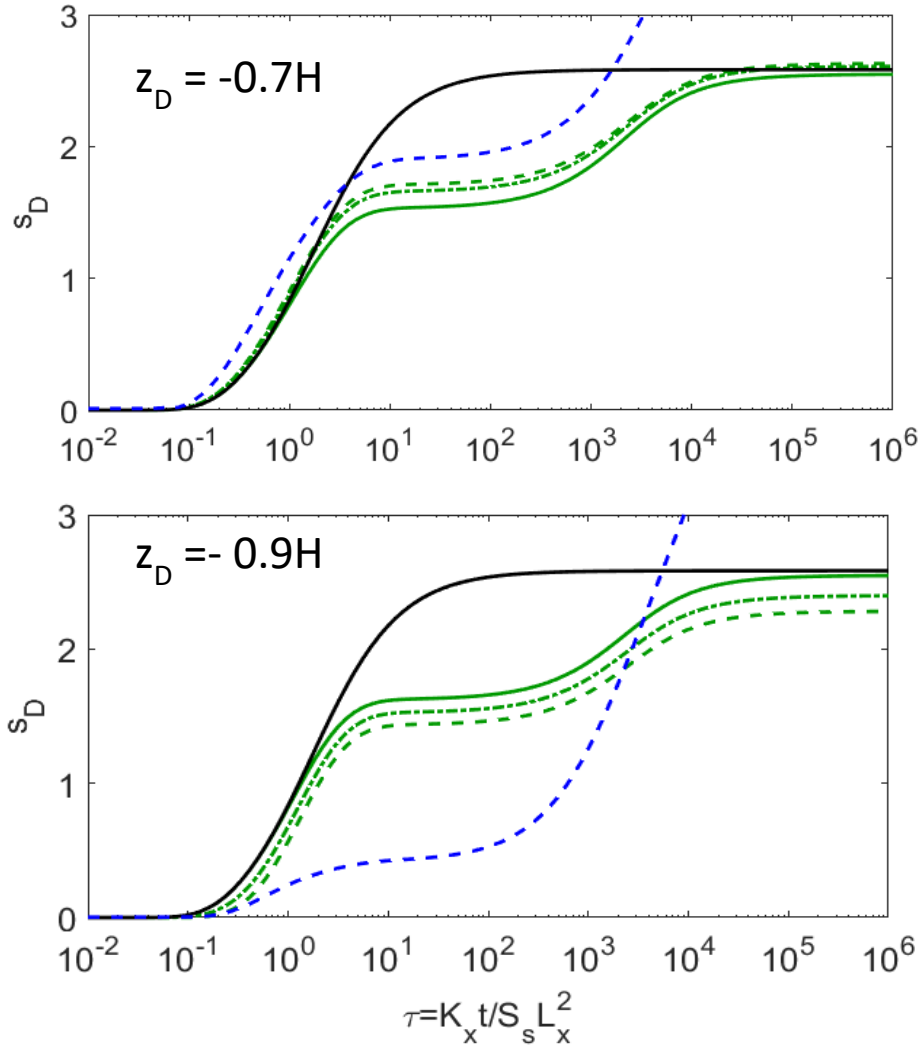

Fig. 3.6. continued. Development of drawdown for wells with $z_{0D} = -0.5$ predicted at $x_D = 1$ and $y_D = 0$ for various reference levels z_D.

Penetration, steady state occurs near the same t_D. The Hantush (1965) model predicts just one value for steady state regardless of the observation level, while the drawdown predicted by the Neuman (1974) model continues to increase because the aquifer is infinite in extent. The differences between the steady values of drawdown in the present model and the Hantush model increase as Λ decreases.

The evolution of unsteady drawdown does not have the symmetry of the steady state drawdown (Fig. 3.6). For a partially penetrating well centered in the aquifer, drawdown is

largest at the middle of the screen (Fig. 3.6c). The drawdown during the intermediate stage develops sooner and is larger when Λ is smaller. The drawdown curves are closer to the Hantush condition as compared to those in Fig. 3.6c. Near the bottom of the aquifer drawdown in the intermediate stage is larger for the fully penetrating well but is smaller for $\Lambda = 0.2$ (Fig. 3.6e). At a higher level in the aquifer water the drawdown during the intermediate stage is smaller than at the center of the aquifer (Fig. 3.6b). Drawdowns during the intermediate stage for all values of Λ are small and grouped together. Drawdown at observation levels near the top of the aquifer are smallest compared to the Hantush curve (Fig. 3.6a). When $\Lambda = 0.2$ and the screen is centered in the aquifer, the dimensionless drawdown is lower during the intermediate stage when a stream is present compared to Neuman's (1974) model for an equivalent well (Fig. 3.6).

Drawdown is largest for wells screened in the center of the saturated thickness and smaller for wells screened near the top and bottom (Fig. 3.7). The drawdowns for screens near the top ($z_{0D} = -0.1$, Fig. 3.7a) and bottom ($z_{0D} = -0.9$, Fig. 3.7c) are nearly identical and about half of the drawdown for a well screened in the center ($z_{0D} = -0.5$, Fig. 3.7b). The drawdown for a well in the center exceeds the drawdown predicted by the Hantush model at steady state, while the drawdown for the other cases is always much less than the Hantush prediction. The drawdown for a well near a river contrasts sharply with the drawdown for a well in an infinite aquifer (Neuman, 1974). For wells screened at the top or in the center (Fig.s 3.7a, b), the drawdown for a well near a river is equal to or slightly less than the drawdown predicted by the Neuman model. However, for a well screened near the bottom

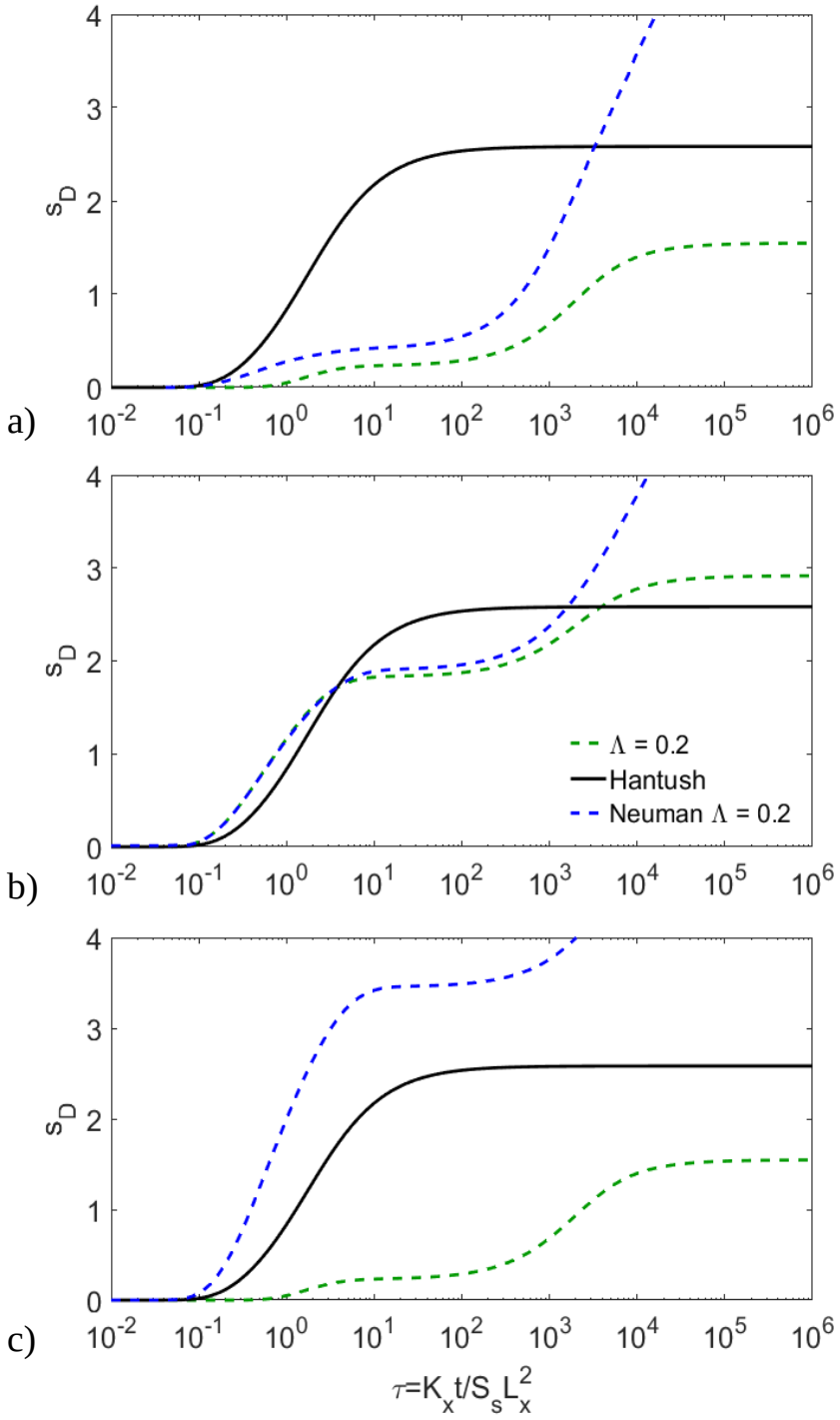

Fig. 3.7. Development of drawdown for wells with a degree of penetration of 0.2. a) top of screen is at top of initial saturated thickness with z_D = 0.1, b) well screen centered at center of initial saturated thickness with z_D = 0.5, and c) base of well screen at the bottom of the aquifer with z_D = 0.9.

(Fig. 3.7c), the drawdown for a well near a river is much less than that predicted by the Neuman model.

3.4. Discussion

3.4.1. Comparison to previous work

The development of the SDR takes longer for a well with small penetration in the same aquifer than for a well that fully penetrates the saturated zone as is described with the Hantush (1965) model with the condition of $S = S_y$ (Fig. 3.3). This phenomenon was noted by Neuman (1974) when comparing the hydraulic head for a partially penetrating well in an unconfined aquifer with the Theis (1935) model using the S_y for gravity drainage. Release of water from storage in the aquifer during the early stage delays the early time development of drawdown. As S/S_y becomes small, the early time period of drawdown decreases. When the degree of penetration of the well is small, the elastic release occurs longer, and the drawdown increases during the intermediate and late stages of flow. This translates to the evolution of SDR. During the early stages when release of water from storage is larger less flow comes from the stream delaying the SDR. This effect becomes more pronounced when z_{0D} is small (i.e., the well is shallow).

Drawdown for a well centered in the aquifer is greatest at the center of the well decreasing above and below the well (Fig. 3.6) indicating that vertical flow occurs from both above and below the center of the well. Drawdown in the intermediate stage is less than the Hantush (1965) model for the condition of $S = S_sH$ also demonstrating the presence of vertical flow. At the center of the well with $\Lambda = 0.2$ (Fig. 3.6c) the present model is similar to the Neuman (1974) model during the intermediate stage; however, the drawdown for the

present model is much less near the top of the aquifer (Fig. 3.7a) due to the contribution of flow from the river. Deeper in the aquifer the present model has a larger drawdown than the Neuman (1974) model; however, the gradient between the center (Fig. 3.6c) and bottom (Fig. 3.6e) of the aquifer is smaller compared to the Neuman (1974) model. Water from the river contributing to flow to the well results in reduced hydraulic gradient from below the center of the well.

Flow from the river provides a source of water to maintain gravity drainage for a well with small Λ located at the bottom of the aquifer. The entire saturated thickness of the aquifer drains toward a well at the bottom of the aquifer. The small drawdown during the intermediate stage for the present model compared to the Neuman (1974) model and during steady state compared to the Hantush (1965) model shows the river is contributing flow to the well through gravity drainage (Fig. 3.7c). Flow from the river through upward flow from below the well regulates the evolution of the drawdown when Λ is small and the well is located at the top of the aquifer (Fig. 3.7a). For the case of $\Lambda = 0.2$ and the well at the top of the aquifer the drawdown during the intermediate stage is close to the Neuman (1974) case and much smaller than the Hantush (1965) model indicating that vertical flow in the aquifer has a large influence on the development of drawdown. The well receives water through vertical flow from below the well, and this flow is maintained by the river.

3.4.2. Analytical versus numerical model

Both the analytical and finite-difference models presented in the chapter require discretization of a semi-infinite domain. While the solution for head of Huang et al. (2012) requires evaluating two improper integrals to invert Fourier and $\mathscr{R}$-transforms, switching to polar coordinates allows one integral to be computed over a finite domain. Still, Eq. (3.12)

for SDR and Eq. (3.19) for hydraulic head each require one numerical evaluation of an improper integral. Although the integrands are highly oscillating, adaptive Gauss-Kronrod quadrature allows them to be evaluated reliably.

The finite-difference representation in the MODFLOW model is also based on a choice of a limited model area. Consideration of a larger finite domain can be addressed with the use of irregular grids and telescopic mesh refinement where a coarse grid models the regional problem which is used to define the boundaries of the smaller domain system (Anderson and Woessner, 2002). A finite-difference model with a large number of nodes requires more computer storage and computational requirements; however, accuracy is improved. The semi-infinite domain of the present model requires the choice of a large area to establish appropriate boundaries and thus a large number of nodes. The data for the present model composed of 350 rows, 250 columns, and 14 layer requires a large amount of computer storage, and the resulting heads continued to change as the grid was refined. The storage requirement for the analytical model is much less than the space utilized for the finite-difference model; however, the analytical model requires a greater computational time to operate for an equivalent number of nodes.

3.4.3. Implications for practice

Drawdown data from aquifer tests can be used with the flow model in Eq. (3.19) to determine vertical and horizontal hydraulic conductivities, storativity, specific yield, and streambed properties for partially penetrating wells located near a stream in an unconfined aquifer of semi-infinite extent as described by Eq. (3.2). Values of α, γ, and χ can be adjusted in Eq. (3.19) to match the drawdown versus time plot from the aquifer test. Increasing χ

shifts the curve earlier in time; increasing κ_z decreases the drawdown during the intermediate stage; and increasing γ increases the duration of the intermediate stage.

A well with a small degree of penetration located at the bottom of the aquifer has a small drawdown and receives more flow from the river, which is an advantage for water supply when river bank filtration is desired. The same well is suited for collection of contamination such as DNAPLs or other contaminants concentrated at the bottom of the aquifer; however, flow from the river will blend with the groundwater. When the degree of penetration is increased and the base of the well is at the bottom of the aquifer, SDR and drawdown decrease along with the average flux in the well. Small drawdown and reduced SDR would aid the collection of a contaminant floating on top or near the water table. A well with small Λ located near the top of the aquifer will meet these requirements. Dewatering wells, which aim to maximize drawdown and minimize SDR, should be placed as high up in the aquifer as possible to reduce SDR but still extend below the required depth of drawdown.

3.5 Conclusion

The Huang et al. (2012) solution for flow to a point sink was modified and used to develop a model for flow to a partially penetrating well near a fully penetrating stream with a reduced permeability streambed in a homogeneous, anisotropic, unconfined aquifer, The point-sink solution for SDR developed by Maroney and Rehmann (2017) was modified for use with a vertical well that partially penetrates an unconfined aquifer and is near a fully-penetrating stream with a reduced permeability streambed. The effects of the degree of penetration of the well screen and location of the well screen in the aquifer were evaluated

and compared to the Hantush (1965) model for flow from a stream to a well and for SDR along with the Neuman (1974) model for flow to a well in an unconfined aquifer.

1. The SDR is reduced during the intermediate stage as the degree of penetration $\Lambda = \ell/H$ decreases or $\kappa_z = K_z/K_x$ increases for a well located at the base of the aquifer and approaches the Hantush (1965) model for SDR with $S = S_y$.
2. For a well with small Λ, the effect from elastic release of water is prolonged as the degree of penetration decreases or the well is higher in the aquifer, and SDR is delayed beyond the limit of the Hantush (1965) condition for SDR with $S = S_y$.
3. The solution in Eq. (3.19) for hydraulic head matches the finite-difference model designed for the same aquifer, stream, and well properties with the models matching well where the finite-difference cells are small but with greater error where the cells are large.
4. Steady state drawdown is symmetric about the midpoint of the saturated thickness decreasing away from the center of the saturated thickness. At the center, drawdown in smaller for larger Λ, while at the top and bottom the opposite occurs with smaller drawdown for smaller Λ.
5. Drawdown for a partially penetrating well located in the middle of the saturated thickness behaves as it would for an infinite aquifer during the intermediate stage of flow. Near the top and bottom of the aquifer drawdowns are smaller due to the source of water from the river.
6. The theoretical model provides quantitative guidance for practical applications. For example, for removing contaminants, a well with small Λ should be placed near the

level of contamination, and for dewatering—which aims for maximum drawdown and minimum SDR, the well should be placed as high in the aquifer as possible.

References

Anderson, M.P., Woessner, W.W., 2002. Applied Groundwater Modeling: Simulation of Flow and Advective Transport. Academic Press, San Diego, California, 381 pages.

Boulton, N.S., 1954. Unsteady radial flow to a pumped well allowing for delayed yield from storage. Proceedings of the Institute of Civil Engineers, no. 3 : 564-579.

Butler, J.J., Zhan, X.Y., Zlotnik, V.A., 2007. Pumping-induced drawdown and stream depletion in a leaky aquifer system. Ground Water, 45(2): 178-186. DOI:10.1111/j.1745-6584.2006.00272.x

Butler, J.J., Zlotnik, V.A., Tsou, M.S., 2001. Drawdown and stream depletion produced by pumping in the vicinity of a partially penetrating stream. Ground Water, 39(5): 651-659. DOI:10.1111/j.1745-6584.2001.tb02354.x

Cleveland, T.G., 1994. Recovery performance for vertical and horizontal wells using semianalytical simulation. Groundwater 32(1): 103-107.

Cooley, R.L., Case, C.M., 1973. Effect of a water table aquitard on drawdonwn in an underlying pumped aquifer. Water Resources Research, 9(2): 434-447. DOI:10.1029/WR009i002p00434

Dagan, G., 1967. A method of determining permeability and effective porosity of unconfined anisotropic aquifers. Water Resources Research, 3(4): 1059-&. DOI:10.1029/WR003i004p01059

Fox, G.A., DuChateau, P., Durnford, D.S., 2002. Analytical model for aquifer response incorporating distributed stream leakage. Ground Water, 40(4): 378-384. DOI:10.1111/j.1745-6584.2002.tb02516.x

Glover, R.E., Balmer, G.G., 1954. River depletion resulting from a pumping well near a river. American Geophysical Union, 35: 468-470.

Hantush, M.S., Jacob, C.E., 1955. Non-steady radial flow in an infinite leaky aquifer, American Geophysical Union Transactions., 36(1), 95-100.

Hantush, M.S., Papadopulos, I.S., 1962. Flow of Ground Water to Collector Wells. Journal of the Hydraulics Division-American Society of Civil Engineers, 88(HY5): 221-244.

Hantush, M.S., 1964. Hydraulics of wells, in Advances in Hydroscience, Vol. 1. Academic, New York, NY, 282-432.

Hantush, M.S., 1965. Wells near streams with semipervious beds. Journal of Geophysical Research, 70(12): 2829-2838. DOI:10.1029/JZ070i012p02829

Harbaugh, A.W., Banta, E.R., Hill, M.C., and McDonald, M.G., 2000, MODFLOW-2000, the U.S. Geological Survey modular ground-water model -- User guide to modularization concepts and the Ground-Water Flow Process: U.S. Geological Survey Open-File Report 00-92, 121 p.

Huang, C.S., Chen, J.J., Yeh, H.D., 2016a. Approximate analysis of three-dimensional groundwater flow toward a radial collector well in a finite-extent unconfined aquifer. Hydrology and Earth System Sciences, 20(1): 55-71. http://dx.doi.org/10.5194/hess-20-55-2016

Huang, C.S., Tsou, P.R., Yeh, H.D., 2012. An analytical solution for a radial collector well near a stream with a low-permeability streambed. Journal of Hydrology, 446: 48-58. DOI:10.1016/j.jhydrol.2012.04.028

Huang, C.S., Tsou, P.R., Yeh, H.D., 2016b. Corrigendum to "An analytical solution for a radial collector well near a stream with a low-permeability streambed" J. Hydrol. 446-447 (2012) 48-58]. J. Hydrol., 542: 1002-1002. http://dx.doi.org/10.1016/j.jhydro1.2016.09.013

Hunt, B., 1999. "Unsteady stream depletion from ground water pumping" by B. Hunt, January-February 1999 issue, v.37, no.1 : 98-102. Author's reply. Ground Water, 37(6): 805-805.

Hunt, B., 2003. Unsteady stream depletion when pumping from semiconfined aquifer. Journal of Hydrologic Engineering, 8(1): 12-19. DOI:10.1061/(asce)1084-0699(2003)8:1(12)

Hunt, B., 2005. Flow to vertical and nonvertical wells in leaky aquifers. Journal of Hydrologic Engineering, 10(6): 477-484. DOI:10.1061/(asce)1084-0699(2005)10:6(477)

Hunt, B., 2006. Characteristics of unsteady flow to wells in unconfined and semi-confined aquifers. Journal of Hydrology, 325(1-4): 154-163. DOI:10.1016/j.jhydrol.2005.10.013

Hunt, B., 2009. Stream Depletion in a Two-Layer Leaky Aquifer System. Journal of Hydrologic Engineering, 14(9): 895-903. DOI:10.1061/(asce)he.1943-5584.0000063

Kawecki, M.W., 2000. Transient flow to a horizontal water well. Ground Water, 38(6): 842-850. DOI:10.1111/j.1745-6584.2000.tb00682.x

Kompani-Zare, M., Zhan, H.B., Samani, N., 2005. Analytical study of capture zone of a horizontal well in a confined aquifer. Journal of Hydrology, 307(1-4): 48-59. DOI:10.1016/j.hydrol.2004.09.021

Maroney, C.L., Rehmann, C.R., 2017. Stream depletion rate for a radial collector well in an unconfined aquifer near a fully penetrating river. J. of Hydrol., 547: 732-741. http://dx.doi.org/10.1016/j.jhydrol.2017.02.010

Murdoch, L.C. 1994. Transient analyses of an interceptor trench. Water Resources Research. 30(11), 3023-3031.

Neuman, S.P., 1972. Theory of flow in unconfined Aquifers considering delayed response of water table. Water Resources Research, 8(4): 1031-1045. DOI:10.1029/WR008i004p01031

Neuman, S. P. 1973. Supplementary comments on 'Theory of flow in unconfined aquifers considering delayed response of the water table'. Water Resources Research, 9(4):1102-1103

Neuman, S.P. 1974, Effect of partial penetration on flow in unconfined aquifers considering delayed gravity response. Water Resources Research, 10(2): 303-312.

Neuman, S.P., 1975. Analysis of pumping test data from anisotropic unconfined aquifers considering delayed gravity response. Water Resources Research, 11(2): 329-342. DOI:10.1029/WR011i002p00329

Sedghi, M.M., Samani, N., Sleep, B., 2009. Three-dimensional semi-analytical solution to groundwater flow in confined and unconfined wedge-shaped aquifers. Advances in Water Resources, 32(6): 925-935. DOI:10.1016/j.advwatres.2009.03.004

Sedghi, M.M., Samani, N., Sleep, B., 2012. Boundary depletion rate and drawdown in leaky wedge-shaped aquifers. Hydrological Processes, 26(20): 3101-3113. DOI:10.1002/hyp.8338

Sun, D.M., Zhan, H.B., 2006. Flow to a horizontal well in an aquitard-aquifer system. Journal of Hydrology, 321(1-4): 364-376. DOI:10.1016/j.jhydrol.2005.08.008

Sun, D., Zhan, H., 2007. Pumping induced depletion from two streams. Advances in Water Resources, 30(4): 1016-1026. DOI:10.1016/j.advwatres.2006.09.001

Theis, C.V., 1935. The relation between the lowering of the piezometric surface and the rate and duration of discharge of a well using ground water storage. Transactions-American Geophysical Union, 16: 519-524.

Theis, C.V., 1941. The effect of a well on the flow of a nearby stream. Transactions-American Geophysical Union, 22: 734-738.

Tsou, P.R., Feng, Z.Y., Yeh, H.D., Huang, C.S., 2010. Stream depletion rate with horizontal or slanted wells in confined aquifers near a stream. Hydrology and Earth System Sciences, 14(8): 1477-1485. DOI:10.5194/hess-14-1477-2010

Turco, M.J., Buchmiller, R.C., 2004. Simulation of ground-water flow in the Cedar River alluvial aquifer flow system, Cedar Rapids, Iowa: U.S. Geological Survey Scientific Investigations Report 2004-5130, 39 pp.

Yeh, H.-D., Chang, Y.-C., Zlotnik, V.A., 2008. Stream depletion rate and volume from groundwater pumping in wedge-shape aquifers. Journal of Hydrology, 349(3-4): 501-511. DOI:10.1016/j.jhydrol.2007.11.025

Zhan, H.B., Cao, J., 2000. Analytical and semi-analytical solutions of horizontal well capture times under no-flow and constant-head boundaries. Advances in Water Resources, 23(8): 835-848. DOI:10.1016/s0309-1708(00)00014-2

Zhan, H.B., Wang, L.V., Park, E., 2001. On the horizontal-well pumping tests in anisotropic confined aquifers. Journal of Hydrology, 252(1-4): 37-50. DOI:10.1016/s0022-1694(01)00453-x

Zhan, H., Zlotnik, V.A., 2002. Groundwater flow to a horizontal or slanted well in an unconfined aquifer. Water Resources Research. 38(7):13-1-13-11. DOI:10.1029/2001wr000401

CHAPTER 4: TRANSPORT TO A VERTICAL WELL IN AN AQUIFER NEAR A STREAM

A paper to be submitted to *Groundwater*

Cynthia Maroney and Chris Rehmann

Abstract

Transport of a contaminant from a stream to a well is computed with a model that includes advection, retardation, and decay. The well and the stream both fully penetrate the saturated thickness of a homogeneous, anisotropic aquifer, and the stream has a reduced conductivity streambed. Dimensional analysis and supporting arguments are used to reduce the dependence of the concentration at the well to four dimensionless parameters: dimensionless time, a streambed conductance coefficient χ, a horizontal anisotropy parameter κ_y, and the Damköhler number, which compares time scales of advection and decay. Concentrations are computed by tracking decay along streamlines calculated for the two-dimensional flow field. For fixed χ and κ_y, the timing and magnitude of the steady state concentration at the well depends only on the Damköhler number, which incorporates aquifer, well, and contaminant properties. The special case of no streambed ($\chi \to \infty$) yields conservative estimates of the time of first arrival, steady state concentration, and (except for small Damköhler number) the time to steady state at the well.

4.1 Introduction

Nonpoint source pollution from bacteria, nitrates, or pesticides poses a risk for water production in agricultural watersheds with shallow groundwater sources. Nitrate is one of the contaminants of concern in the alluvial aquifer system in Iowa. The cost for the Des Moines

area to add a nitrate treatment facility was $4.1 million with operating costs of up to $7,000 per day (Des Moines Water Works, 2015). Riverbank filtration serves as a pretreatment process for high capacity water supply wells located near streams and reduces the risk of nonpoint source contaminants entering the pumping effluent. Understanding the transport of contaminants between a river and wells aids in assessing, managing, and controlling nonpoint source contaminants; planning and operating water collection systems that use the hydraulic connection between the river and well; and developing regulations to protect connected ecosystems and public health.

Methods to assess of nonpoint source contamination in alluvial aquifers include index based methods, statistical methods, and physical process based methods for analyzing contaminant transport between streams and wells. Index or overlay methods use soil type, surface slope, depth of unsaturated zone, and regional climate along with other properties to develop risk maps (Aller et al., 1987). Statistical methods include national regression models (Nolan and Hitt, 2006; Lee et al., 2003) and artificial neural networks (Al-Mahallawi et al., 2012). Physical process based methods involve solving groundwater flow and contaminant transport equations either numerically or analytically. Fully three-dimensional transport solutions have high—and sometimes prohibitive—costs (Kourakos and Harter, 2014). Process based models, such as those created using MODFLOW coupled with MT3DMS (Jiang and Somers, 2009; Gallardo et al, 2005), are useful for point source problems where site specific information is desired (Kourakos et al., 2012).

Streamline transport is an alternative to a full three-dimensional transport model (Kourakos and Harter, 2014). Kourakos et al. (2012) developed a streamline model for contaminant transport referred to as the NonPoint Source Assessment Toolbox (NPSAT)

composed of steady state groundwater flow, backward particle tracking, and one-dimensional unsteady transport along the streamlines which allows for the effect of nonpoint source contaminants to be evaluated. Kourakos et al. (2012) applied NPSAT to an aquifer in an irrigated agricultural region and found that time for nitrates to appear in wells is controlled by recharge and well pumping rates along with the effective porosity of the aquifer.

Existing analytical solutions for contaminant transport to wells are primarily for one-dimensional or uniform flow fields. They include the van Genuchten and Alves (1982) solutions for the one-dimensional advection and dispersion equation and the widely used Domenico (1987) model with a finite source of contaminant subject to one-dimensional groundwater flow, dispersion, and decay. One-dimensional analytical models have even been applied to the riverbank filtration problem. By approximating the flow and transport as one-dimensional, Mustafa et al. (2016) computed the increase in contamination caused by increasing the pumping rate or pumping time.

Analytical solutions are difficult to achieve in two- and three-dimensions because in general flow fields are non-uniform and dispersion coefficients vary (Zhan and Sun, 2007). Batu (1996, 1997) developed a three-dimensional model of advection, dispersion, retardation, and decay to compute transport from rectangular sources of constant concentration in vertical planes normal to the unidirectional flow. The calculations of Taylor and Guha (2017) of transport from a point source of contamination in uniform unidirectional flow to a stream show that the timing and magnitude of the peak concentration entering the stream depend on the Damköhler number, or the ratio of the advection and decay times, and the Péclet number, or the ratio of the dispersion and advection times. In particular, the peak concentration can

occur sooner and reach larger values than when only advection, retardation and decay are considered (Taylor and Guha, 2017).

A few analytical solutions have been developed that include varying dispersion coefficients in flow to a well. For confined aquifers Chen et al. (2002) computed radial dispersion and transport for flow to a fully penetrating well, and Chen (2010) considered a partially penetrating well. Tartakovsky (2000) applied the Dupuit approximation and used conformal mapping to obtain a solution for two-dimensional flow to a well. Lai et al. (2016) applied a Laplace transform in time and a generalized integral transform for the spatial dimension to produce an exact solution for radial advection and dispersion. However, none of these solutions include a stream or nonpoint source pollution.

This chapter presents a model to produce a breakthrough curve for a contaminant drawn from a stream by a nearby fully penetrating well in an unconfined aquifer. The model neglects dispersion but accounts for decay, retardation, and advection by the two-dimensional flow—as well as the effects of a streambed with reduced conductivity on the flow. In section 4.2, the model is developed, and dimensional analysis is used to identify the key relationships controlling the breakthrough curve. Results for important features of the breakthrough curve, including magnitude and timing of steady state concentration, are presented in section 4.3 and discussed in section 4.4. Conclusions are summarized in section 4.5.

4.2 Methods

4.2.1. Two-dimensional model of the aquifer and stream

Transport of a decaying contaminant from a stream to a well is computed (Fig. 4.1). The stream fully penetrates the aquifer, and it has a streambed with reduced hydraulic conductivity K' and thickness of b'. The fully penetrating vertical well with constant discharge Q uniformly distributed over the screen is installed a distance L_x from the stream. The aquifer is homogeneous and anisotropic with hydraulic conductivities K_x and K_y in the x- and y-directions, respectively. No contamination exists in the aquifer before time $t = 0$, and at $t = 0$ a contaminant of constant concentration C_0 arrives in the stream. In general, transport occurs through advection, dispersion, and decay.

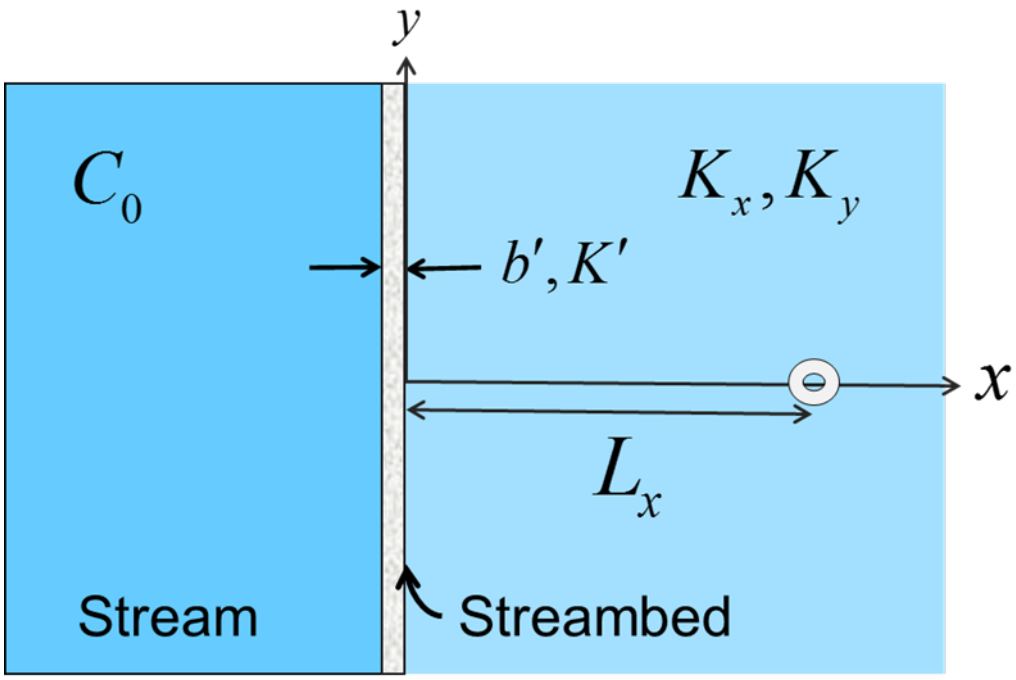

Fig. 4.1. Conceptual model for a fully penetrating vertical well installed in an unconfined aquifer adjacent to a fully penetrating stream with constant contamination in the stream (plan view).

4.2.2. Dimensional analysis

Dimensional analysis helps to identify the key parameters that affect C_w, the concentration of the contaminant reaching the well. Along with the time t, saturated thickness H of the aquifer, streambed properties, and concentration in the river, C_w depends on parameters related to decay (the decay rate λ of the contaminant), advection (hydraulic conductivities, the pumping rate, distance from the stream to the well, effective porosity η_e, and retardation coefficient R_c), and dispersion (the linear and transverse hydrodynamic dispersion coefficients D_L and D_T, respectively):

$$C_w = f\left(t, H, K', b', C_0, \lambda, K_x, K_y, Q, L_x, \eta_e, R_c, D_L, D_T\right) \tag{4.1}$$

The large number of parameters can be reduced with several observations. The pumping rate, saturated thickness, and porosity should appear only in the average linear velocity—that is, in the form $Q/\eta_e HL_x$. The governing equation for the contaminant concentration shows that only product of the decay rate and retardation coefficient—not the individual parameters—is important, and the solution of Maroney and Rehmann (2017) suggests that the effects of aquifer conductivities and streambed parameters can be expressed with the parameters $\kappa_y = K_y/K_x$ and $\chi = K'L_x / K_x b'$. Then dimensional analysis gives

$$\frac{C_w}{C_0} = f\left(\frac{t}{T_0}, \lambda R_c T_0, \chi, \kappa_y, \frac{L}{a_L}, \frac{a_T}{a_L}\right) = f\left(\frac{t}{T_0}, Da, \chi, \kappa_y, Pe, \frac{a_T}{a_L}\right) \tag{4.2}$$

where $T_0 = \eta_e HL_x^2 / Q$ is a travel time. The ratio of the advection time to reaction time is known as the Damköhler number $Da = \lambda R_c T_0$; the ratio of advection time to dispersion time is the Péclet number Pe; and the ratio of transverse to longitudinal dispersion coefficients simplifies to the ratio of transverse to longitudinal dispersivities a_T/a_L.

To simplify the problem further, dispersion is neglected, and only the effects of advection and decay are considered. Dispersion occurs through mechanical processes such as spreading from the center of mass of the contaminant caused by velocity gradients in the pores and dispersion along preferred flow pathways; the latter produces the scale effect of increasing dispersivity as the area of measurement increases. Schulze-Makuch (2005) quantified the relationship of flow scale L_f to longitudinal dispersivity as $a_L = cL_f^m$ where L_f and a_L are in meters, c is a property of the geologic material and m is a scaling exponent which ranges from 0.40 to 0.94 for geologic material. Neglecting dispersion is justified when $P_e >> 1$, or dispersion is small relative to advection. For the flow paths of L_x = 5 m and L_x = 200 m, the corresponding a_L are 0.35 m and 6.21 m for Pe = 14 and Pe = 32, respectively. Thus longitudinal dispersion is small related to advection and can be neglected. Because longitudinal dispersivity is 5 to 20 times larger than the transverse dispersivity (Charbeneau, 2000), transverse dispersion can be neglected also, and Equation (4.2) shows that the concentration at the well depends on four dimensionless parameters: dimensionless time, the Damköhler number, the streambed coefficient, and the ratio κ_y.

4.2.3. Calculating the breakthrough curve

Breakthrough curves for contaminants entering a well were developed using an approach that accounts for advection and decay (Charbeneau 2000, section 6.5). Quantifying advection requires computing the average linear velocity

$$v_{\ell x} = -\frac{K}{\eta_e}\frac{\partial h}{\partial x} \quad \text{and} \quad v_{\ell y} = -\frac{K}{\eta_e}\frac{\partial h}{\partial y} \tag{4.3}$$

Average linear velocities were computed using a special case of Eqs. (16) and (17) of Huang et al. (2012). For the flow, stream, and well described in section 4.2.1, the velocities are

$$
\begin{aligned}
v_{\ell x} = \; & \frac{Q}{\pi HL\kappa_y^{1/2}\eta_e}\int_0^\infty \frac{e^{-|y_D-y'_D|\omega/\kappa_y^{1/2}}}{\omega^2+\chi^2}\times \\
& \left\{\chi^2\cos(\omega x_D)\sin(\omega x'_D)+\chi\omega\cos\left[\omega(x_D+x'_D)\right]-\omega^2\sin(\omega x_D)\cos(\omega x'_D)\right\}d\omega \\
v_{\ell y} = \; & \frac{Q\,\mathrm{sgn}\left(y_D-y'_D\right)}{\pi HL\eta_e}\int_0^\infty \frac{e^{-|y_D-y'_D|\omega/\kappa_y^{1/2}}}{\omega^2+\chi^2}\times \\
& \left\{\chi^2\sin(\omega x_D)\sin(\omega x'_D)+\chi\omega\sin\left[\omega(x_D+x'_D)\right]+\omega^2\cos(\omega x_D)\cos(\omega x'_D)\right\}d\omega
\end{aligned}
\tag{4.4}
$$

For most of the aquifer, the integrals in Eq. (4.4) were evaluated using adaptive Gauss-Kronrod quadrature. When $y = y'$, however, the lack of exponential decay in the integrand for $v_{\ell x}$ makes numerical integration difficult. Instead the head was computed in part with adaptive quadrature and in part by expressing integrals in terms of the Meijer *G* function; then the average linear velocities were computed with finite differences and Darcy's law.

The decay of the contaminant along streamlines was computed, and the breakthrough curve was constructed. Streamlines were generated from the velocity field using Matlab's streamline function, and average linear velocities interpolated along the streamline were used to estimate the travel time of the water. By the method of characteristics (Charbeneau 2000, p. 326), the concentration of contaminant arriving at the well in the i^{th} streamtube is $C_0\exp(-\lambda R_c T_i)$, where T_i is the travel time of water in the streamtube. The contamination arriving in each streamtube is combined in time using a discrete form of a convolution integral (Charbeneau 2000, p. 327) to produce the breakthrough curve:

$$
C_w\left(t\right) = C_0\sum_{i=1}^{N_s} H\left(t-R_cT_i\right)e^{-\lambda R_cT_i}\Delta F_i \tag{4.5}
$$

where N_s is the number of streamlines, H(z) is the Heaviside step function, and ΔF_i is the fraction of the total flow carried by the i^{th} streamtube.

4.3 Results

The streamline pattern depends strongly on the streambed conductance coefficient χ (Fig. 4.2). Large streambed conductance produces a large flow field from the river that wraps around the well at $(x, y) = (L_x, 0)$—or $(x/L_x, y/L_x) = (1, 0)$, and small streambed conductance results in a thin flow field that remains close to the river at $x = 0$. Although the streamlines extend about the same distance in y, the spacing, which reflects a constant fraction of the well's flow, increases as the streambed becomes more conductive. As χ increases, the streamlines become nearly perpendicular to the stream, and the river approaches a constant-head boundary. The drop in hydraulic head across the streambed affects the hydraulic

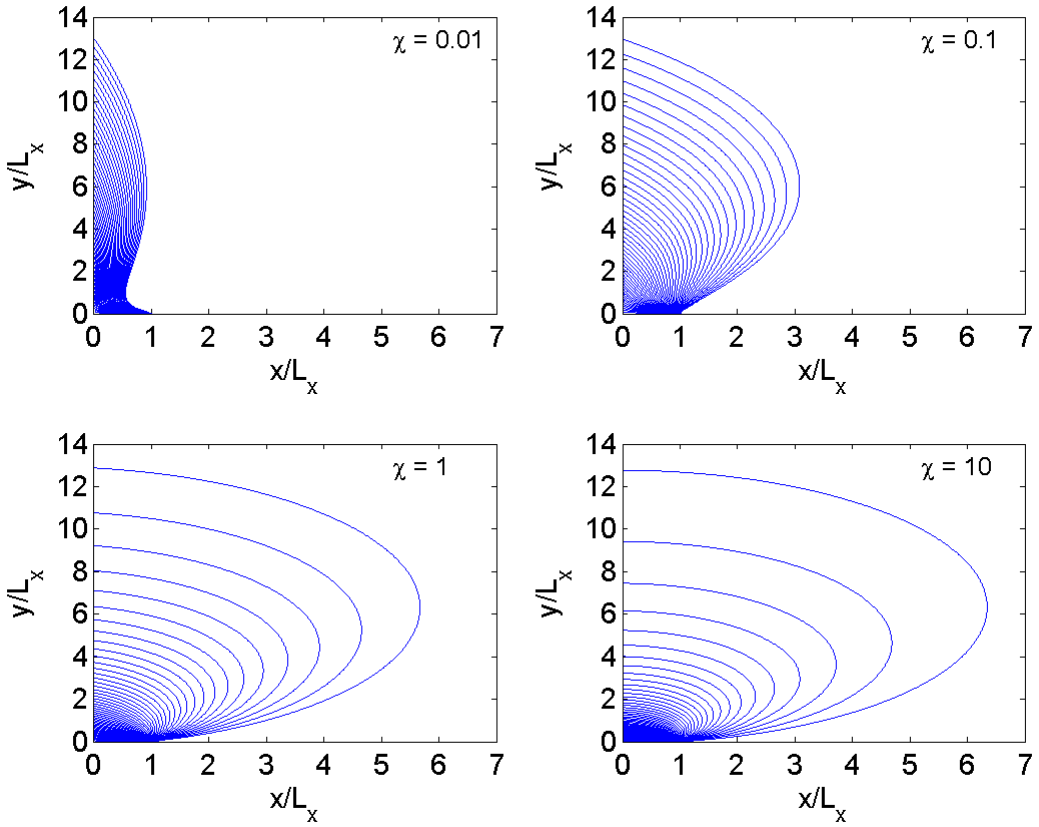

Fig. 4.2. Effect of the streambed conductance coefficient χ on the streamlines for $\kappa_y = 1$. The well is at $(x/L_x, y/L_x) = (1, 0)$, the river is at $x/L_x = 0$, and the fraction of flow between adjacent streamlines is constant.

gradient between the river and well. A small χ, which can result from low streambed permeability or large streambed thickness, leads to increased head loss across the streambed and reduced head difference between the aquifer side of the streambed and the well.

Travel time along streamlines is larger for streamlines farther from the well, and except for the streamlines far from the well, the travel time increases as the streambed conductance decreases (Fig. 4.3). The lengths of the streamlines close to the well (i.e., the ones for which the fraction of the total flow is small) do not vary much with χ, and the larger times for small χ reflect the smaller gradients in the aquifer. The travel times increase with the length of the streamline, and because the streamlines far from the well are much longer for large χ than for small χ, the travel time is larger when χ is larger.

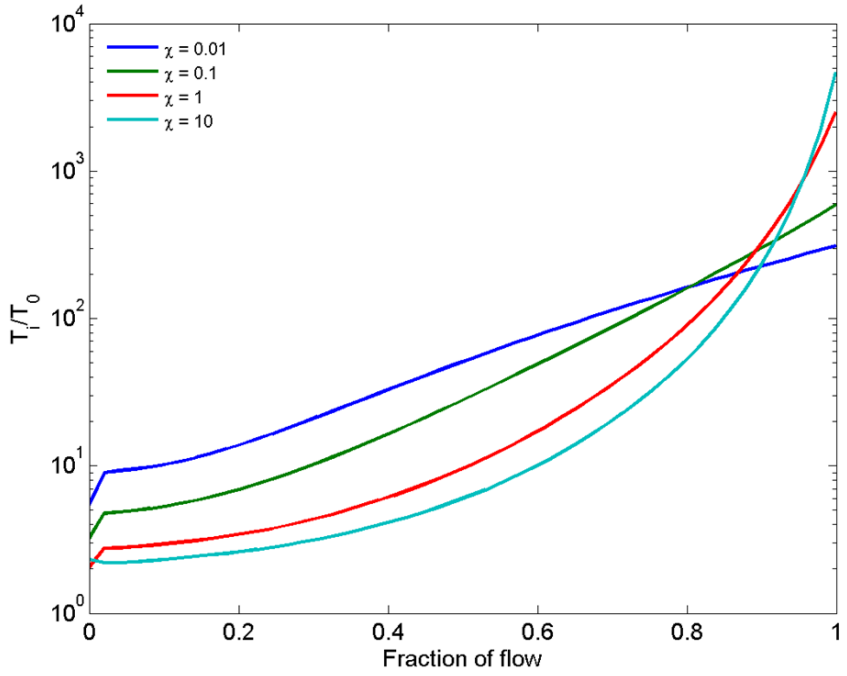

Fig. 4.3. Arrival of water at the well as a function of Damköhler number for various values of streambed conductance coefficient χ with $\kappa_y = 1$.

The Damköhler number strongly affects the time to reach steady state concentration at the well (Fig. 4.4). For a large pumping rate, well close to the river, or small aquifer properties of effective porosity or saturated thickness, or a large rate of decay, the Damköhler number is large and a small time is required for the flow of the contaminant to accumulate at the well. When decay occurs quickly compared to advection (i.e., large *Da*), streamlines farther from the well contribute little contaminant because it has mostly decayed. As the Damköhler number decreases, the time required for the flow of contaminant to accumulate to steady state takes longer because more of the streamtubes contribute to the concentration at the well. The plateaus occur because at low *Da* almost no decay occurs, and the

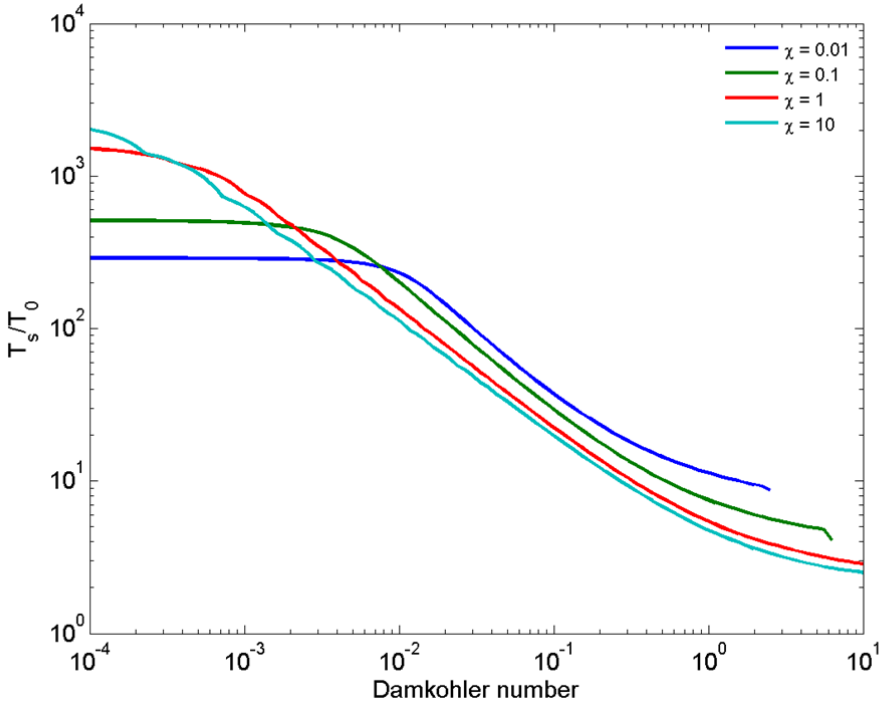

Fig. 4.4. Times to reach steady state in the breakthrough curve as a function of Damköhler number and streambed conductance coefficient for $\kappa_y = 1$. The time T_s to steady state is defined such that the concentration is 99% of the steady state value.

concentration at the well equals the concentration in the river. For fixed χ and κ_y, these results hold for any combination of pumping rate, distance between the well and river, effective porosity, saturated thickness, and decay rate. The dependence of the time to steady on streambed conductance coefficient reflects the results in Fig. 4.3: When *Da* is large and the main contribution comes from the first few streamlines, times are larger for smaller χ. However, when *Da* is small and most of the streamlines contribute to contamination at the well, times are larger for larger χ.

The steady state concentration of the contaminant at the well decreases sharply with Damköhler number (Fig. 4.5). For small Damköhler number—that is, when the advection time is smaller than the decay time, contaminant reaches the well without much decay, and concentrations are close to the concentration in the stream. When the Damköhler number is large, the time for flow to accumulate at the well is large compared to the time for decay, and concentrations at the well approach zero. For intermediate values of the Damköhler number, the concentrations reflect the results in Fig. 4.4: For $10^{-2} < Da < 1$, the times to steady state decrease with increasing χ. Therefore, the concentrations increase with increasing χ.

Horizontal anisotropy in hydraulic conductivities has a minor effect on the steady state concentration of contaminant at the well (Fig. 4.6). When K_x is larger than K_y (i.e., $\kappa_y < 1$) and the Damköhler number is small, the concentration at steady state is slightly reduced and when the Damköhler number is large, the concentration is increased. The reverse is true when K_y is larger as the symmetry of the hydraulic system is rotated. When concentrations are high (i.e., small *Da*), the relative differences between concentration curves is small. For $Da > 0.07$, the differences between the cases with $\kappa_y = 1$ and $\kappa_y = 0.5$ exceed 10%.

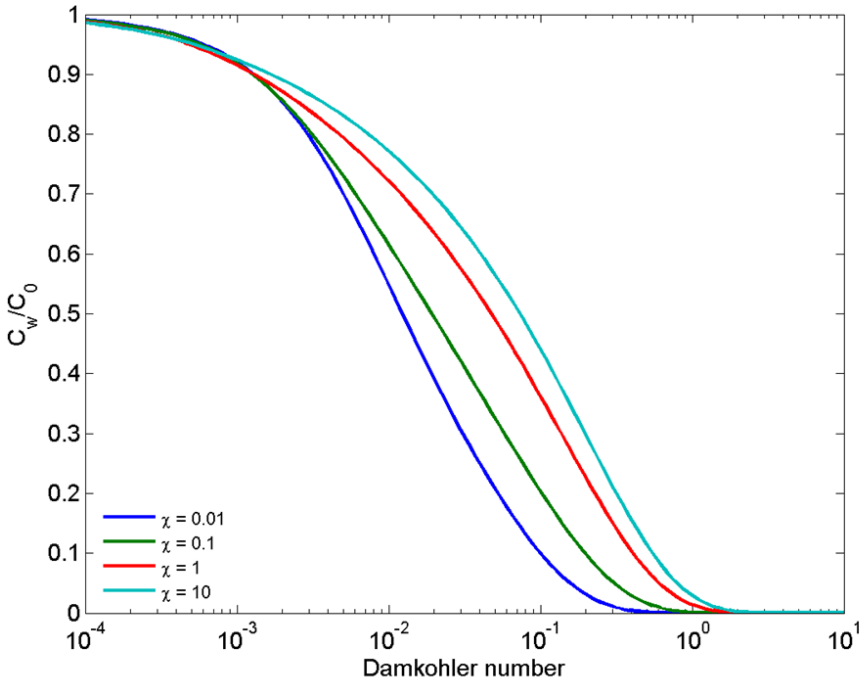

Fig. 4.5. Steady state concentration of contaminant at the well as a function of Damköhler number and streambed conductance coefficient for $\kappa_y = 1$.

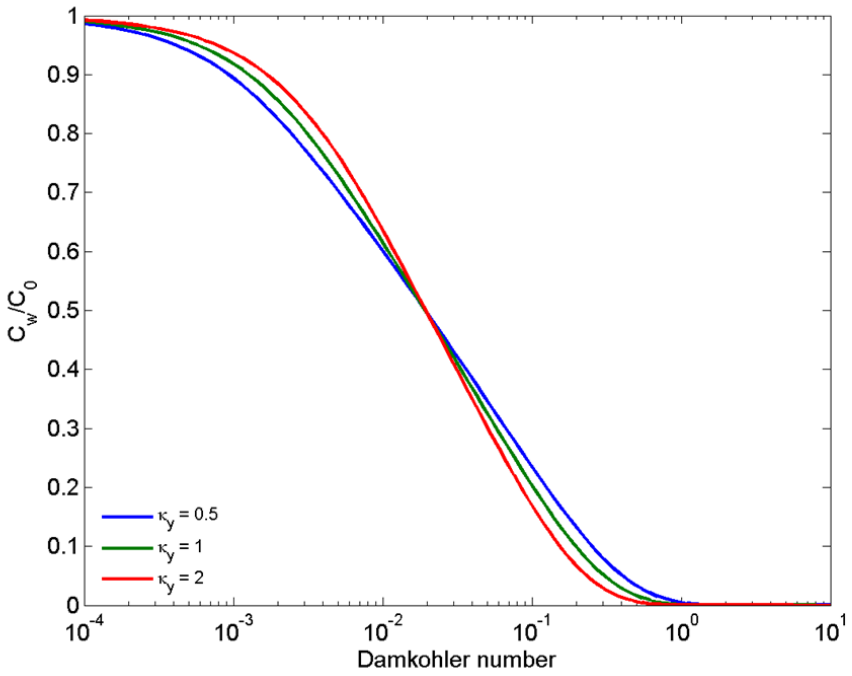

Fig. 4.6. Dependence of steady state concentration at the well on horizontal anisotropy parameter κ_y and Damköhler number.

4.4 Discussion

The relationships in the previous section can be used to predict the steady state concentration of a contaminant at a pumping well. For example, Figs. 4.4 and 4.5 provide information to estimate the timing and magnitude of contamination in wells near the Des Moines River (Moore et al., 2012). Conditions for their site 1 include H = 15 m, L_x = 30.5 m, and Q = 2800 m^3/d. The aquifer material is composed of sand and gravel with an effective porosity estimated to be 0.25 (Fetter, 2001). Aquifer hydraulic conductivity of K_x = 58.8 m/d and streambed resistance of b'/K' = 2.8 d yield a streambed conductance coefficient χ = 0.2. With a retardation coefficient of R_c = 1 and decay rates estimated as λ = 1 d^{-1} for bacteria (Hipsey et al., 2008) and λ = 0.75 d^{-1} for nitrate (Chapra, 1997), the Damköhler numbers are 0.12 and 0.09 respectively. Then Fig 4.5 gives C_w/C_0 of 0.2 for bacteria and 0.24 for nitrate in steady state. Fig. 4.4 gives T_x/T_0 of 24 and 30, or times of 3.0 and 3.7 d, for bacteria and nitrate.

To simplify the analysis leading to the relationships discussed in section 4.3, the flow was assumed to be steady. In terms of the temporal development of the concentration at the well, that assumption leads to conservative estimates. A well that has been pumping for a long time with an established flow pattern has a greater risk of a contaminant entering the pumping effluent compared to a well that just begins to pump and has an undeveloped zone of influence. The times estimated by Maroney and Rehmann (2017) for the flow field to reach steady state are typically much smaller than the durations of pumping for water supply wells. Therefore, assuming a steady flow field is not only conservative but also practical.

The relationships in section 4.3 allow accounting for the effects of the streambed through the conductance coefficient χ, but in practice determining the thickness and

hydraulic conductivity of the streambed is challenging. However, if the main concern is the maximum concentration of the contaminant, then assuming no streambed (i.e., $\chi \to \infty$) gives a conservative, estimate as shown in Fig. 4.5. Neglecting the streambed also would give the smallest times of arrival in many cases. Fig. 4.3 shows that the time of first arrival, which occurs for a fraction of zero, decreases as χ increases, and except at low *Da* the time to the steady state concentration is smallest for large χ.

As shown in section 4.2.2, dispersion is of secondary importance compared to advection. However, it does contribute to the transport of contaminants. Taylor and Guha (2017) found that for transport from an instantaneous release in a well to a river, the peak concentration can occur sooner and can be higher with dispersion than when only advection and retardation are considered. The case presented here is for a constant nonpoint source flow toward a well, but similar results can be expected. Accounting for dispersion in this case would require a numerical solution because the dispersion coefficients vary throughout the aquifer.

The model presented in this chapter does not consider the travel time through the streambed. Flow takes longer to pass through a streambed with a low conductance, allowing more time for decay to occur. Therefore, the concentrations in Fig. 4.5 are conservative (i.e., high) because they account for only decay in the aquifer. Assessing the importance of decay in the streambed involves comparing the travel times through the streambed and to the well. Identifying the value of y at which the travel time through the streambed is the largest fraction of the total travel time is not clear. The largest head drop across the streambed—and therefore the smallest travel time—occurs at $y = y'$, but the smallest travel time in the aquifer occurs there as well.

4.5 Conclusions

The transport of a contaminant from a river to well installed in a homogeneous, anisotropic aquifer was investigated using flow vectors generated from a special case of the flow model presented in Chapter 3 for two-dimensional flow. Both the river and the well fully penetrate the saturated thickness, and the river has a streambed with reduced conductivity. Dimensional analysis showed that the concentration at the well is a function of 14 parameters but can be reduced to a function of 5 dimensionless parameters. The Péclet number was greater than 1 showing that that dispersion time is small compared to advection time, and dispersion can be neglected reducing the number of parameters to four. Then the time to reach steady state and steady state concentration at the well were evaluated as functions of Damköhler number, streambed conductance coefficient χ, and horizontal anisotropy parameter κ_y. Significant findings are as follows:

1. The effects of advection, retardation, and decay are captured by the Damköhler number, which includes properties of the well, aquifer, and contaminant. If dispersion is negligible, then for fixed values of χ and κ_y, the concentration at the well and the time for the steady state concentration can be predicted with the Damköhler number alone.
2. Many streamlines are short when the streambed is less conductive (i.e., χ is smaller), but because the hydraulic gradient in the aquifer between the river and the well is smaller, the travel times are higher and concentrations at the well are smaller for a given Damköhler number.
3. The case of no streambed (i.e., $\chi \to \infty$) provides conservative estimates of the steady state concentration, time of first arrival, and—except for low *Da*—time to steady state concentration.

4. Effects of horizontal anisotropy on the steady state concentrations are small. At large *Da*, the differences between concentrations for different κ_y are relatively larger because the concentrations themselves are small.

References

Al-Mahallawi, K., Mania, J., Hani, A., Shahrour, I., 2012. Using of neural networks for the prediction of nitrate groundwater contamination in rural and agricultural areas. Environmental Earth Sciences, 65(3): 917-928. DOI:10.1007/s12665-011-1134-5

Aller, L., Bennett, T., Lehr, J.H., Petty, R.J., and Hackett, G., 1987. DRASTIC: A standardized system for evaluating groundwater pollution potential using hydrogeologic settings. U.S. Environmental Protection Agency report EPA-600/2-87-035, 641 pages.

Batu, V., 1996. A generalized three-dimensional analytical solute transport model for multiple rectangular first-type sources. Journal of Hydrology, 174(1-2): 57-82. DOI:10.1016/0022-1694(95)02752-1

Batu, V., 1997. A generalized three-dimensional analytical solute transport model for multiple rectangular first-type sources (vol 174, pg 57, 1996). Journal of Hydrology, 191(1-4): 372-372.

Chapra, S. C. (1997). Surface Water-Quality Modeling, McGraw-Hill, New York, NY.

Charbeneau, R.J., 2000. Groundwater Hydraulics and Pollutant Transport. Prentice-Hall, Inc., New Jersey, 593 pages.

Chen, J.S., 2010. Analytical model for fully three-dimensional radial dispersion in a finite-thickness aquifer. Hydrological Processes, 24(7): 934-945. DOI:10.1002/hyp.7541

Chen, J.S., Liu, C.W.I., Liao, C.M., 2002. A novel analytical power series solution for solute transport in a radially convergent flow field. Journal of Hydrology, 266(1-2): 120-138. DOI:10.1016/s0022-1694(02)00119-1

Des Moines Water Works, 2015. “Fact sheet: Nitrate removal facility.” http://www.dmww.com/upl/documents/water-quality/lab-reports/fact-sheets/nitrate-removal-facility.pdf

Domenico, P.A., 1987. An analytical model for multidimensional transport of a decaying contaminant species. Journal of Hydrology, 91(1-2): 49-58. DOI:10.1016/0022-1694(87)90127-2

Fetter, C.W., 2001. Applied Hydrogeology. Prentice-Hall, Inc., Upper Saddle River, New Jersey, 603 pages.

Gallardo, A.H., Reyes-Borja, W., Tase, N., 2005. Flow and patterns of nitrate pollution in groundwater: a case study of an agricultural area in Tsukuba City, Japan. Environmental Geology, 48(7): 908-919. DOI:10.1007/s00254-005-0029-8

Hipsey, M. R., Antenucci, J. P., and Brookes, J. D., 2008. A generic, process-based model of microbial pollution in aquatic systems. Water Resour. Res., 44(7), W07408, DOI: 07410.01029/02007wr006395.

Jiang, Y.F., Somers, G., 2009. Modeling effects of nitrate from non-point sources on groundwater quality in an agricultural watershed in Prince Edward Island, Canada. Hydrogeology Journal, 17(3): 707-724. DOI:10.1007/s10040-008-0390-2

Kourakos, G., Harter, T., 2014. Vectorized simulation of groundwater flow and streamline transport. Environmental Modelling & Software, 52: 207-221. DOI:10.1016/j.envsoft.2013.10.029

Kourakos, G., Klein, F., Cortis, A., Harter, T., 2012. A groundwater nonpoint source pollution modeling framework to evaluate long-term dynamics of pollutant exceedance probabilities in wells and other discharge locations. Water Resources Research, 48. DOI:10.1029/2011wr010813

Lai, K.H., Liu, C.W., Liang, C.P., Chen, J.S., Sie, B.R., 2016. A novel method for analytically solving a radial advection-dispersion equation. Journal of Hydrology, 542: 532-540. DOI:10.1016/j.jhydrol.2016.09.027

Lee, S.M., Min, K.D., Woo, N.C., Kim, Y.J., Ahn, C.H., 2003. Statistical models for the assessment of nitrate contamination in urban groundwater using GIS. Environmental Geology, 44(2): 210-221. DOI:10.1007/s00254-002-0747-0

Maroney, C.L., Rehmann, C.R., 2017. Stream depletion rate for a radial collector well in an unconfined aquifer near a fully penetrating river. Journal of Hydrology, 547: 732-741. http://dx.doi.org/10.1016/j.jhydrol.2017.02.010

Moore, R., Kelson, V., Wittman, J., Rash, V., 2012. A Modeling Framework for the Design of Collector Wells. Ground Water, 50(3): 355-366. DOI:10.1111/j.1745-6584.2011.00850.x

Mustafa, S., Bahar, A., Aziz, Z.A., Suratman, S., 2016. Modeling Water Chemistry Change and Contaminant Transport in Riverbank Filtration Systems, 2nd International Conference on Mathematical Sciences and Statistics (ICMSS). AIP Conference Proceedings. Amer Inst Physics, Kuala Lumpur, MALAYSIA. DOI:10.1063/1.4952520

Nolan, B.T., Hitt, K.J., 2006. Vulnerability of shallow groundwater and drinking-water wells to nitrate in the United States. Environmental Science & Technology, 40(24): 7834-7840. DOI:10.1021/es060911u

Schulze-Makuch, D., 2005. Longitudinal dispersivity data and implications for scaling behavior. Ground Water, 43(3): 443-456. DOI:10.1111/j.1745-6584.2005.0051.x

Tartakovsky, D.M., 2000. An analytical solution for two-dimensional contaminant transport during groundwater extraction. Journal of Contaminant Hydrology, 42(2-4): 273-283. DOI:10.1016/s0169-7722(99)00086-8

Taylor, S.W., Guha, H., 2017. Time and Magnitude of Peak Concentration of Reactive Groundwater Contaminants Discharged to a River. Groundwater, 55(1): 63-72. DOI:10.1111/gwat.12478

van Genuchten, M.T., 1982. A comparison of numerical solutions of the one-dimensional unsaturated-saturated flow and mass transport equations. Advances in Water Resources, 5(1): 47-55. DOI:10.1016/0309-1708(82)90028-8

Zhan, H.B., Sun, D.M., 2007. Travel-time distribution from a finite line contamination source to an extraction well with regional flow. Advances in Water Resources, 30(3): 389-398. DOI:10.1016/j.advwatres.2006.05.008

CHAPTER 5: GENERAL CONCLUSIONS

5.1 Summary

Planning and operating high capacity riverbank filtration systems requires knowledge about the stream depletion rate, drawdown, and quality of the water pumped by these systems. In Chapter 2 an analytical model of a radial collector well was used to evaluate SDR in terms of dimensionless parameters that include properties of the aquifer, streambed, and well. The parameters examined were the streambed conductance coefficient χ; vertical to horizontal anisotropy of the aquifer κ_z; the ratio $\gamma = S_y / S_s H$, which includes the effects of vertical flow; the ratio of length of the well screen to saturated thickness of the aquifer Λ; the orientation of the lateral well screens θ_i; dimensionless distance from the river to the caisson ρ_x; and dimensionless depth of the lateral well screens ρ_z. Although Huang et al. (2012) had computed the SDR for unsteady flow to a radial collector well, the work in Chapter 2 corrects an error and systematically studies the effects of the dimensionless parameters on the SDR.

The research for the radial collector well in Chapter 2 leads to extensions for other well configurations. Chapter 3 evaluated the SDR and drawdown caused by a partially penetrating vertical well near a stream. The systematic evaluation of the dimensionless parameters in Chapter 2 allowed the work in Chapter 3 to focus on how the depth and degree of penetration affects SDR and drawdown for partially penetrating wells. These models can be used to provide guidance for the design and operation of water supply, remediation, or dewatering systems.

A special case of the flow model presented in Chapter 3 is used in Chapter 4 to predict the concentration of a contaminant at a fully penetrating well located near a stream with a streambed with reduced conductivity. Dimensional analysis and arguments regarding the importance of dispersion were used to express the concentration as a function of four dimensionless parameters: dimensionless time, a horizontal anisotropy parameter, the streambed conductance coefficient χ, and the Damköhler number Da, which measures the relative importance of advection and decay. Streamlines were computed for the velocity flow field generated from the special case model, and the concentration at the well was computed by summing the contributions of individual streamtubes. The effects of three dimensionless parameters on the timing and magnitude of the steady state concentration at the well were evaluated.

5.2 Significant Findings

The models pertaining to flow and transport from a stream with a reduced conductivity streambed to a well in an unconfined aquifer provided the following important contributions:

- The analytical solution for SDR for a radial collector well provides an efficient solution involving only one numerical integration compared to the five required by Huang et al. (2012).
- SDR for a point sink at steady state is shown analytically to be one for a well located near a river in a semi-infinite, unconfined aquifer.
- When the streambed conductance defined as $\chi = K'L_x/K_xb'$ or $\alpha = -K'H/K_xb'$ is smaller SDR is smaller. Both parameters are better for describing the effects of the streambed

than just the ratio of streambed hydraulic conductivity K' to aquifer hydraulic conductivity K_x because the streambed thickness is included.

- The ratio of vertical to horizontal hydraulic conductivity K_z/K_x controls the value of SDR during the intermediate stage and the ratio of specific yield to storativity controls the duration of the intermediate stage.
- The streambed properties, aquifer anisotropy, and distance between the well and the stream affect SDR more than the length, depth, and orientation of the laterals of a radial collector well.
- For a partially penetrating vertical well SDR is reduced during the intermediate stage when $\kappa_z = K_z/K_x$ is large or the degree of penetration $\Lambda = \ell/H$ is small and the well is at the base of the aquifer.
- Drawdown for a partially penetrating vertical well vertically centered in an aquifer and located near a stream is similar to that observed for an infinite aquifer. However, a partially penetrating well located near the top or bottom of the aquifer experiences smaller drawdown due to the river supplying water.
- The Damköhler number combines the effects of advection, retardation, and decay and includes well, aquifer, and contaminant properties. For negligible dispersion and fixed streambed conductance coefficient and horizontal anisotropy ratio, the steady state concentration at the well and time to reach the steady concentration can be predicted from the Damköhler number.
- A low conductivity streambed shortens many of the streamlines but reduces the hydraulic gradient between the stream and the well. The reduced gradient results in longer travel time to the well and smaller concentration for a specific Damköhler number.

- Conservative estimates for the steady state concentration, time of first arrival, and (except at low *Da*) time to steady concentration can be predicted with the case of no streambed.

5.3 Future Work

Further work on this topic includes pursuing practical applications of the analytical models and exploring the implications of the assumptions in more detail. An example of the former would be to investigate the extent of the effects of partial penetration of a well—that is, to determine the conditions under which the partially penetrating well can be treated as fully penetrating and thus simplifying the application of the formulas derived in Chapter 3. The analytical solution in Chapter 3 provides physical insight into how the various parameters affect drawdown. Future work could involve developing a method for determining aquifer and streambed parameters from aquifer testing based on the analytical solution. It could also evaluate averaging the hydraulic head in observation wells as an alternative approach in the analysis of the evolution of drawdown.

Although the models in Chapter 2 to 4 are accompanied by discussions of the assumptions and their implications, further work to explore the implications of relaxing the assumptions would provide more information about how generally the models apply. The assumption of a straight river, fully penetrating river can be examined with numerical simulations of a sinuous or shallow stream to recompute SDR, drawdown, and transport and compare to the results from the analytical models. Dispersion can be added to the analysis of Chapter 4 with a finite-difference model of the transport accounting for variable dispersion coefficients; such a study would show whether dispersion decreases the arrival time and increases the peak concentration at the well.

APPENDIX MODEL VARIATIONS

The conceptual model for a slanted well near a stream in a homogeneous, anisotropic, unconfined aquifer is the more general version of the models given in Chapters 2 and 3. The stream fully penetrates the aquifer, the stream stage is constant and the flow rate through the well screen is uniform. The origin of the coordinate system is at the intersection of the streambed and pre-pumping water level with the *x*-direction in line with the well as shown in Fig. A.1. The point sink Q is located at (L_x, L_y, L_z). The governing equation, boundary conditions, and initial conditions are given in Chapter 2.

For flow that is uniform along the screen section of the well, the SDR for a vertical, slanted, or horizontal well can be found by integrating the SDR for a point sink (Eq. (2.37)) over the screened portion of the well. For any well, the integration points are

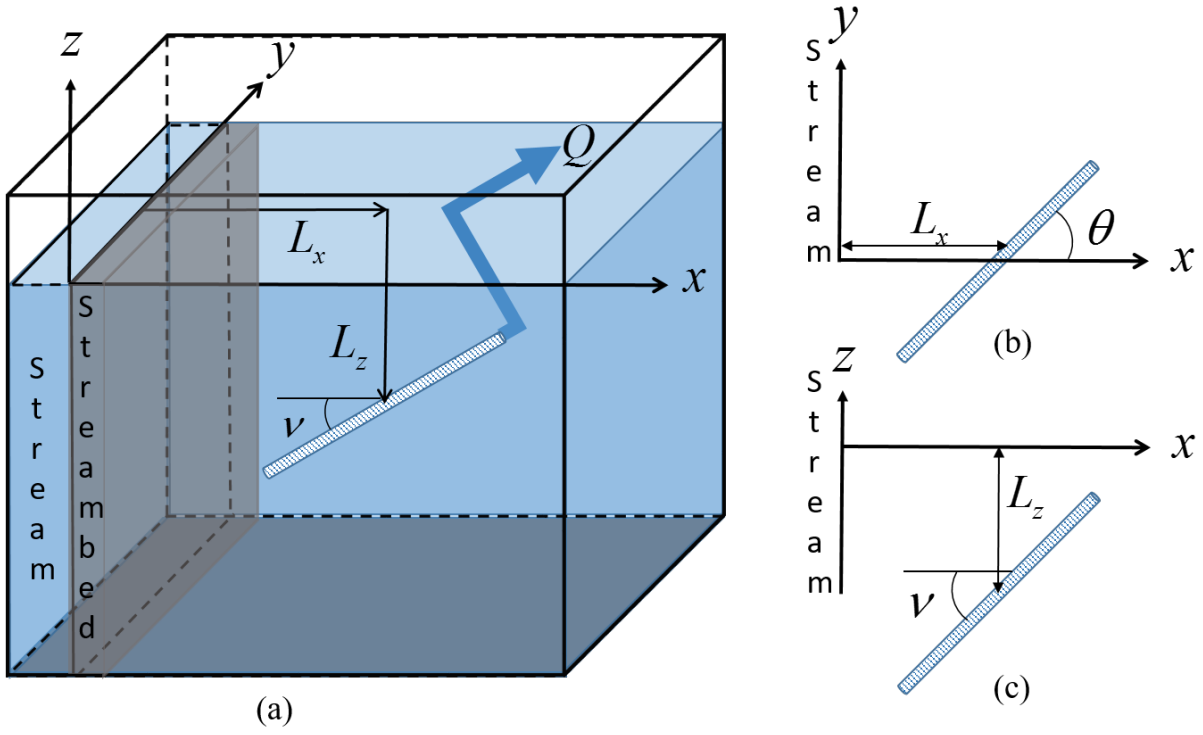

Fig. A.1. Conceptual model for a slanted well installed in an anisotropic, unconfined aquifer adjacent to a fully penetrating stream: (a) 2-D view, (b) plan view, (c) profile view.

$$x'_D = \sigma\cos(\theta)\cos(\nu) + \rho_x \tag{A.1}$$

$$z'_D = \sigma\sin(\nu) + \rho_z \tag{A.2}$$

where ρ_x and ρ_z are the coordinates of the center of the well screen, normalized by H and μ_0, μ_n, ζ_0, and ζ_n as defined in Chapter 2. This gives

$$SDR = 1 + \frac{2\alpha}{\Lambda\pi}\int_0^\infty \left\{ \left(\Phi_{0s}R_{0s} + \Phi_{0c}R_{0c}\right) + \sum_{n=1}^{\infty}\left(\Phi_{ns+}R_{ns+} + \Phi_{ns-}R_{ns-} + \Phi_{nc+}R_{nc+} + \Phi_{nc-}R_{nc-}\right)\right\} d\omega \tag{A.3}$$

where

$$\Phi_{0s} = \frac{2\gamma\sinh\left[\zeta_0(1+\rho_z)\right]e^{\mu_0\tau}}{\zeta_0\left[(2\gamma+1)\zeta_0\kappa_z\cosh(\zeta_0) + (\kappa_z+\gamma\mu_0)\sinh(\zeta_0)\right]\left\{\left[\omega\cos(\theta)\cos(\nu)\right]^2 + \left[\zeta_0\sin(\nu)\right]^2\right\}} \tag{A.4}$$

$$\Phi_{0c} = \frac{2\gamma\cosh\left[\zeta_0(1+\rho_z)\right]e^{\mu_0\tau}}{\zeta_0\left[(2\gamma+1)\zeta_0\kappa_z\cosh(\zeta_0) + (\gamma\mu_0+\kappa_z)\sinh(\zeta_0)\right]\left\{\left[\omega\cos(\theta)\cos(\nu)\right]^2 + \left[\zeta_0\sin(\nu)\right]^2\right\}} \tag{A.5}$$

$$\Phi_{ns+} = \frac{2\gamma\zeta_n\sin(\nu)\sin\left[\zeta_n\left(1+\rho_z+\frac{\Lambda}{2}\sin(\nu)\right)\right]e^{-\mu_n\tau}}{\zeta_n\left[(2\gamma+1)\zeta_n\kappa_z\cos(\zeta_n) + (\kappa_z-\gamma\mu_n)\sin(\zeta_n)\right]\left\{\left[\omega\cos(\theta)\cos(\nu)\right]^2 + \left[\zeta_n\sin(\nu)\right]^2\right\}} \tag{A.6}$$

$$\Phi_{ns-} = \frac{2\gamma\zeta_n\sin(\nu)\sin\left[\zeta_n\left(1+\rho_z-\frac{\Lambda}{2}\sin(\nu)\right)\right]e^{-\mu_n\tau}}{\zeta_n\left[(2\gamma+1)\zeta_n\kappa_z\cos(\zeta_n) + (\kappa_z-\gamma\mu_n)\sin(\zeta_n)\right]\left\{\left[\omega\cos(\theta)\cos(\nu)\right]^2 + \left[\zeta_n\sin(\nu)\right]^2\right\}} \tag{A.7}$$

$$\Phi_{nc+}=\frac{2\gamma\omega\cos(\theta)\cos(\nu)\cos\left[\zeta_n\left(1+\rho_z+\frac{\Lambda}{2}\sin(\nu)\right)\right]e^{-\mu_n\tau}}{\zeta_n\left[(2\gamma+1)\zeta_n\kappa_z\cos(\zeta_n)+(\kappa_z-\gamma\mu_n)\sin(\zeta_n)\right]\left\{\left[\omega\cos(\theta)\cos(\nu)\right]^2+\left[\zeta_n\sin(\nu)\right]^2\right\}} \tag{A.8}$$

$$\Phi_{nc-}=\frac{2\gamma\omega\cos(\theta)\cos(\nu)\cos\left[\zeta_n\left(1+\rho_z-\frac{\Lambda}{2}\sin(\nu)\right)\right]e^{-\mu_n\tau}}{\zeta_n\left[(2\gamma+1)\zeta_n\kappa_z\cos(\zeta_n)+(\kappa_z-\gamma\mu_n)\sin(\zeta_n)\right]\left\{\left[\omega\cos(\theta)\cos(\nu)\right]^2+\left[\zeta_n\sin(\nu)\right]^2\right\}} \tag{A.9}$$

$$\begin{aligned}R_{0s}=\frac{\omega}{\left(\omega^2+\alpha^2\right)}\Bigg\{&2\omega\cos(\theta)\cos(\nu)\sinh\left[\frac{\Lambda}{2}\zeta_0\sin(\nu)\right]\cos\left[\frac{\Lambda}{2}\omega\cos(\theta)\cos(\nu)\right]\\&\left[\omega\sin(\omega\rho_x)-\alpha\cos(\omega\rho_x)\right]\\&-\zeta_0\sin(\nu)\cosh\left[\frac{\Lambda}{2}\zeta_0\sin(\nu)\right]\\&\left\{\alpha\left\{\sin\left[\omega\left(\rho_x+\frac{\Lambda}{2}\cos(\theta)\cos(\nu)\right)\right]-\sin\left[\omega\left(\rho_x-\frac{\Lambda}{2}\cos(\theta)\cos(\nu)\right)\right]\right\}\right.\\&\left.-\omega\left\{\cos\left[\omega\left(\rho_x+\frac{\Lambda}{2}\cos(\theta)\cos(\nu)\right)\right]-\cos\left[\omega\left(\rho_x-\frac{\Lambda}{2}\cos(\theta)\cos(\nu)\right)\right]\right\}\right\}\Bigg\}\end{aligned} \tag{A.10}$$

$$\begin{aligned}R_{0c}=\frac{\omega}{\left(\omega^2+\alpha^2\right)}\Bigg\{&\omega\cos(\theta)\cos(\nu)\cosh\left[\frac{\Lambda}{2}\zeta_0\sin(\nu)\right]\\&\left\{\alpha\left\{\cos\left[\omega\left(\rho_x+\frac{\Lambda}{2}\cos(\theta)\cos(\nu)\right)\right]-\cos\left[\omega\left(\rho_x-\frac{\Lambda}{2}\cos(\theta)\cos(\nu)\right)\right]\right\}\right.\\&\left.+\omega\left\{\sin\left[\omega\left(\rho_x+\frac{\Lambda}{2}\cos(\theta)\cos(\nu)\right)\right]-\sin\left[\omega\left(\rho_x-\frac{\Lambda}{2}\cos(\theta)\cos(\nu)\right)\right]\right\}\right\}\\&-\zeta_0\sin(\nu)\sinh\left[\frac{\Lambda}{2}\zeta_0\sin(\nu)\right]\left\{2\alpha\cos\left[\frac{\Lambda}{2}\omega\cos(\theta)\cos(\nu)\right]\sin(\omega\rho_x)\right.\\&\left.+\omega\left\{\cos\left[\omega\left(\rho_x+\frac{\Lambda}{2}\cos(\theta)\cos(\nu)\right)\right]-\cos\left[\omega\left(\rho_x-\frac{\Lambda}{2}\cos(\theta)\cos(\nu)\right)\right]\right\}\right\}\Bigg\}\end{aligned} \tag{A.11}$$

$$R_{ns+} = \frac{\omega\left\{\omega co\,\mathrm{s}\left[\omega\left(\rho_x + \frac{\Lambda}{2}\cos(\theta)\cos(\nu)\right)\right] - \alpha\sin\left[\omega\left(\rho_x + \frac{\Lambda}{2}\cos(\theta)\cos(\nu)\right)\right]\right\}}{\left(\omega^2 + \alpha^2\right)} \quad \text{(A.12)}$$

$$R_{ns-} = \frac{-\omega\left\{\omega\cos\left[\omega\left(\rho_x - \frac{\Lambda}{2}\cos(\theta)\cos(\nu)\right)\right] - \alpha\sin\left[\omega\left(\rho_x - \frac{\Lambda}{2}\cos(\theta)\cos(\nu)\right)\right]\right\}}{\left(\omega^2 + \alpha^2\right)} \quad \text{(A.13)}$$

$$R_{nc+} = \frac{-\omega\left\{\omega\sin\left[\omega\left(\rho_x + \frac{\Lambda}{2}\cos(\theta)\cos(\nu)\right)\right] + \alpha\cos\left[\omega\left(\rho_x + \frac{\Lambda}{2}\cos(\theta)\cos(\nu)\right)\right]\right\}}{\left(\omega^2 + \alpha^2\right)} \quad \text{(A.14)}$$

$$R_{nc-} = \frac{\omega\left\{\omega\sin\left[\omega\left(\rho_x - \frac{\Lambda}{2}\cos(\theta)\cos(\nu)\right)\right] + \alpha\cos\left[\omega\left(\rho_x - \frac{\Lambda}{2}\cos(\theta)\cos(\nu)\right)\right]\right\}}{\left(\omega^2 + \alpha^2\right)} \quad \text{(A.15)}$$